Ultrafast Spectroscopy and Drug Delivery of the Medicinal Pigment Curcumin in Molecular Assemblies

Takaaki Harada

Department of Chemistry

The University of Adelaide

This dissertation is submitted in total fulfilment of the requirements

for the degree of Doctor of Philosophy

July 2015

Declaration

I certify that this work contains no material which has been accepted for the award of any other degree or diploma in my name in any university or other tertiary institution and, to the best of my knowledge and belief, contains no material previously published or written by another person, except where due reference has been made in the text. In addition, I certify that no part of this work will, in the future, be used in a submission in my name for any other degree or diploma in any university or other tertiary institution without the prior approval of the University of Adelaide and where applicable, any partner institution responsible for the joint award of this degree.

I give consent to this copy of my thesis when deposited in the University Library, being made available for loan and photocopying, subject to the provisions of the Copyright Act 1968.

The author acknowledges that copyright of published works contained within this thesis resides with the copyright holder(s) of those works.

I also give permission for the digital version of my thesis to be made available on the web, via the University's digital research repository, the Library Search and also through web search engines, unless permission has been granted by the University to restrict access for a period of time.

Takaaki Harada
July 2015

Acknowledgements

First and foremost, I would like to express my appreciation to my supervisor, A/Prof. Tak W. Kee, who has supported my PhD projects with his enthusiasm, encouragement, advice and immense knowledge. He has also got me interested in ultrafast spectroscopy and excited state dynamics. I would also like to thank for giving me the opportunities to work not only in Physical Chemistry but also in other disciplines. I believe I have gained important skills as a researcher.

I would also like to express my gratitude to Prof. Lincoln and his research group members. I have learnt a lot about how to write research manuscripts and data presentations through our publications. Special thanks go to Dr. Duc-Truc Pham for his support and advice during my polymer syntheses. I would not be able to accomplish my PhD projects without the fancy host molecules and polymers synthesised in his laboratory.

I would like to appreciate Dr. Grant Buchanan and his research group members, especially, Dr. Eleanor F. Need, Dr. Lauren Giorgio, Dr. Damien A. Leach, and Ms. Tiffany Harris, in School of Medicine at the University of Adelaide, who have given me enormous support to achieve a publication. As a Chemistry researcher, it was great opportunities to work with them and learn different skills for *in vitro* experiments. I also appreciate A/Prof. Brendon Coventry in Discipline of Surgery at the University of Adelaide, for his support and engagement with Dr. Grant Buchanan and his research group members.

I would also like to thank A/Prof. David Beattie and his research group members, at Ian Wark Research Institute at University of South Australia, for access to an experimental instrument which has provided insight into the macromolecular spectroscopic properties in a publication.

I wish to thank Mr. Philip Clements for his support on two-dimensional NMR experiments. Furthermore, I appreciate Mr. Matthew Bull, Mr. Graham Bull, Mr. Peter Apoefis, and Mr. Gino Farese for their support to build and repair instruments and other equipments. Without their contributions, I would not be able to make good progress in research.

I would like to thank friends, Postdocs, PhD candidates, and Honours students for their advice and the happy working environment. Special thanks go to Dr. Scott N. Clafton for his support and training on the ultrafast laser systems.

Finally, I would like to thank my parents for their financial support which has led to the opportunity to be awarded a PhD. I hope they will understand and acknowledge what I have achieved in the past few years. Last but not the least, I would like express appreciation to my girlfriend / lab buddy, Dr. Mandy H. M. Leung. Throughout our PhD life, she have encouraged and supported me, and we share good and bad outcomes. Thank you!

Abstract

Curcumin is a natural pigment extracted from turmeric. It is well known as a spice and herbal medicine in east Asia. The medicinal effects of curcumin have been demonstrated for cancer, inflammation, Alzheimer's disease, and cystic fibrosis. Recent studies have explored a number of delivery systems to suppress rapid aqueous degradation of curcumin and improve its bioavailability. Previously, we have demonstrated that diamide linked γ-cyclodextrin dimers, namely 66γCD$_2$su and 66γCD$_2$ur, suppress the degradation of curcumin by forming strong 1:1 cooperative binding complexes under physiological conditions. This result indicates the potential for 66γCD$_2$su and 66γCD$_2$ur as curcumin delivery systems.

As a part of the thesis work, both 66γCD$_2$su and 66γCD$_2$ur are used as molecular-scale delivery agents for curcumin in potential treatment of cancer. Cellular viability assays and gene regulation in human prostate cancer (PC-3) cells show an anti-proliferative effect of curcumin complexed with 66γCD$_2$su and 66γCD$_2$ur, which is comparable with that of curcumin alone. Both 66γCD$_2$su and 66γCD$_2$ur carriers show a lack of toxicity to the cells. Fluorescence studies show the intracellular delivery of curcumin by 66γCD$_2$su and 66γCD$_2$ur. Our results strongly suggest the potential of these carriers for future studies involving animal models.

To further understand the properties of curcumin, particularly its photo-therapeutic effect, ultrafast dynamics of curcumin complexed with 66γCD$_2$su and 66γCD$_2$ur are investigated using femtosecond transient absorption spectroscopy. Both curcumin complexes show only an excited state absorption (ESA) band without any stimulated emission signals. The ESA decay kinetics reveals the non-radiative relaxation of curcumin through solvent reorganization, excited state intramolecular hydrogen atom transfer, and other slow dynamics of inclusion molecules and flexibility of the γ-CD moieties of 66γCD$_2$su and 66γCD$_2$ur. In addition, transient absorption anisotropy studies reveal slow rotational motions of the curcumin complexes due to their large hydrodynamic volumes.

Hydrophobically modified polyacrylates are also potential delivery systems for curcumin because they suppress its degradation under physiological conditions. The

3 % octadecyl randomly substituted polyacrylate, PAAC18, shows a remarkable ability to suppress the degradation of curcumin, which is attributed to strong hydrophobic interactions between curcumin and the octadecyl substituents of PAAC18 within the micelle-like aggregates and the hydrogel. In contrast, the 3 % dodecyl randomly substituted polyacrylate, PAAC12, shows a negligible effect on slowing the degradation of curcumin, which is consistent with the dodecyl substituents being insufficiently long to capture curcumin in an adequately hydrophobic environment.

The ultrafast dynamics of water molecules and curcumin in the PAAC18 hydrogel are also studied using ultrafast spectroscopic techniques. The solvation dynamics (reorganization) of water molecules in the PAAC18 hydrogel exhibit a triexponential characteristic, as shown using femtosecond fluorescence upconversion spectroscopy. We attribute the slow solvation dynamics to the confinement of water molecules in the three-dimensional cross-linking network of the octadecyl substituents of PAAC18. Moreover, non-radiative relaxation processes of curcumin were investigated using femtosecond transient absorption spectroscopy.

List of Publications

The following publications are presented as a part of the thesis work.

- Leung, M. H. M.[†]; Harada, T.[†]; Kee, T. W., Delivery of Curcumin and Medicinal Effects of the Copper(II)-Curcumin Complexes. *Curr. Pharm. Des.* **2013**, 19, 2070-2083 (Published in April 2013). [†]These authors contribute equally to this review article. Reprinted by permission of Eureka Science Ltd. Copyright (2013) Eureka Science Ltd.

- Harada, T.; Giorgio, L.; Harris, T. J.; Pham, D.-T.; Ngo, H. T.; Need, E. F.; Coventry, B. J.; Lincoln, S. F.; Easton, C. J.; Buchanan, G.; Kee, T. W., Diamide Linked γ-Cyclodextrin Dimers as Molecular-scale Delivery Systems for the Medicinal Pigment Curcumin to Prostate Cancer Cells. *Mol. Pharmaceutics* **2013**, 10, 4481-4490 (Published in December 2013). Adapted with permission from this journal article. Copyright (2013) American Chemical Society.

- Harada, T.; Pham, D.-T.; Lincoln, S. F.; Kee, T. W., The Capture and Stabilization of Curcumin Using Hydrophobically Modified Polyacrylate Aggregates and Hydrogels. *J. Phys. Chem. B* **2014**, 118, 9515–9523 (Published in July 2014). Adapted with permission from this journal article. Copyright (2014) American Chemical Society.

- Harada, T.; McTernan, H. L.; Pham, D.-T.; Lincoln, S. F.; Kee, T. W., Femtosecond Transient Absorption Spectroscopy of the Medicinal Agent Curcumin in Diamide Linked γ-Cyclodextrin Dimers *J. Phys. Chem. B* **2015**, 119, 2425-2433 (Published in September 2014). Adapted with permission from this journal article. Copyright (2015) American Chemical Society.

The following publication is presented as a part of the thesis work and will be submitted to a journal article.

- Harada, T.; Pham, D.-T.; Lincoln, S. F.; Kee, T. W., Ultrafast Dynamics of the Medicinal Pigment Curcumin and Solvation Dynamics of Water in Octadecyl Substituted Polyacrylate Hydrogel (In preparation).

Contents

List of Abbreviations

BBO	β-Barium borate
10%-PAAC12	10 % Dodecyl randomly substituted polyacrylate
10%-PAAC18	10 % Octadecyl randomly substituted polyacrylate
PAAC12	3 % Dodecyl randomly substituted polyacrylate
PAAC18	3 % Octadecyl randomly substituted polyacrylate
66γCD$_2$su	*N,N'*-Bis(6^A-deoxy-γ-cyclodextrin-6^A-yl)succinamide
66γCD$_2$ur	*N,N'*-Bis(6^A-deoxy-γ-cyclodextrin-6^A-yl)urea
DMPC	1,2-Dimyristoyl-*sn*-glycero-3-phosphocholine
DHAQ	1,8-Dihydroxy-9,10-anthraquinone
NMP	1-Methyl-2-pyrrolidone
6γCDN$_3$	6^A-Azido-6^A-deoxy-γ-cyclodextrin
6γCDTs	6^A-*O*-(4-methylbenzenesulfonyl)-γ-cyclodextrin
AOT	Aerosol OT
AR	Analytical Reagent
BSA	Bovine Serum Albumin
BRCA2	Breast Cancer 2 gene
CTAB	Cetyltrimethylammonium bromide
CMOS	Complementary Metal–Oxide–Semiconductor
CW	Continuous Wave

CD	Cyclodextrin
COX-II	Cyclooxygenase-II
CFTR	Cystic Fibrosis Transmembrane Conductance Regulator
DNA	Deoxyribonucleic acid
DCC-FBS	Dextran-Coated Charcoal Stripped Fetal Bovine Serum
DCC	Dicyclohexylcarbodiimide
DMSO	Dimethyl sulphoxide
DPSS	Diode-Pumped Solid State
DTAB	Dodecyltrimethylammonium bromide
eq	Equation
ESA	Excited State Absorption
ESIHT	Excited-State Intramolecular Hydrogen atom Transfer
FBS	Fetal Bovine Serum
FDA	Food and Drug Administration
FWHM	Full Width at Half Maximum
GVD	Group Velocity Dispersion
GADD45A	Growth Arrest and DNA-Damage-inducible protein alpha gene
IC50	Half maximal inhibitory concentration
HMOX1	Heme Oxygenase 1 gene
HPLC	High Pressure Liquid Chromatography
PC-3	Human Prostate Cancer
HSA	Human Serum Albumin
H/D exchange	Hydrogen/Deuterium exchange
IgG	Immunoglobulin G

LBO	Lithium triborate
mp	melting point
mRNA	messenger Ribonucleic acid
Mw	Molecular weight
NIR	Near Infra-Red
Nd:YLF	Neodymium-doped yttrium lithium fluoride
Nd:YVO_4	Neodymium-doped yttrium vanadate
n.s.	not significant
NFκBIA	Nuclear Factor κ light polypeptide gene enhancer in B-cells Inhibitor, Alpha gene
NRF2	Nuclear Factor like 2
NMR	Nuclear Magnetic Resonance
NOESY	Nuclear Overhauser Effect Spectroscopy
OD	Optical Density
OC	Output Coupler
PPAR	Peroxisome Proliferator-Activated Receptor
PRF	Phenol Red-Free
PBS	Phosphate Buffer Saline
PD	Photodiode Detector
PC	Pockels Cell
PLGA	Poly(lactic-*co*-glycolic acid)
QPCR	Quantitative Real Time Polymerase Chain Reaction
RI	Refractive Index
SPM	Self Phase Modulation

SDS	Sodium dodecyl sulphate
SD	Standard Deviation
SEM	Standard Error of the Mean
SE	Stimulated Emission
Mw/Mn	The Weight Average Molecular Weigh over The Number Average Molecular Weight
Ti:sapphire	Titanium-doped sapphire
TX-100	Triton-X 100
TNFRSF10B	Tumour Necrosis Factor Receptor Superfamily, member 10B gene
UV-Vis	Ultraviolet-Visible
VRR	Vertical Retro-Reflectors

Chapter 1

Introduction - Medicinal Pigment Curcumin

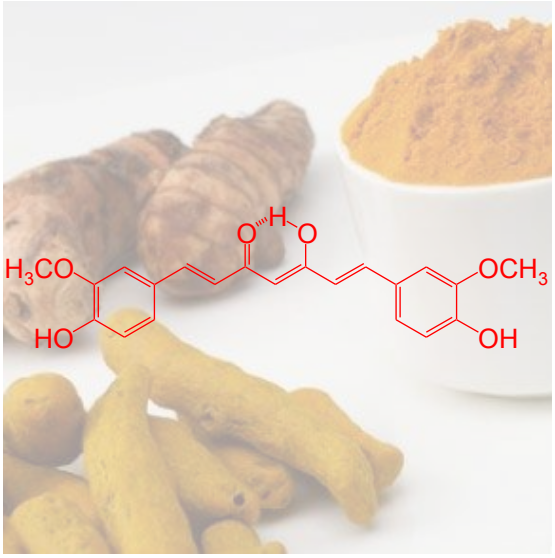

Statement of Authorship

By signing the Statement of Authorship, each author certifies that their stated contribution to the publication above is accurate and that permission in granted for the publication to be included in this thesis.

- Leung, M. H. M.[†]; Harada, T.[†]; Kee, T. W., Delivery of Curcumin and Medicinal Effects of the Copper(II)-Curcumin Complexes. *Curr. Pharm. Des.* **2013**, 19, 2070-2083 (Published on April 2013). [†]These authors contribute equally to this review article. Reprinted by permission of Eureka Science Ltd. Copyright (2013) Eureka Science Ltd.

Author Contributions

Name of First Author (Candidate)	Takaaki Harada
Contribution to the Paper	Literature search and preparation for sections shown in this chapter, and editing the manuscript
Signature	
Date	17/07/2014

Name of First Author	Mandy H. M. Leung
Contribution to the Paper	Literature search and preparation and editing for manuscript (not shown in this chapter)
Signature	
Date	02/10/2014

Name of Co-Author	Tak W. Kee
Contribution to the Paper	Supervision of the candidate, editing manuscript, and acted as corresponding author
Signature	
Date	02/10/2014

1.1 Abstract

Curcumin, a yellow pigment extracted from the rhizome of *Curcuma longa*, commonly known as turmeric, is the most active agent of this herbal medicine. The therapeutic activities of curcumin are exemplified not only by its enhancement in wound healing but also in the treatment of inflammation, cystic fibrosis, Alzheimer's disease and cancer. There are two critical issues involving low aqueous stability and solubility that limit the bioavailability and application of curcumin as a therapeutic agent. To address these issues, delivery systems of curcumin including surfactant micelles, liposomes, polymer nanoparticles, casein micelles, plasma proteins and cyclodextrins have been developed and characterised.

Figure 1.1. Pictures of *Curcuma longa* and turmeric powder.

1.2 History and Biosynthesis of Curcumin and Curcuminoids

Turmeric powder is the dried ground rhizome of *Curcuma longa*, a member of the ginger family *Zingiberaceae* (Figure 1.1) [1]. This intensely yellow powder has a long history of useful benefits and widespread applications in India and other Asian countries as turmeric is a key ingredient in Indian and Thai cuisines [2]. It was also introduced in a remedial theory called Ayurveda, the knowledge for long life, in which a system of traditional medicine and health maintenance was established in India over 2000 years ago [3]. The yellow colour and therapeutic activities of turmeric powder are derived from a group of active molecules, called curcuminoids.

Curcuminoids are present at 3–5 % in turmeric powder after liquid extraction and filtration [1, 4]. In 1815, Vogel and Pelletier et al. were the first to isolate curcuminoids [5]. Curcuminoids consist of three major components, with curcumin being the predominant species (77 %), which is followed by demethoxycurcumin (17 %) and bisdemethoxycurcumin (3 %) (Figures 1.2a−1.2c, respectively). In addition to these three curcuminoids, a recent study showed that a trace amount of a fourth curcuminoid, cyclocurcumin, is also present [6]. In 1973, Roughly and Whiting et al. investigated the biosynthesis of the major curcuminoids using ^{14}C-labelled precursors and proposed two possible pathways (Scheme 1.1) [4]. Scheme 1.1a depicts the synthesis of curcumin using two portions of ferulic acid and a portion of malonic acid. In addition, Scheme 1.1b shows the reaction between cinnamic acid and multiple malonic acid units through a condensation reaction to produce 7-methoxy-8-hydroxy-curcumin (curcumin without the methoxy and hydroxyl groups on one

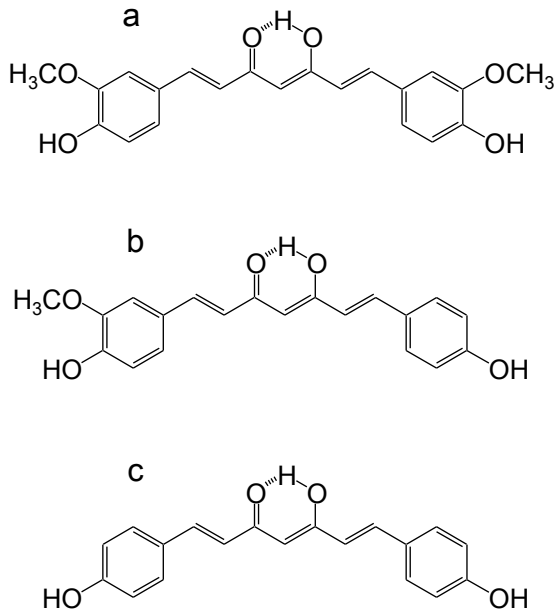

Figure 1.2. Structures of curcuminoids; (a) curcumin, (b) demethoxycurcumin and (c) bisdemethoxycurcumin.

side). This research was further investigated [7], in which ^{13}C-nuclear magnetic resonance (NMR) results were used to propose a more detailed biosynthesis of curcuminoids (Scheme 1.2) [7, 8]. In the major pathway, the curcumin skeleton intermediate called bisdeshydroxybisdesmethoxycurcumin is first synthesised from two units of cinnamic acid and one unit of malonic acid, which is followed by modification at the phenyl groups to form bisdemethoxycurcumin, demethoxycurcumin and then finally curcumin. Alternatively, cinnamic acid is modified to form *p*-coumaric acid and ferulic acid which randomly react with malonic acid to generate other curcuminoids in the minor pathway. This recently proposed biosynthesis scheme supports the earlier proposed pathway by Roughly and Whiting et al. (Scheme 1.1a) [4].

1.3 Physical Properties of Curcumin

Curcumin, (1*E*,6*E*)-1,7-bis(4-hydroxy-3-methoxyphenyl)-1,6-heptadiene-3,5-dione, is an orange-yellow solid at room temperature (Mw = 368.38 g/mol, mp = 183 °C), also known as E100 or Natural Yellow 3. Curcumin exists in two tautomeric forms, the keto-enol and di-keto tautomers (Schemes 1.3a and 1.3b, respectively). The predominant tautomer of curcumin is the keto-enol form when it is present in polar organic solvents such as methanol and DMSO [9]. This tautomer possesses intramolecular hydrogen bonding in the keto-enol moiety and π-conjugation is main-

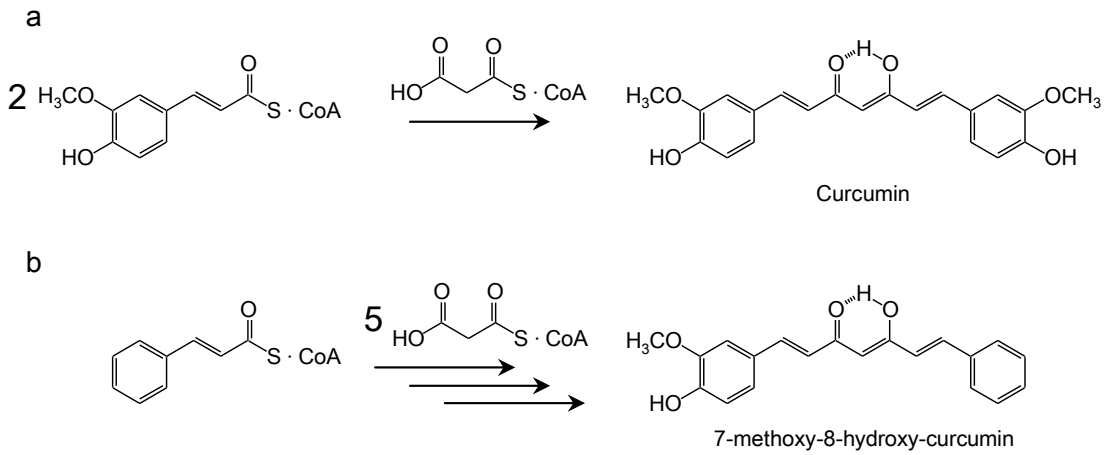

Scheme 1.1. Proposed mechanisms of biosynthesis of curcumin by Roughley and Whiting [4].

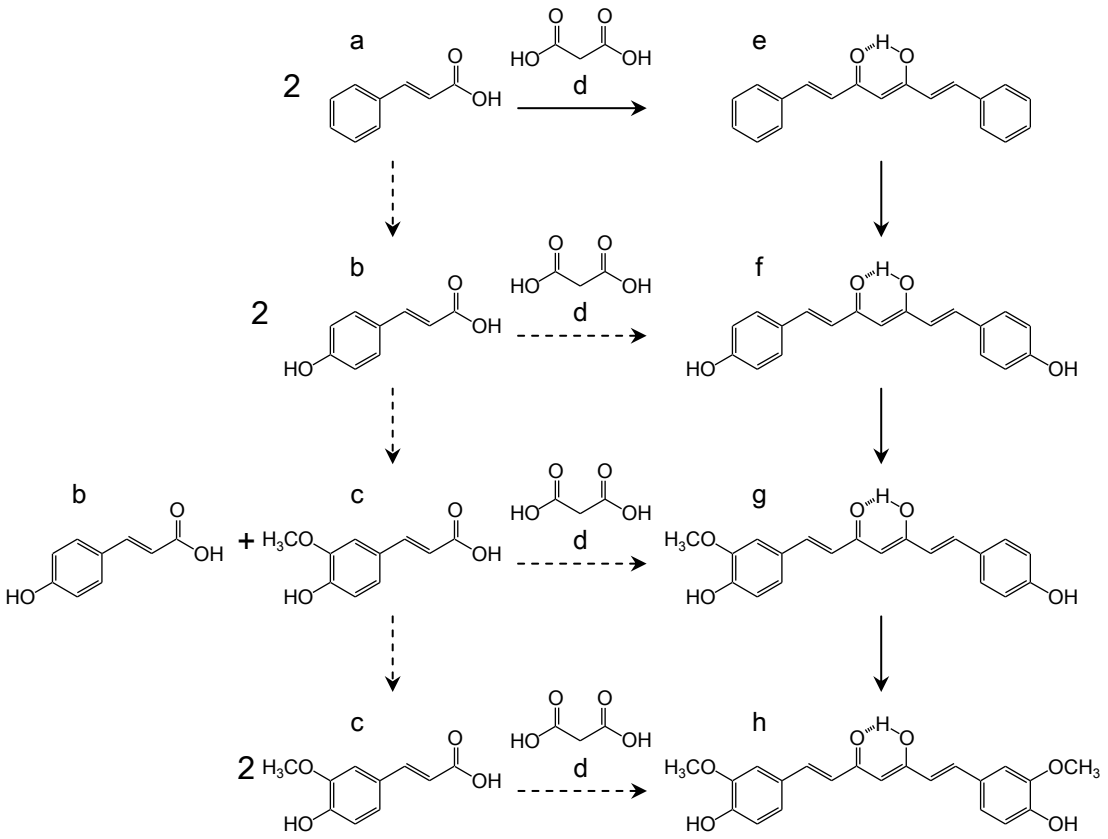

Scheme 1.2. Proposed major (solid arrows) and minor (dashed arrows) mechanisms of biosynthesis of curcumin and curcuminoids by Kita et al. [7]. The letters represent the following molecules; (a) cinnamic acid, (b) *p*-coumaric acid, (c) ferulic acid, (d) malonic acid, (e) bisdeshydoxybisdesmethoxycurcumin, (f) bisdemethoxycurcumin, (g) demethoxycurcumin and (h) curcumin.

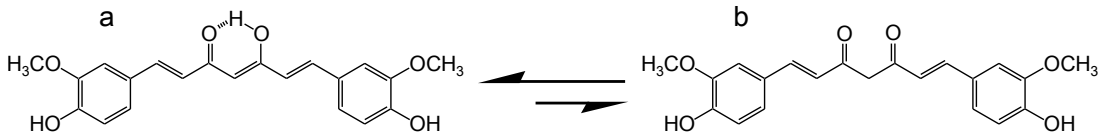

Scheme 1.3. Tautomerisation of curcumin in (a) keto-enol and (b) di-keto forms.

tained across the molecule, which results in an ultraviolet-visible (UV-Vis) absorption peak around 420 nm [10]. The strongly allowed $\pi - \pi^*$ transition gives rise to a high molar extinction coefficient of 30.000–70.000 $M^{-1}\,cm^{-1}$ at the absorption peak in water, methanol or ethanol [11]. Although curcumin is essentially non-fluorescent in water, it has a fluorescence quantum yield of 2–10 % in polar organic solvents, lipid membranes, and hydrophobic environment including non-polar solvents [11]. Several groups have used time-resolved fluorescence spectroscopy to investigate the rapid intramolecular hydrogen atom transfer in the keto-enol moiety of curcumin in the excited state [12–15]. In addition, the keto-enol tautomer possesses three hydroxyl groups of which the enolic and phenolic hydrogens can be deprotonated under alkaline conditions. The p*K*a values of the enolic and phenolic hydrogens are 8.3 and ∼10, respectively, in aqueous environment [16]. Hence, curcumin is expected to remain protonated at physiological pH (7.4).

In contrast, the conjugation length of the minor di-keto tautomer is significantly shorter, extending over only half the length of curcumin. The shorter conjugation length is due to the presence of an sp^3 hybridised carbon between the two carbonyl groups in the di-keto moiety of this tautomer (Scheme 1.3) [17, 18], which results in an absorption maximum around 350 nm. The presence of the di-keto form is indicated by an absorption shoulder around 350 nm when curcumin is solubilised in water.

1.4 Solubility and Stability of Curcumin

Although turmeric powder has a long history of medicinal applications in Asia, two critical issues involving low aqueous solubility and stability must be addressed in order for curcumin to be utilised as an effective therapeutic agent. Because curcumin is a moderately hydrophobic molecule with polar moieties, it has a high solubility and stability in polar organic solvents such as methanol, ethanol, acetone and DMSO. Although these solvents can solubilise curcumin at a high concentration, it is crucial to consider its solubility and stability in the aqueous environment for biological applications. The water solubility of curcumin is only approximately 30 nM, which is equivalent to 11 µg/L [19, 20]. In the presence of micelles, vesicles or polymer

nanoparticles, curcumin partitions largely into the hydrophobic domains under either slightly acidic or neutral condition due to its hydrophobicity [21]. However, under alkaline condition, the aqueous solubility of curcumin is improved due to deprotonation of the enolic and phenolic groups such that it becomes negatively charged. Under this condition, curcumin decomposes rapidly in water by a retro-aldol hydrolysis reaction, which is catalysed by hydroxide and followed by molecular fragmentation [22, 23]. The degradation of curcumin leads to formation of several metabolites, including *trans*-6-(4'-hydroxy-3'-methoxyphenyl)- 2,4-dioxo-5-hexenal (*half*-curcumin), vanillin, ferulic acid and feruloyl methane.

The poor aqueous stability of curcumin reduces an effective uptake *in vivo* and as such frequent doses may be required to maintain a sufficient curcumin level for effective medicinal response [23]. Therefore, a number of research groups are focusing on encapsulation of curcumin using delivery agents to improve the aqueous solubility and stability, with the ultimate goal of enhancing bioavailability of curcumin in the treatment of diseases. Such delivery agents require two key features to achieve a high solubility and stability of curcumin under physiological environment. First, encapsulation of curcumin by delivery agents with either a hydrophobic interior or moiety is essential to stabilise curcumin as well as segregate curcumin from water to prevent rapid hydrolysis. Second, a hydrophilic exterior is necessary to disperse the delivery agents in the aqueous environment. Recent work has demonstrated curcumin delivery using agents such as micelles, liposomes, polymer nanoparticles, plasma proteins and cyclodextrins.

1.5 Curcumin Encapsulation by Micelles, Liposomes and Polymer Nanoparticles

Micelles and liposomes are often used as cell membrane mimics because of the similar microscopic environment produced by these self-assembled structures. Surfactant and lipid molecules consist of long alkyl tail(s) and a charged head group [24, 25]. In the formation of micelles in the aqueous environment, the long alkyl tails of surfactants aggregate and form a hydrophobic core, while the polar head groups provide charges on the surface of the micellar particle to facilitate interaction with the surrounding water molecules. However, this aggregation can only occur above the critical micelle concentration [24]. Surfactant micelles are often used for solubilising and stabilising hydrophobic molecules. Curcumin is stable in anionic and neutral micelles including those of sodium dodecyl sulphate (SDS) and Triton-X 100 [26,

27]. Cationic micelles such as cetyltrimethylammonium bromide (CTAB) and dodecyltrimethylammonium bromide (DTAB) also show significant stabilisation of curcumin, especially under alkaline condition as rapid hydrolysis is expected [11, 18]. A measurable fluorescence quantum yield of approximately 4 % indicates a strong interaction between curcumin and the hydrophobic domain of the micelles (as curcumin is non-fluorescent in water), resulting in segregation of curcumin from water molecules and hence inhibition of hydrolysis [18].

Similarly, lipid molecules aggregate to form vesicles with a lipid bilayer and they are also known as liposomes [28]. The core and the surrounding environment of the vesicle are composed of water with which the polar head groups interact, allowing the vesicles to remain suspended in an aqueous solution. Aggregation of the long alkyl tails of the lipid molecules provides a hydrophobic environment to accommodate hydrophobic species including drugs inside the bilayers [29–31]. Stabilisation of curcumin using liposomes has been demonstrated in physiological environment [32, 33]. In 1993, Tønnesen et al. first showed stabilisation of curcumin using liposomes [32]. In a separate study, Barry et al. determined the orientation of curcumin using 1,2-dimyristoyl-*sn*-glycero-3-phosphocholine (DMPC) vesicles in order to infer the interaction between curcumin and the membrane [34]. At low concentrations, curcumin binds to either side of DMPC bilayer through hydrogen bonding with the phosphate group of the lipids. At high concentrations of curcumin, however, linear dimers of curcumin that are held by hydrogen bonding between the phenol moieties bind across the lipid bilayer.

Synthetic polymers also form micellar aggregates to yield polymer nanoparticles, which are useful for curcumin delivery. Bisht et al. demonstrated the synthesis and characterisation of 50-nm polymeric nanoparticles which are aggregates of cross-linked and random copolymers of *N*-isopropylacrylamide, with *N*-vinyl-2-pyrrolidone and poly(ethyleneglycol)monoacrylate [35]. The micellar nanoparticles solubilise curcumin in water at a concentration that curcumin alone would precipitate. In addition, Mohanty et al. achieved stabilisation of curcumin using copolymeric micelles composed of methoxy(polyethyleneglycol) and poly-ε-caprolactone [36]. The curcumin-loaded micellar nanoparticles, which were present in 65 % humidity for three months, were able to maintain a curcumin level of approximately 56 % at the end of the study.

1.6 Curcumin Binding with Protein Micelles and Plasma Proteins

In spite of the high stabilisation effects on curcumin using micelles, liposomal vehicles and polymer nanoparticles, their potential incompatibility *in vivo* may become issues in clinical trials. While surfactants may have a low toxicity to humans, their degradation products may be harmful [37, 38]. An alternative delivery method to improve the bioavailability of curcumin is to use milk proteins and plasma proteins to resolve the potential toxicity issue.

Food proteins possess potential abilities not only to suppress curcumin degradation but also to exhibit biocompatibility. Casein is the major protein in mammalian milk and widely used in the food industry [39]. Cross-linking of caseins using glutaraldehyde enables formation of micellar microspheres [39, 40]. Casein micelles exhibit a stabilisation effect of curcumin with a strong binding constant on the order of $10^5\,\mathrm{M}^{-1}$ [39, 41, 42]. Cytotoxicity assays of curcumin in the presence and absence of casein micelles revealed that curcumin encapsulated in casein micelles is as effective as curcumin alone against cancer cells [39, 41], indicating a potential application in clinical trials.

Plasma proteins play an important role as transporters in physiological functions [43, 44]. Multiple binding sites of plasma proteins provide possible interaction with a variety of ligands including metal ions, fatty acids, amino acids and drugs [43, 45]. Serum albumin is the most abundant plasma protein and its hydrophobic pockets allow curcumin to form a complex in the aqueous environment [44]. Absorption and fluorescence quenching studies on the serum albumin-curcumin complex resulted in a binding constant of 10^4–$10^5\,\mathrm{M}^{-1}$ [44]. Furthermore, we have previously investigated stabilisation of curcumin using plasma proteins including human serum albumin (HSA), fibrinogen, transferrin and immunoglobulin G (IgG) under physiological conditions [46]. The spectroscopic studies revealed that both HSA and fibrinogen suppress hydrolysis of curcumin, whereas neither transferrin nor IgG stabilises curcumin [46]. The stabilisation effect of HSA and fibrinogen is enabled by the strong binding of curcumin to the hydrophobic domains of the proteins. The binding constants of curcumin to HSA and fibrinogen are $(1.22 \pm 0.35) \times 10^5$ and $(5.99 \pm 1.75) \times 10^4\,\mathrm{M}^{-1}$, respectively [46]. In addition, denatured HSA at $50\,^{\circ}\mathrm{C}$ shows a significantly weaker ability to stabilise curcumin than wild type, which is indicative of a weaker interaction between curcumin and the hydrophobic pockets [46]. In short, delivery of curcumin using plasma proteins, particularly HSA and fib-

rinogen, may be a practical method in clinical trials. Curcumin can be delivered *in vivo* using the patient's own plasma proteins through intravenous delivery.

1.7 Stabilisation of Curcumin by Cyclodextrins and Diamide Linked γ-Cyclodextrin Dimers

Oral dosage of curcumin may be achieved by using cyclodextrins as delivery agents. Cyclodextrins are naturally occurring cyclic oligosaccharides, appearing as white crystalline powder at room temperature. The Food and Drug Administration (FDA) has approved the clinical use of cyclodextrins due to their non-toxic properties [47–49]. There are mainly three types of cyclodextrins; α-, β- and γ-cyclodextrins, consisting of six, seven and eight glucopyranoside units, respectively, which are linked with α-1,4 glycosidic bonds in a toroidal shape [50, 51]. Cyclodextrins have a hydrophilic exterior and a hydrophobic interior. The hydrophobic interior interacts with the hydrophobic moieties of the bound molecule, typically with the aromatic ring by van der Waals interactions [51, 52]. In a drug carrier system, cyclodextrins act as hosts to capture hydrophobic guest molecules [53, 54]. The driving force for this self-assembly is the entropy increase due to exclusion of water molecules from the cyclodextrin cavity [51, 55], which must overcome the corresponding decrease due to host-guest complexation to result in a successful binding event. A significant advantage of this delivery system is its high structural integrity. Micellar particles may lose their structural properties below critical micelle concentrations, and plasma proteins may denature depending on pH and temperature. Cyclodextrins, however, retain their structural properties as drug delivery systems under a wide range of physiological conditions, exhibiting more potential for drug delivery than micelles and plasma proteins.

The low toxicity of cyclodextrins and the structural characteristics lead to a possible delivery pathway for curcumin using cyclodextrin-curcumin complexation. However, neither α- nor β-cyclodextrin stabilises curcumin even at 100 : 1 cyclodextrin : curcumin molar ratio under physiological conditions, while γ-cyclodextrin at the same molar ratio shows some stabilisation effect, resulting in a short degradation half-life of curcumin of approximately (4.46 ± 0.12) h [56]. The short half-lives of curcumin in the presence of α-, β- and γ-cyclodextrins imply a rather weak interaction between curcumin and cyclodextrins. Therefore, synthetic modifications of cyclodextrins are essential to improve the cyclodextrin-curcumin interaction and to increase the aqueous stability of curcumin. (2-Hydroxypropyl)-α-cyclodextrin, (2-

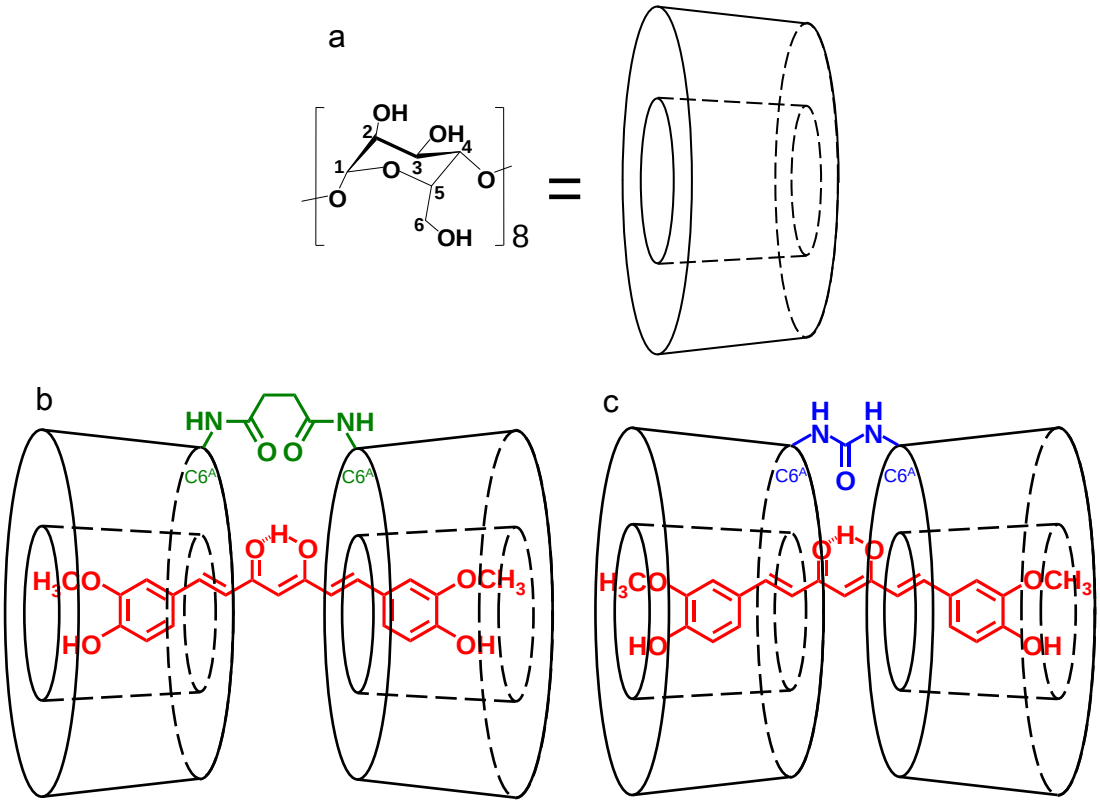

Figure 1.3. Structures of (a) γ-cyclodextrin, (b) 66γCD$_2$su-curcumin and (c) 66γ-CD$_2$ur-curcumin complexes.

hydroxypropyl)-β-cyclodextrin and (2-hydroxypropyl)-γ-cyclodextrin are modified cyclodextrins with enhanced hydrophobicity. Suppression of curcumin degradation has been demonstrated in the presence of these modified cyclodextrins at 30 °C [57]. Baglole et al. and Singh et al. have demonstrated stronger interactions between the modified cyclodextrins and curcumin, and the level of 1 : 1 host-guest complexation is increased by $3-10$-fold [58, 59]. Another possible modification of cyclodextrin is to introduce a linker between two cyclodextrins in order to induce cooperative interaction with a guest molecule. Pham et al. has established the synthesis of diamide linked cyclodextrin dimers for β- and γ-cyclodextrins [60, 61]. Our previous study has demonstrated strong cooperative binding and effective stabilisation of curcumin using diamide linked γ-cyclodextrin dimers, *N,N'*-bis(6^A-deoxy-γ-cyclodextrin-6^A-yl)succinamide, 66γCD$_2$su, and *N,N'*-bis(6^A-deoxy-γ-cyclodextrin-6^A-yl)urea, 66γ-CD$_2$ur (Figure 1.3) [56]. Both 66γCD$_2$su and 66γCD$_2$ur stabilise curcumin at the 1 : 1 molar ratio and the half-life of curcumin is extended by at least $180-750$ times, when compared to curcumin alone [56]. The binding constants of 66γCD$_2$su-curcumin and 66γCD$_2$ur-curcumin complexes are $(8.7\pm0.4)\times10^6$ and $(2.0\pm0.1)\times10^6$ M^{-1}, re-

spectively [56]. Overall, the remarkable and effective suppression of curcumin degradation using diamide linked γ-cyclodextrin dimers, 66γCD$_2$su and 66γCD$_2$ur, provide a potentially attractive method for oral dosage.

1.8 Medicinal Activities of Curcumin

Turmeric has been utilised not only as a dietary herbal medicine but also as a topical agent for wound healing enhancement for centuries [62]. Despite the limited bioavailability of curcumin as described before, the therapeutic activities of curcumin have been demonstrated for diseases including inflammation [63–70], cystic fibrosis [71–73], Alzheimer's disease [74–77], and cancer [62, 68, 78–82] without significant side effects in the past decades. A recent clinical trial indicated that a large oral dose of curcumin shows insignificant toxicity [83].

1.8.1 Wound Healing and Anti-Inflammatory Activities of Curcumin

Wound healing is a complex process of cell proliferation and migration involving different types of cells [84]. Inadequate treatment of the wound further causes inflammatory response at the trauma. The use of herbal medicine including turmeric as wound dressing has been documented in ancient Indian medical literature [62]. An *in vitro* study has revealed that curcumin is more effective in suppressing inflammation than demethoxycurcumin and bisdemethoxycurcumin [63]. In addition, recent *in vivo* studies have also demonstrated that curcumin possesses the ability to reduce inflammation and enhance wound healing [64–66]. The anti-inflammatory activity of curcumin has been related to the inhibition of the NF-κB activation pathways [68]. Other proposed mechanisms are inhibition of cyclooxygenase-II (COX-II) transcription and expression [63, 68], activation of peroxisome proliferator-activated receptors (PPARs) and urokinase plasminogen mRNA [66], and scavenging of oxidative radicals [62, 66, 68].

1.8.2 Anti-Cystic Fibrosis Activities of Curcumin

Cystic fibrosis is a life threatening disease caused by mutations in the gene expressing the cystic fibrosis transmembrane conductance regulator (CFTR). Misfolded CFTR proteins interact with calcium-dependant chaperones in the endoplasmic reticulum, resulting in degradation by the proteasome in the cytoplasm before CFTR

proteins activate the chloride ion channel across epithelial membranes [72]. Consequently, the elevated level of chloride ions induces influx of sodium ions [73], which causes dehydration of the tissue surface and production of viscous secretions typically in the lungs and nose. Egan et al. have demonstrated a potential use of curcumin to treat the cystic fibrosis defect [72]. The results of immunoblot assay and surface density measurements are indicative of an enhanced level of CFTR proteins in the cytoplasm after doses of curcumin. It is possible that binding of curcumin corrects the CFTR protein expression and/or the tertiary structure of CFTR proteins [72]. An alternative mechanism suggests that curcumin decreases the calcium level in the endoplasmic reticulum and inhibits calcium-dependent chaperones [73]. Hence, the reduced level of proteasomal degradation of CFTR proteins leads to efflux of chloride ions, even though the misfolded CFTR proteins can act as a chloride channel [73]. Moreover, encapsulation of curcumin using poly(lactic-*co*-glycolic acid) (PLGA) nanoparticles enhances the activity of curcumin against the cystic fibrosis defect owing to a possible delivery of curcumin into the endoplasmic reticulum [71].

1.8.3 Alzheimer's Disease and Activities of Curcumin

A proposed cause of Alzheimer's disease is aggregation of amyloid β-peptides and accumulation of β-amyloid fibrils in the brain tissue [85]. The potential ability of curcumin to treat Alzheimer's disease has been studied both *in vitro* and *in vivo* [75–77]. Solutions of amyloid β-peptides and β-amyloid fibrils were prepared in the absence and presence of curcumin in order to study its effect on preventing aggregation of β-amyloid fibrils. The results show that curcumin binds to the end of β-amyloid fibril and/or amyloid β-peptide, and hence it inhibits further aggregation of β-amyloid fibrils [75, 76]. Yanagisawa et al. have revealed molecular insight into the binding of curcumin to amyloid β-peptides by discovering that the keto-enol and di-keto tautomerisation of curcumin is essential to inhibit amyloid β-peptide aggregation [86]. In an *in vivo* study, although the curcumin concentration in the mouse brain was as low as 1 µM, curcumin was still able to either reduce aggregation or promote the destabilisation of amyloid β-peptides and β-amyloid fibrils [76]. Furthermore, curcumin also reduces oxidative stress and inflammation of the brain due to Alzheimer's disease [74]. Overall, curcumin exhibits a considerable promise to promote neuroprotective treatment for Alzheimer's disease.

1.8.4 Anti-Cancer Activities of Curcumin

Cancer (malignant neoplasm) is classified as a disease in which a group of cells exhibits uncontrolled growth, destruct adjacent tissues, and spread to other body parts by either the lymph nodes, blood stream, or both [87]. A statistical report has estimated that 10.9 million new cancer cases were found and 6.7 million deaths were recorded worldwide in 2002 [88]. The most common and lethal cancers are lung, stomach and liver cancers [88]. The anticancer activities of curcumin have been widely investigated using different types of cells and animal models [1, 62, 68, 78–82]. The anti-proliferative effect of curcumin has been determined in previous studies, using different delivery agents including PLGA nanoparticles [89], β-cyclodextrins [90], glycerol manooleate based nanoparticles, copolymeric nanoparticles of Pluronic F-127 and polyvinyl alcohol [91], and *O*-carboxymethyl chitosan nanoparticles [92]. It is also known that curcumin induces cellular apoptosis [93–95]. Although the proposed mechanisms are complicated, there are two roles of curcumin in its anti-cancer activities. First, curcumin activates and/or inhibits some of the regulators and receptors involving cellular proliferation, migration and transcription [89–92]. These indirect activities of curcumin seem to explain its efficacy against multiple types of cancerous cells. Second, curcumin interacts and directly damages deoxyribonucleic acid (DNA), which leads to apoptosis [93–95]. The ability of curcumin to cause DNA damage often involves transition metals including copper and iron.

1.9 References

(1) Sa, G.; Das, T. Anti-Cancer Effects of Curcumin: Cycle of Life and Death. *Cell Division* **2008**, *3*, 1–14.

(2) Ammon, H. P. T.; Wahl, M. A. Pharmacology of Curcuma longa. *Planta Med.* **1991**, *57*, 1–7.

(3) Mishra, S.; Palanivelu, K. The Effect of Curcumin (Turmeric) on Alzheimer's Disease: An Overview. *Ann. Indian Acad. Neurol.* **2008**, *11*, 13–19.

(4) Roughley, P. J.; Whiting, D. A. Experiments in Biosynthesis of Curcumin. *J. Chem. Soc. Perkin. Trans. 1* **1973**, 2379–2388.

(5) Vogel, E.; Pellertier, S. *J. Pharm.* **1815**, *2*, 50–54.

(6) Kiuchi, F.; Goto, Y.; Sugimoto, N.; Akao, N.; Kondo, K.; Tsuda, Y. Nematocidal Activity of Turmeric - Synergistic Action of Curcuminoids. *Chem. Pharm. Bull.* **1993**, *41*, 1640–1643.

(7) Kita, T.; Imai, S.; Sawada, H.; Kumagai, H.; Seto, H. The Biosynthetic Pathway of Curcuminoid in Turmeric (Curcuma Longa) as Revealed by ^{13}C-Labeled Precursors. *Biosci. Biotechnol. Biochem.* **2008**, *72*, 1789–1798.

(8) Katsuyama, Y.; Kita, T.; Horinouchi, S. Identification and Characterization of Multiple Curcumin Synthases from the Herb Curcuma Longa. *FEBS Lett.* **2009**, *583*, 2799–2803.

(9) Payton, F.; Sandusky, P.; Alworth, W. L. NMR Study of the Solution Structure of Curcumin. *J. Nat. Prod.* **2007**, *70*, 143–146.

(10) Chignell, C. F.; Bilskj, P.; Reszka, K. J.; Motten, A. G.; Sik, R. H.; Dahl, T. A. Spectral and Photochemical Properties of Curcumin. *Photochem. Photobiol.* **1994**, *59*, 295–302.

(11) Wang, Z. F.; Leung, M. H. M.; Kee, T. W.; English, D. S. The Role of Charge in the Surfactant-Assisted Stabilization of the Natural Product Curcumin. *Langmuir* **2010**, *26*, 5520–5526.

(12) Adhikary, R.; Mukherjee, P.; Kee, T. W.; Petrich, J. W. Excited-State Intramolecular Hydrogen Atom Transfer and Solvation Dynamics of the Medicinal Pigment Curcumin. *J. Phys. Chem. B* **2009**, *113*, 5255–5261.

(13) Adhikary, R.; Carlson, P. J.; Kee, T. W.; Petrich, J. W. Excited-State Intramolecular Hydrogen Atom Transfer of Curcumin in Surfactant Micelles. *J. Phys. Chem. B* **2010**, *114*, 2997–3004.

(14) Nardo, L.; Andreoni, A.; Másson, M.; Haukvik, T.; Tønnesen, H. H. Studies on Curcumin and Curcuminoids. XXXIX. Photophysical Properties of Bisdemethoxycurcumin. *J. Fluorescence* **2011**, *21*, 627–635.

(15) Priyadarsini, K. I. Photophysics, Photochemistry and Photobiology of Curcumin: Studies from Organic Solutions, Bio-Mimetics and Living Cells. *J. Photoch. Photobio. C* **2009**, *10*, 81–95.

(16) Bernabe-Pineda, M.; Ramirez-Silva, M. T.; Romero-Romo, M.; Gonzadlez-Vergara, E.; Rojas-Hernandez, A. Determination of Acidity Constants of Curcumin in Aqueous Solution and Apparent Rate Constant of Its Decomposition. *Spectrochim. Acta A* **2004**, *60*, 1091–1097.

(17) Shen, L.; Ji, H.-F. Theoretical Study on Physicochemical Properties of Curcumin. *Spectrochim acta A* **2007**, *67*, 619–623.

(18) Leung, M. H. M.; Colangelo, H.; Kee, T. W. Encapsulation of Curcumin in Cationic Micelles Suppresses Alkaline Hydrolysis. *Langmuir* **2008**, *24*, 5672–5675.

(19) Kaminaga, Y.; Nagatsu, A.; Akiyama, T.; Sugimoto, N.; Yamazaki, T.; Maitani, T.; Mizukami, H. Production of Unnatural Glucosides of Curcumin with Drastically Enhanced Water Solubility by Cell Suspension Cultures of Catharanthus Roseus. *FEBS Lett.* **2003**, *555*, 311–316.

(20) Letchford, K.; Liggins, R.; Burt, H. Solubilization of Hydrophobic Drugs by Methoxy Poly(ethylene glycol)-block-polycaprolactone Diblock Copolymer Micelles: Theoretical and Experimental Data and Correlations. *J. Pharm. Sci.* **2008**, *97*, 1179–1190.

(21) Anand, P.; Kunnumakkara, A. B.; Newman, R. A.; Aggarwal, B. B. Bioavailability of Curcumin: Problems and Promises. *Mol. Pharmaceutics* **2007**, *4*, 807–818.

(22) Tønnesen, H. H.; Karlsen, J. Studies on Curcumin and Curcuminoids. 6. Kinetics of Curcumin Degradation in Aqueous Solution. *Z. Lebensm. Unters. Forsch.* **1985**, *180*, 402–404.

(23) Wang, Y. J.; Pan, M. H.; Cheng, A. L.; Lin, L. I.; Ho, Y. S.; Hsieh, C. Y.; Lin, J. K. Stability of Curcumin in Buffer Solutions and Characterization of Its Degradation Products. *J. Pharm. Biomed. Anal.* **1997**, *15*, 1867–1876.

(24) Wennerstrom, H.; Lindman, B. Micelles - Physical-Chemistry of Surfactant Association. *Phys. Rep.* **1979**, *52*, 1–86.

(25) Nagarajan, R.; Ruckenstein, E. Theory of Surfactant Self-Assembly - A Predictive Molecular Thermodynamic Approach. *Langmuir* **1991**, *7*, 2934–2969.

(26) Iwunze, M. O. Binding and Distribution Characteristics of Curcumin Solubilized in CTAB Micelle. *J. Mol. Liq.* **2004**, *111*, 161–165.

(27) Tønnesen, H. H. Solubility, Chemical and Photochemical Stability of Curcumin in Surfactant Solutions - Studies of Curcumin and Curcuminolds, XXVIII. *Pharmazie* **2002**, *57*, 820–824.

(28) Bangham, A. D. Physical Structure and Behavior of Lipids and Lipid Enzymes. *Adv. Lipid Res.* **1963**, *1*, 65–104.

(29) Alving, C. R. Liposomes as Carriers of Antigens and Adjuvants. *J. Immunol. Methods* **1991**, *140*, 1–13.

(30) Lian, T.; Ho, R. J. Y. Trends and Developments in Liposome Drug Delivery Systems. *J. Pharm. Sci.* **2001**, *90*, 667–680.

(31) Huwyler, J.; Wu, D. F.; Pardridge, W. M. Brain Drug Delivery of Small Mole-cules Using Immunoliposomes. *P. Natl. Acad. Sci. USA* **1996**, *93*, 14164–14169.

(32) Tønnesen, H. H.; Smistad, G.; Agren, T.; Karlsen, J. Studies on Curcumin and Curcuminoids. 23. Effects of Curcumin on Liposomal Lipid-Peroxidation. *Int. J. Pharm.* **1993**, *90*, 221–228.

(33) Chen, C.; Johnston, T. D.; Jeon, H.; Gedaly, R.; McHugh, P. R.; Burke, T. G.; Ranjan, D. An In Vitro Study of Liposomal Curcumin: Stability, Toxicity and Biological Activity in Human Lymphocytes and Epstein-Barr Virus-Transform-ed Human B-Cells. *Int. J. Pharm.* **2009**, *366*, 133–139.

(34) Barry, J.; Fritz, M.; Brender, J. R.; Smith, P. E. S.; Lee, D.-K.; Ramamoorthy, A. Determining the Effects of Lipophilic Drugs on Membrane Structure by Solid-State NMR Spectroscopy: The Case of the Antioxidant Curcumin. *J. Am. Chem. Soc.* **2009**, *131*, 4490–4498.

(35) Bisht, S.; Feldmann, G.; Soni, S.; Ravi, R.; Karikar, C.; Maitra, A.; Maitra, A. Polymeric Nanoparticle-Encapsulated Curcumin ("Nanocurcumin"): A Novel Strategy for Human Cancer Therapy. *J. Nanobiotechnology* **2007**, *5*, 18.

(36) Mohanty, C.; Acharya, S.; Mohanty, A. K.; Dilnawaz, F.; Sahoo, S. K. Curcumin-Encapsulated MePEG/PCL Diblock Copolymeric Micelles: A Novel Controlled Delivery Vehicle for Cancer Therapy. *Nanomedicine* **2010**, *5*, 433–449.

(37) Scott, M. J.; Jones, M. N. The Biodegradation of Surfactants in the Environment. *BBA Biomemb.* **2000**, *1508*, 235–251.

(38) Yam, J.; Booman, K. A.; Broddle, W.; Geiger, L.; Heinze, J. E.; Lin, Y. J.; McCarthy, K.; Reiss, S.; Sawin, V.; Sedlak, R. I.; Slesinski, R. S.; Wright, G. A. Surfactants: A Survey of Short-Term Genotoxicity Testing. *Food Chem. Toxicol.* **1984**, *22*, 761–769.

(39) Sahu, A.; Kasoju, N.; Bora, U. Fluorescence Study of the Curcumin-Casein Micelle Complexation and Its Application as a Drug Nanocarrier to Cancer Cells. *Biomacromolecules* **2008**, *9*, 2905–2912.

(40) Huppertz, T.; Fox, P. F.; Kelly, A. L. Properties of Casein Micelles in High Pressure-Treated Bovine Milk. *Food Chem.* **2004**, *87*, 103–110.

(41) Esmaili, M.; Ghaffari, S. M.; Moosavi-Movahedi, Z.; Atri, M. S.; Sharifizadeh, A.; Farhadi, M.; Yousefi, R.; Chobert, J. M.; Haertle, T.; Moosavi-Movahedi, A. A. Beta Casein-Micelle as a Nano Vehicle for Solubility Enhancement of Curcumin; Food Industry Application. *LWT–Food Sci. Technol.* **2011**, *44*, 2166–2172.

(42) Yazdi, S. R.; Corredig, M. Heating of Milk Alters the Binding of Curcumin to Casein Micelles, A Fluorescence Spectroscopy Study. *Food Chem.* **2012**, *132*, 1143–1149.

(43) Kragh-Hansen, U. Molecular Aspects of Ligand Binding to Serum Albumin. *Pharmacol. Rev.* **1981**, *33*, 17–53.

(44) Barik, A.; Priyadarsini, K. I.; Mohan, H. Photophysical Studies on Binding of Curcumin to Bovine Serum Albumin. *Photochem. Photobiol.* **2003**, *77*, 597–603.

(45) Naik, P. N.; Chimatadar, S. A.; Nandibewoor, S. T. Study on the Interaction between Antibacterial Drug and Bovine Serum Albumin: A Spectroscopic Approach. *Spectrochim. Acta A* **2009**, *73*, 841–845.

(46) Leung, M. H. M.; Kee, T. W. Effective Stabilization of Curcumin by Association to Plasma Proteins: Human Serum Albumin and Fibrinogen. *Langmuir* **2009**, *25*, 5773–5777.

(47) alpha cyclodexrin., Food and Drug Administration, `http://www.accessdata.fda.gov/scripts/fcn/fcnDetailNavigation.cfm?rpt=grasListing&id=155`.

(48) beta cyclodexrin., Food and Drug Administration, http://www.accessdata.fda.gov/scripts/fcn/fcnDetailNavigation.cfm?rpt=grasListing&id=74.

(49) gamma cyclodexrin., Food and Drug Administration, http://www.accessdata.fda.gov/scripts/fcn/fcnDetailNavigation.cfm?rpt=grasListing&id=46.

(50) Szejtli, J. Introduction and General Overview of Cyclodextrin Chemistry. *Chem. Rev.* **1998**, *98*, 1743–1753.

(51) Lincoln, S. F.; Pham, D.-T. *Supramol. Chem.* John Wiley & Sons, Ltd: 2012.

(52) Hoshino, M.; Imamura, M.; Ikehara, K.; Hama, Y. Fluorescence Enhancement of Benzene-Derivatives by Forming Inclusion Complexes With β-Cyclodextrin in Aqueous Solutions. *J. Phys. Chem.* **1981**, *85*, 1820–1823.

(53) Loftsson, T.; Duchene, D. Cyclodextrins and Their Pharmaceutical Applications. *Int. J. Pharm.* **2007**, *329*, 1–11.

(54) Loftsson, T.; Konradsdottir, F.; Másson, M. Influence of Aqueous Diffusion Layer on Passive Drug Diffusion from Aqueous Cyclodextrin Solutions through Biological Membranes. *Pharmazie* **2006**, *61*, 83–89.

(55) Rekharsky, M. V.; Inoue, Y. Complexation Thermodynamics of Cyclodextrins. *Chem. Rev.* **1998**, *98*, 1875–1917.

(56) Harada, T.; Pham, D.-T.; Leung, M. H. M.; Ngo, H. T.; Lincoln, S. F.; Easton, C. J.; Kee, T. W. Cooperative Binding and Stabilization of the Medicinal Pigment Curcumin by Diamide Linked γ-Cyclodextrin Dimers: A Spectroscopic Characterization. *J. Phys. Chem. B* **2011**, *115*, 1268–1274.

(57) Tønnesen, H. H.; Másson, M.; Loftsson, T. Studies of Curcumin and Curcuminoids. XXVII. Cyclodextrin Complexation: Solubility, Chemical and Photochemical Stability. *Int. J. Pharm.* **2002**, *244*, 127–135.

(58) Baglole, K. N.; Boland, P. G.; Wagner, B. D. Fluorescence Enhancement of Curcumin upon Inclusion into Parent and Modified Cyclodextrins. *J. Photochem. Photobiol. A* **2005**, *173*, 230–237.

(59) Singh, R.; Tønnesen, H. H.; Vogensen, S. B.; Loftsson, T.; Másson, M. Studies of Curcumin and Curcuminoids. XXXVI. The Stoichiometry and Complexation Constants of Cyclodextrin Complexes as Determined by the Phase-Solubility Method and UV-Vis Titration. *J. Incl. Phenom. Macro.* **2010**, *66*, 335–348.

(60) Pham, D. T.; Clements, P.; Easton, C. J.; Papageorgiou, J.; Maya, B. L.; Lincoln, S. F. Complexation of 6-(4'-(toluidinyl)naphthalene-2-sulfonate by β-Cyclodextrin and Linked β-Cyclodextrin Dimers. *New J. Chem.* **2008**, *32*, 712–718.

(61) Pham, D. T.; Ngo, H. T.; Lincoln, S. F.; May, B. L.; Easton, C. J. Synthesis of C6(A)-to-C6(A) and C3(A)-to-C3(A) Diamide Linked γ-Cyclodextrin Dimers. *Tetrahedron* **2010**, *66*, 2895–2898.

(62) Hatcher, H.; Planalp, R.; Cho, J.; Tortia, F. M.; Torti, S. V. Curcumin: From Ancient Medicine to Current Clinical Trials. *Cell. Mol. Life Sci.* **2008**, *65*, 1631–1652.

(63) Lantz, R. C.; Chen, G. J.; Solyom, A. M.; Jolad, S. D.; Timmermann, B. N. The Effect of Turmeric Extracts on Inflammatory Mediator Production. *Phytomedicine* **2005**, *12*, 445–452.

(64) Gopinath, D.; Ahmed, M. R.; Gomathi, K.; Chitra, K.; Sehgal, P. K.; Jayakumar, R. Dermal Wound Healing Processes with Curcumin Incorporated Collagen Films. *Biomaterials* **2004**, *25*, 1911–1917.

(65) Jagetia, G. C.; Rajanikant, G. K. Curcumin Treatment Enhances the Repair and Regeneration of Wounds in Mice Exposed to Hemibody γ-Irradiation. *Plast. Reconstr. Surg.* **2005**, *115*, 515–528.

(66) Jagetia, G. C.; Rajanikant, G. K. Acceleration of Wound Repair by Curcumin in the Excision Wound of Mice Exposed to Different Doses of Fractionated γ Radiation. *Int. Wound J.* **2012**, *9*, 76–92.

(67) Legeza, V.; Galenko-Yaroshevskii, V.; Zinov'ev, E.; Paramonov, B.; Kreichman, G.; Turkovskii, I.; Gumenyuk, E.; Karnovich, A.; Khripunov, A. Effects of New Wound Dressings on Healing of Thermal Burns of the Skin in Acute Radiation Disease. *Bull. Exp. Biol. Med.* **2004**, *138*, 311–315.

(68) Aggarwal, B. B.; Kumar, A.; Bharti, A. C. Anticancer Potential of Curcumin: Preclinical and Clinical Studies. *Anticancer Res.* **2003**, *23*, 363–398.

(69) Suresh, M. V.; Wagner, M. C.; Rosania, G. R.; Stringer, K. A.; Min, K. A.; Risler, L.; Shen, D. D.; Georges, G. E.; Reddy, A. T.; Parkkinen, J.; Reddy, R. C. Pulmonary Administration of Water-Soluble Curcumin Complex Reduces Severity of Acute Lung Injury. *Am. J. Respir. Cell Mol. Biol.* **2012**, *47*, 280–287.

(70) Park, J. H.; Kim, H. A.; Park, J. H.; Lee, M. Amphiphilic Peptide Carrier for the Combined Delivery of Curcumin and Plasmid DNA into the Lungs. *Biomaterials* **2012**, *33*, 6542–6550.

(71) Cartiera, M. S.; Ferreira, E. C.; Caputo, C.; Egan, M. E.; Caplan, M. J.; Saltzman, W. M. Partial Correction of Cystic Fibrosis Defects with PLGA Nanoparticles Encapsulating Curcumin. *Mol. Pharmaceutics* **2010**, *7*, 86–93.

(72) Egan, M. E.; Pearson, M.; Weiner, S. A.; Rajendran, V.; Rubin, D.; Glockner-Pagel, J.; Canny, S.; Du, K.; Lukacs, G. L.; Caplan, M. J. Curcumin, a Major Constituent of Turmeric, Corrects Cystic Fibrosis Defects. *Science* **2004**, *304*, 600–602.

(73) Zeitlin, P. Can Curcumin Cure Cystic Fibrosis? *N. Engl. J. Med.* **2004**, *351*, 606–608.

(74) Lim, G. P.; Chu, T.; Yang, F. S.; Beech, W.; Frautschy, S. A.; Cole, G. M. The Curry Spice Curcumin Reduces Oxidative Damage and Amyloid Pathology in an Alzheimer Transgenic Mouse. *J. Neurosci.* **2001**, *21*, 8370–8377.

(75) Ono, K.; Hasegawa, K.; Naiki, H.; Yamada, M. Curcumin Has Potent Anti-Amyloidogenic Effects for Alzheimer's β-Amyloid Fibrils In Vitro. *J. Neurosci. Res.* **2004**, *75*, 742–750.

(76) Yang, F. S.; Lim, G. P.; Begum, A. N.; Ubeda, O. J.; Simmons, M. R.; Ambegaokar, S. S.; Chen, P. P.; Kayed, R.; Glabe, C. G.; Frautschy, S. A.; Cole, G. M. Curcumin Inhibits Formation of Amyloid β Oligomers and Fibrils, Binds Plaques, and Reduces Amyloid In Vivo. *J. Biol. Chem.* **2005**, *280*, 5892–5901.

(77) Jiang, T.; Zhi, X.-L.; Zhang, Y.-H.; Pan, L.-F.; Zhou, P. Inhibitory Effect of Curcumin on the Al(III)-Induced Aβ_{42} Aggregation and Neurotoxicity In Vitro. *BBA-Mol. Basis Dis.* **2012**, *1822*, 1207–1215.

(78) Anand, P.; Sundaram, C.; Jhurani, S.; Kunnumakkara, A. B.; Aggarwal, B. B. Curcumin and Cancer: An "Old-Age" Disease with an "Age-Old" Solution. *Cancer Lett.* **2008**, *267*, 133–164.

(79) Huang, M. T.; Lou, Y. R.; Ma, W.; Newmark, H. L.; Reuhl, K. R.; Conney, A. H. Inhibitory Effects of Dietary Curcumin on Forestomach, Duodenal, and Colon Carcinogenesis in Mice. *Cancer Res.* **1994**, *54*, 5841–5847.

(80) Rao, C. V.; Rivenson, A.; Simi, B.; Reddy, B. S. Chemoprevention of Colon Carcinogenesis by Dietary Curcumin, A Naturally-Occurring Plant Phenolic Compound. *Cancer Res.* **1995**, *55*, 259–266.

(81) Sharma, R. A.; Gescher, A. J.; Steward, W. P. Curcumin: The Story So Far. *Eur. J. Cancer* **2005**, *41*, 1955–1968.

(82) Caruso, F.; Rossi, M.; Benson, A.; Opazo, C.; Freedman, D.; Monti, E.; Gariboldi, M. B.; Shaulky, J.; Marchetti, F.; Pettinari, R.; Pettinari, C. Ruthenium-Arene Complexes of Curcumin: X-Ray and Density Functional Theory Structure, Synthesis, and Spectroscopic Characterization, In Vitro Antitumor Activity, and DNA Docking Studies of (p-cymene)Ru(curcuminato)-chloro. *J. Med. Chem.* **2011**, *55*, 1072–1081.

(83) Lao, C. D.; Ruffin, M. T. t.; Normolle, D.; Heath, D. D.; Murray, S. I.; Bailey, J. M.; Boggs, M. E.; Crowell, J.; Rock, C. L.; Brenner, D. E. Dose Escalation of a Curcuminoid Formulation. *BMC Complem. Altern. M.* **2006**, *6*, 10.

(84) Martin, P. Wound Healing - Aiming for Perfect Skin Regeneration. *Science* **1997**, *276*, 75–81.

(85) Hardy, J.; Selkoe, D. J. Medicine - the Amyloid Hypothesis of Alzheimer's Disease: Progress and Problems on the Road to Therapeutics. *Science* **2002**, *297*, 353–356.

(86) Yanagisawa, D.; Shirai, N.; Amatsubo, T.; Taguchi, H.; Hirao, K.; Urushitani, M.; Morikawa, S.; Inubushi, T.; Kato, M.; Kato, F.; Morino, K.; Kimura, H.; Nakano, I.; Yoshida, C.; Okada, T.; Sano, M.; Wada, Y.; Wada, K.-n.; Yamamoto, A.; Tooyama, I. Relationship between the Tautomeric Structures of Curcumin Derivatives and their Aβ-Binding Activities in the Context of Therapies for Alzheimer's Disease. *Biomaterials* **2010**, *31*, 4179–4185.

(87) Diaz-Cano, S. J. General Morphological and Biological Features of Neoplasms: Integration of Molecular Findings. *Histopathology* **2008**, *53*, 1–19.

(88) Parkin, D. M.; Bray, F.; Ferlay, J.; Pisani, P. Global Cancer Statistics, 2002. *CA. Cancer J. Clin.* **2005**, *55*, 74–108.

(89) Yallapu, M. M.; Gupta, B. K.; Jaggi, M.; Chauhan, S. C. Fabrication of Curcumin Encapsulated PLGA Nanoparticles for Improved Therapeutic Effects in Metastatic Cancer Cells. *J. Colloid Interface Sci.* **2010**, *351*, 19–29.

(90) Yallapu, M. M.; Jaggi, M.; Chauhan, S. C. β-Cyclodextrin-Curcumin Self-Assembly Enhances Curcumin Delivery in Prostate Cancer Cells. *Colloids Surf., B.* **2010**, *79*, 113–125.

(91) Mohanty, C.; Sahoo, S. K. The In Vitro Stability and In Vivo Pharmacokinetics of Curcumin Prepared as an Aqueous Nanoparticulate Formulation. *Biomaterials* **2010**, *31*, 6597–6611.

(92) Anitha, A.; Maya, S.; Deepa, N.; Chennazhi, K. P.; Nair, S. V.; Tamura, H.; Jayakumar, R. Efficient Water Soluble *O*-Carboxymethyl Chitosan Nanocarrier for the Delivery of Curcumin to Cancer Cells. *Carbohydr. Polym.* **2011**, *83*, 452–461.

(93) Bush, J. A.; Cheung, K. J. J.; Li, G. Curcumin Induces Apoptosis in Human Melanoma Cells through a Fas Receptor/Caspase-8 Pathway Independent of p53. *Exp. Cell Res.* **2001**, *271*, 305–314.

(94) Jaiswal, A. S.; Marlow, B. P.; Gupta, N.; Narayan, S. B-Catenin-Mediated Transactivation and Cell - Cell Adhesion Pathways are Important in Curcumin (diferuylmethane)-Induced Growth Arrest and Apoptosis in Colon Cancer Cells. *Oncogene* **2002**, *21*, 8414–8427.

(95) Nagai, S.; Kurimoto, M.; Washiyama, K.; Hirashima, Y.; Kumanishi, T.; Endo, S. Inhibition of Cellular Proliferation and Induction of Apoptosis by Curcumin in Human Malignant Astrocytoma Cell Lines. *J. Neurooncol.* **2005**, *74*, 105–111.

Chapter 2

Diamide Linked γ-Cyclodextrin Dimers as Molecular-Scale Delivery Systems for the Medicinal Pigment Curcumin to Prostate Cancer Cells

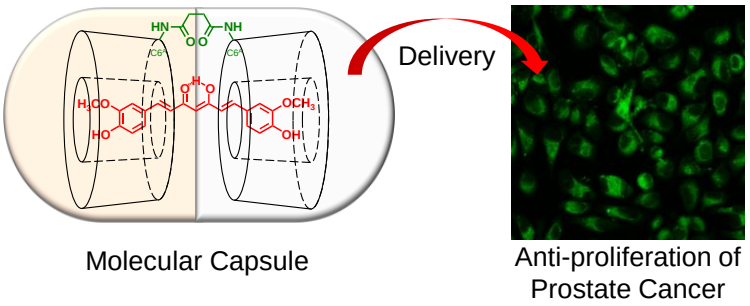

Statement of Authorship

By signing the Statement of Authorship, each author certifies that their stated contribution to the following publication is accurate and that permission in granted for the publication to be included in this thesis.

- Harada, T.; Giorgio, L.; Harris, T. J.; Pham, D.-T.; Ngo, H. T.; Need, E. F.; Coventry, B. J.; Lincoln, S. F.; Easton, C. J.; Buchanan, G.; Kee, T. W., Diamide Linked γ-Cyclodextrin Dimers as Molecular-scale Delivery Systems for the Medicinal Pigment Curcumin to Prostate Cancer Cells. *Mol. Pharmaceutics* **2013**, 10, 4481-4490 (Published in December 2013). Adapted with permission from this journal article. Copyright (2013) American Chemical Society.

Author Contributions

Name of First Author (Candidate)	Takaaki Harada
Contribution to the Paper	Sample preparations, data acquisition and analysis, and preparation and editing for manuscript
Signature	
Date	17/07/2014

Name of Co-Author	Lauren Giorgio
Contribution to the Paper	Data acquisition and analysis, and editing manuscript
Signature	
Date	22/08/2014

Name of Co-Author	Tiffany J. Harris
Contribution to the Paper	Data acquisition and analysis
Signature	
Date	21/08/2014

(Continued.)

Name of Co-Author	Duc-Truc Pham
Contribution to the Paper	Synthesis of samples
Signature	
Date	21/08/2014

Name of Co-Author	Huy Tien Ngo
Contribution to the Paper	Synthesis of samples
Signature	
Date	21/08/2014

Name of Co-Author	Eleanor F. Need
Contribution to the Paper	Supervision of the candidate, data analysis and editing manuscript
Signature	
Date	21/08/2014

Name of Co-Author	Brendon J. Coventry
Contribution to the Paper	Supervision of the candidate and editing manuscript
Signature	
Date	20/10/2014

Name of Co-Author	Stephen F. Lincoln
Contribution to the Paper	Supervision of the candidate and editing manuscript
Signature	
Date	02/10/2014

(Continued.)

Name of Co-Author	Christopher J. Easton
Contribution to the Paper	Supervision for sample synthesis
Signature	
Date	02/09/2014

Name of Co-Author	Grant Buchanan
Contribution to the Paper	Supervision of the candidate, data analysis, editing manuscript, and acted as corresponding author
Signature	
Date	21/08/2014

Name of Co-Author	Tak W. Kee
Contribution to the Paper	Supervision of the candidate, data analysis, editing manuscript, and acted as corresponding author
Signature	
Date	02/10/2014

2.1 Abstract

Diamide linked γ-cyclodextrin (γ-CD) dimers are proposed as molecular-scale delivery agents for the anticancer agent curcumin. *N,N'*-bis(6^A-deoxy-γ-cyclodextrin-6^A-yl)succinamide (66γCD$_2$su) and *N,N'*-bis(6^A-deoxy-γ-cyclodextrin-6^A-yl)urea (66-γCD$_2$ur) markedly suppress the degradation of curcumin by forming a strong 1 : 1 cooperative binding complexes. The results presented in this study describe the potential efficacy of 66γCD$_2$su and 66γCD$_2$ur for intracellular curcumin delivery to cancer cells. Cellular viability assays demonstrated a dose-dependent anti-proliferative effect of curcumin in human prostate cancer (PC-3) cells that was preserved by the curcumin-66γCD$_2$su complex. In contrast, delivery of curcumin by 66γCD$_2$ur significantly delayed the anti-proliferative effect. We observed similar patterns of gene regulation in PC-3 cells for curcumin complexed with either 66γCD$_2$su or 66γCD$_2$ur in comparison to curcumin alone, although curcumin delivered by either 66γCD$_2$su or 66γCD$_2$ur induces a slightly higher up-regulation of heme oxygenase-1. Highlighting their non-toxic nature, neither 66γCD$_2$su nor 66γCD$_2$ur carriers alone had any measurable effect on cell proliferation or candidate gene expression in PC-3 cells. Finally, confocal fluorescence imaging and uptake studies were used to demonstrate the intracellular delivery of curcumin by 66γCD$_2$su and 66γCD$_2$ur. Overall, these results demonstrate effective intracellular delivery and action of curcumin when complexed with 66γCD$_2$su and 66γCD$_2$ur, providing further evidence of their potential applications to deliver curcumin effectively in cancer and other treatment settings.

2.2 Introduction

Prostate cancer remains a worldwide health concern, with approximately 913 000 new cases diagnosed each year, or around 14 % of all male cancers [1]. The treatment options for men diagnosed with early stage prostate cancer include surgery and/or radiation and are often curative. For men diagnosed with cancer that has already spread beyond the prostate gland, however, treatment options are essentially palliative and often involve removal of the gland and/or surgical or chemical castration. While these treatments are initially effective, many patients eventually relapse, after which the only remaining treatments are chemotherapy or blockade of androgen metabolism, which have limited efficacy and significant side effects [2–4]. It is unsurprising, therefore, that there is considerable interest in developing adjuvant or alternative cancer agents to improve treatment response or prolong progression and/or quality of life or have fewer side effects. One potential agent in this regard is the naturally occurring compound curcumin, found in the Indian spice plant turmeric (*Curcuma longa*), which has previously been shown to possess chemo-preventive properties with low toxicity [5, 6].

Turmeric contains a group of yellow pigments, namely, curcuminoids, which are mainly comprised of curcumin ($\sim$ 77 %), demethoxycurcumin (17 %), and bisdemethoxycurcumin (3 %) [7]. In the past decade, curcumin has been investigated intensively and is shown to have anticancer [8–10], anti-inflammatory [10, 11], anti-Alzheimer's [12], anti-cystic fibrosis [13], and wound healing activities [9, 10]. In a phase I clinical study, Cheng et al. demonstrated that curcumin is non-toxic up to 8 g/day when orally administrated for three months, but at that dose it did not significantly affect a variety of either pre-malignant or high-risk lesions [5]. Poor bioavailability is likely to be a major contributor to the disparity between *in vitro* and *in vivo* effects of curcumin, which is poorly soluble in water ($\sim$ 11 µg/L) [14, 15], and prone to hydrolysis and fragmentation, resulting in significant degradation within 30 min [16–19]. These challenges must be overcome to increase the practical applicability of this compound. Previous studies have demonstrated effective stabilisation of curcumin using a range of potential delivery agents, including micelles [19–22], liposomes [23–25], polymers [26–28], and proteins [17, 29–32]. Each of these large-scale supramolecular assemblies may, however, limit intracellular delivery of curcumin, as they typically undergo significant structural perturbation upon contact with cellular membranes [33]. The development of molecular-scale delivery agents for curcumin and other agents is therefore of significant interest, because they have the potential to be more effective at delivering these agents to the intracellular milieu

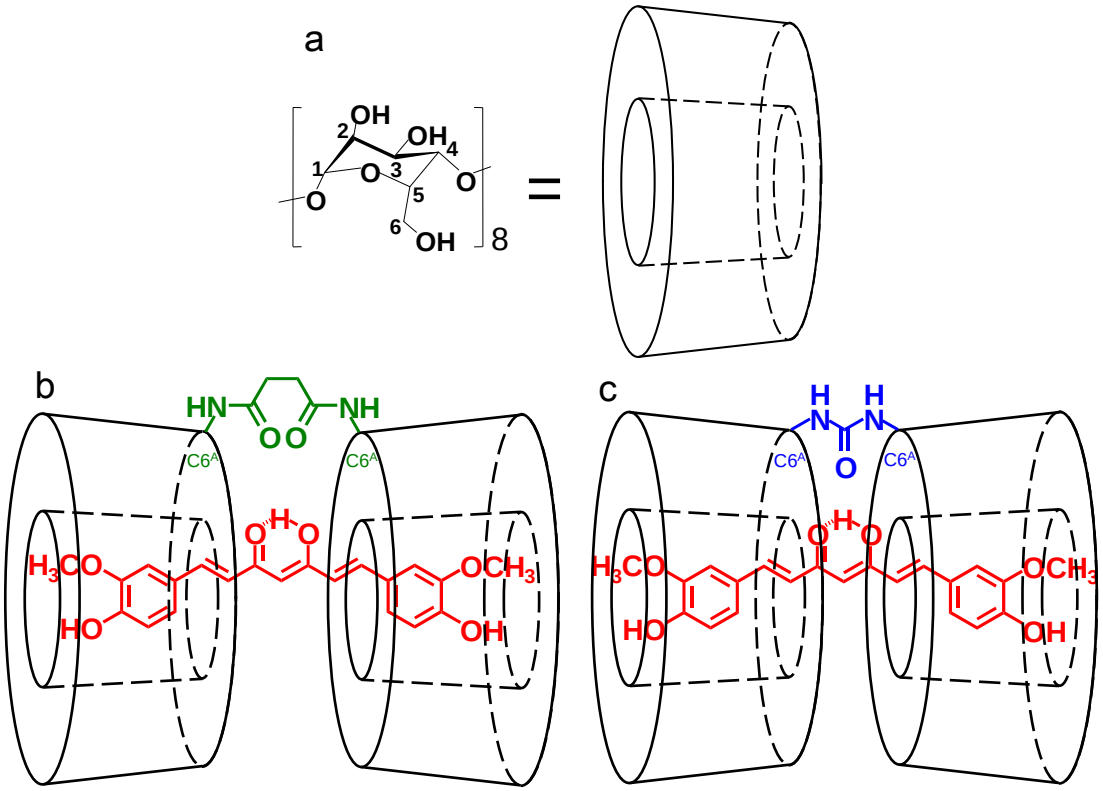

Figure 2.1. Structures of (a) γ-CD and curcumin complexed in (b) 66γCD_2su and (c) 66γCD_2ur.

while maintaining their structural integrity [33]. Our previous study has shown that diamide linked γ-cyclodextrin dimers possess many desirable properties for molecular encapsulation and delivery of curcumin, including a high structural stability and the ability to suppress degradation of curcumin under physiological conditions [16].

Cyclodextrins (CDs) are natural cyclic oligosaccharides that are FDA-approved [34–36] and are already utilised in the food and cosmetic industries [37]. γ-Cyclodextrin (γ-CD), which consists of eight glucopyranoside units in a toroidal structure, possesses a hydrophobic interior and hydrophilic exterior (Figure 2.1a). As such, γ-CD can act as a host to encapsulate and solubilise hydrophobic guest species in water through host-guest complexation [38, 39]. Recently, Pham et al. established the synthesis of γ-CD dimers linked with either succinamide or urea substituted onto the $C6^A$ site of a glucopyranose unit in each of the γ-CD, namely, *N,N'*-bis(6^A-deoxy-γ-cyclodextrin-6^A-yl)succinamide, 66γCD_2su, and *N,N'*-bis(6^A-deoxy-γ-cyclodextrin-6^A-yl)urea, 66γCD_2ur (Figures 2.1b and 2.1c) [40]. These diamide linked γ-CD dimers are excellent systems for drug delivery because (i) of their small size relative to other delivery agents mentioned above and (ii) the diamide linker can be hydrolysed

by intracellular enzymes to release the encapsulated species. The close proximity of the two γ-CDs in the dimers results in cooperative binding to the guest molecule. In the case of curcumin, the resulting molecular encapsulation by the diamide linked γ-CD dimers at the 1 : 1 molar ratio suppresses the rates of curcumin degradation substantially under physiological conditions [16]. Cooperative binding of the diamide linked γ-CD dimers to curcumin results in a high binding constant of $10^6\ M^{-1}$, which is indicative of an entrapment efficiency of nearly 100 % in water. In addition, a high concentration of curcumin of at least 1.3 mg/mL (3.3 mM) in aqueous solution can be achieved with either 66γCD$_2$su or 66γCD$_2$ur at a 1 : 1 molar ratio, which is more than 100 times higher than the aqueous solubility of curcumin ($\sim$ 11 µg/L) [14, 15]. Moreover, this high concentration of curcumin is unachievable with single γ-CDs, demonstrating the importance of cooperative binding by 66γCD$_2$su and 66γCD$_2$ur. Thus, they possess the potential to be effective and non-toxic delivery systems for curcumin.

Here, we report for the first time the intracellular delivery of curcumin using 66-γCD$_2$su and 66γCD$_2$ur and the biological consequences to human prostate cancer (PC-3) cells. Using cell viability assays, we observed a significant, dose-dependent decrease in cellular proliferation in response to encapsulated curcumin without any observable effect from the carrier 66γCD$_2$su or 66γCD$_2$ur alone. The intracellular delivery of curcumin to PC-3 cells by 66γCD$_2$su and 66γCD$_2$ur and the maintenance of biological activity of curcumin delivered by these carriers were verified by a variety of techniques, including confocal fluorescence imaging, uptake studies using fluorescence spectroscopy, and expression of several well-characterised curcumin target genes. Overall, the results indicate the potential of 66γCD$_2$su and 66γCD$_2$ur as effective and non-toxic delivery agents for curcumin in cancer treatment.

2.3 Experimental Section

2.3.1 Materials

Curcumin was obtained from LKT Laboratories (purity $> 98\,\%$). Methanol (AR grade, 99.5 %) from Merck Pty Ltd. was used as received. The phosphate buffer solution (50 mM) used in the stability study was prepared with deionised water from a Millipore Milli-Q NANO pure water system, and the pH was adjusted to 7.4. The human prostate cancer (PC-3) cell line was obtained from American Type Culture Collection (VA, USA). RPMI 1640 cell culture medium with and without phenol red were purchased from Invitrogen (Mulgrave, VIC, Australia). Dimethyl sulphoxide (DMSO, $\geq 99.7\,\%$, sterile filtered), fetal bovine serum (FBS), dextran-coated charcoal stripped fetal bovine serum (DCC-FBS), bovine serum albumin (BSA), and 0.1 % trypan blue diluted with PBS (endotoxin free) were purchased from Sigma-Aldrich (Castle Hill, NSW, Australia). RNA was extracted using the RNeasy mini kit (Qiagen, VIC, Australia) and cDNA generated using the iScript cDNA synthesis kit (Biorad, NSW, Australia). Cells were maintained in RPMI supplemented with 10 % FBS. For cell treatments, phenol red-free (PRF) RPMI was supplemented with 10 % DCC-FBS.

2.3.2 Synthesis of Diamide Linked γ-CD Dimers

The C6^A-to-C6^A diamide linked γ-CD dimers, *N,N'*-bis(6^A-deoxy-γ-cyclodextrin-6^A-yl)succinamide, 66γCD$_2$su, and *N,N'*-bis(6^A-deoxy-γ-cyclodextrin-6^A-yl)urea, 66-γCD$_2$ur, were synthesised using methods established by Pham et al. [40]. Briefly, the native *gamma*-CDs were substituted with 4-toluenesulfonylchloride for activation at the C6^A position, which yielded 6^A-*O*-(4-methylbenzenesulfonyl)-γ-cyclodextrin (6γCDTs). For the synthesis of 66γCD$_2$su, the reaction between 6γCDTs and ammonium bicarbonate produced 6^A-amino-6^A-deoxy-γ-cyclodextrin, 6γCDNH$_2$, which was then dimerised by the reaction with bis(4-nitrophenyl)succinate as the linker. For the synthesis of 66γCD$_2$ur, the reaction between 6γCDTs and sodium azide produced 6^A-azido-6^A-deoxy-γ-cyclodextrin, 6γCDN$_3$, which was then dimerised by the reaction with carbon dioxide as the linker.

2.3.3 Measurement of Cell Viability

A 50 mM solution of curcumin in DMSO and 8 mg/mL solutions of 66γCD$_2$su and 66γCD$_2$ur in PBS were used as stock solutions. PC-3 cells (5×10^3 cells/well

in 24-well plates) were plated in phenol red free RPMI 1640 (PRF RPMI 1640) media containing 10 % dextran-charcoal stripped fetal bovine serum (DCC-FBS) and allowed to attach for 24 h. Cells were washed with PBS once and treated in quadruplicates with curcumin (3.1–50.0 µM), 66γCD_2su (12.5 µM), 66γCD_2ur (12.5 µM), curcumin-66γCD_2su (12.5 µM), or curcumin-66γCD_2ur (12.5 µM) in PRF RPMI 1640 media containing 10 % DCC-FBS, and the plates were incubated for 1–5 days. Owing to curcumin's low solubility and stability in PBS, it was delivered to PC-3 cells using a small quantity of DMSO. As a consequence, each solution contained a total of 0.03 vol% DMSO as vehicle control to maintain consistency in each study. The negligible quantity of DMSO was expected to have an insignificant effect on cell viability. The curcumin stock solution was mixed with either the 66γCD_2su or 66γCD_2ur solution to facilitate the diamide linked γ-CD dimer-curcumin complexation before being added to the medium. Viable and dead cells were manually counted using a haemocytometer on the day of treatment (Day 0) and at Days 1–5 post-treatment by trypan blue exclusion as described previously [41, 42].

2.3.4 Curcumin Target Gene Expression in PC-3 Cells

PC-3 cells (2×10^5 cells/well in 6-well plates) were plated in PRF RPMI 1640 containing 5 % DCC-FBS and allowed to attach for 24 h. Cells were treated in triplicate for 12 h with curcumin (6.3–25.0 µM), 66γCD_2su (25.0 µM), 66γCD_2ur (25.0 µM), curcumin-66γCD_2su (6.3–25.0 µM), or curcumin-66γCD_2ur (6.3–25.0 µM) in PRF RPMI 1640 containing 5 % DCC-FBS. Each solution contained a total of 0.05 vol% DMSO as vehicle control for the reason stated above. For the studies involving a diamide linked γ-CD dimer, the control was either 25.0 µM 66γCD_2su or 66γCD_2ur, in addition to a total of 0.05 vol% DMSO without curcumin. RNA was extracted using the RNeasy mini kit and DNase treated using the RNase free DNase kit according to the manufacturer's instructions (Qiagen, VIC, Australia). RNA was reverse transcribed using the iScript cDNA synthesis kit according to the manufacturer's protocol (Biorad, VIC, Australia). Quantitative real time PCR (QPCR) was performed using iQ SYBR green supermix (Biorad) on a Biorad CFX96 real time PCR machine. Data are presented as the average of three biological replicates in technical duplicates, with gene expression normalised to the reference genes *GAPDH* and *RPL32*.

2.3.5 Qualitative and Quantitative Cellular Uptake of Curcumin

The qualitative cellular uptake studies involved imaging PC-3 cells with curcumin with a laser scanning confocal fluorescence microscope (Leica TCS SP5). The purpose of these studies is to confirm cellular uptake of curcumin. PC-3 cells (1.6×10^3 cells/well in 8-well chamber slides) in PRF RPMI 1640 containing 10 % DCC-FBS and allowed to attach for 24 h. Cells were washed once with PBS and treated with 12.5 µM curcumin, 66γCD$_2$su, 66γCD$_2$ur, curcumin-66γCD$_2$su, or curcumin-66γCD$_2$ur in PRF RPMI 1640 containing 10 % DCC-FBS, and incubated for 1–5 days. Each of these solutions contained a total of 0.08 vol% DMSO as vehicle control for the reason stated above. Prior to imaging, cells were washed with PBS twice (0.5 mL/well) so that only intracellular curcumin was detected. The excitation and emission wavelengths used were λ_{ex} = 405 nm and λ_{em} = 470–600 nm, respectively. The excitation source was a PicoQuant PDL 800-B pulse diode laser with a repetition rate of 4 MHz. The average excitation power used was 3 mW. The excitation light was focused onto the sample using a Leica HCX PL APO 63× N.A. 1.20 water-immersion objective with a 220 µm working distance. The emission was collected by the same objective, separated from the excitation source using a dichroic mirror and dispersed using a built-in spectrometer. Each image was acquired using line and frame averaging of 1 and 8, respectively. The images were 700 µm^2 × 700 µm^2, and each image acquisition time was approximately 3 s.

The first set of quantitative cellular uptake studies was performed using a FLUOstar OPTIMA microplate reader (λ_{ex} = 400 nm, λ_{em} = 520 nm). PC-3 cells (5×10^4 cells/well in 24-well plates) were plated in the same culture media and allowed to attach for 24 h. Cells were washed with PBS once and treated in sextuplicates with 12.5 µM curcumin, 66γCD$_2$su, 66γCD$_2$ur, curcumin-66γCD$_2$su, or curcumin-66γCD$_2$ur in PBS and incubated for the time periods. Cells were subsequently washed twice with PBS. At each incubation time point, 200 µL of chilled 100 % methanol was used to lyse the cells in the six replicate wells. Lysates were combined and transferred to a well of a 96-well plate on ice in order to reduce methanol evaporation. Curcumin fluorescence intensity relative to untreated cells was measured. Data were normalised to the saturation intensity of curcumin (Appendix A, Table A.1) and was obtained by fitting with first-order binding kinetics.

The second set of quantitative studies was aimed at investigating the role of BSA in cellular uptake of curcumin. A 4.0 mg/mL BSA solution was prepared in PBS, which corresponds to the concentration of BSA in PRF RPMI 1640 containing 10 % DCC-FBS used in our cell viability and confocal fluorescence imaging assays [43–

45]. Cells were incubated with either 0.0 mg/mL or 4.0 mg/mL BSA solution supplemented with 12.5 µM curcumin, curcumin-66γCD$_2$su, or curcumin-66γCD$_2$ur for 10 or 90 min, where fluorescence intensity was found to be within the error range of the half or full saturation value described above. The curcumin stock solution was mixed with either 66γCD$_2$su or 66γCD$_2$ur solution prior to dilution with the BSA solution. The curcumin fluorescence intensity of 200 µL of chilled 100 % methanol lysates was measured using the microplate reader described above with identical wavelength settings. Fluorescence intensities were normalised to the half or full saturation intensity of each sample in PBS without BSA after 10 min or 90 min incubation, respectively.

2.3.6 Statistical Analyses

All data, except for cellular viability assays, are presented as mean ± standard deviation for three independently performed experiments unless described. The data from cellular viability assays are presented as mean ± standard error of the mean (SEM) of viable or dead cells per well in quadruplicates. Statistical analyses were performed by two-way ANOVA for paired comparisons of means. Values of $p > 0.05$ were indicative of insignificant differences, whereas those of $p < 0.001$ were indicative of very significant differences.

2.4 Results

2.4.1 PC-3 Viability in the Presence of Curcumin and Encapsulated by Diamide Linked γ-CD Dimers

The anti-proliferative effects of curcumin on PC-3 cells were evaluated using trypan blue exclusion, as described previously [41, 42]. We observed a dose-dependent decrease in cell proliferation between 3.1 µM and 50.0 µM curcumin, with a 50 % maximal inhibitory response (IC50) observed at 12.5 µM over a 5 day period (Figure 2.2a). The duration of our studies is consistent with that of previous studies [46–51]. Curcumin treatment did not appear to lead to an increased incidence of dead cells determined by trypan blue exclusion over the course of the experiments (Figure A.2 in Appendix A). An IC50 concentration of 12.5 µM was determined and used for further investigation using 66γCD$_2$su and 66γCD$_2$ur as delivery agents.

The effect of curcumin encapsulated in either 66γCD$_2$su or 66γCD$_2$ur, namely curcumin-66γCD$_2$su and curcumin-66γCD$_2$ur, on PC-3 cells was investigated next over a 5 day period. Figure 2.2b shows the anti-proliferative effect of curcumin in the absence and presence of 66γCD$_2$su or 66γCD$_2$ur. Compared to vehicle, curcumin alone and curcumin-66γCD$_2$su were equally effective at inhibiting cell proliferation at all time points ($p > 0.05$). While curcumin-66γCD$_2$ur also inhibited cell proliferation effectively compared to vehicle at all time points ($p < 0.001$), it was only 73 % as effective as curcumin or curcumin-66γCD$_2$su after Day 3 ($p < 0.001$; Figure 2.2b), indicating a delayed response. Importantly, neither 66γCD$_2$su nor 66γCD$_2$ur alone affected PC-3 cell proliferation compared to vehicle control ($p > 0.05$; Figure 2.2c).

2.4.2 Curcumin-Induced Gene Expression in the PC-3 Cell Line

Heme oxygenase 1 gene (*HMOX1*) is an inducible stress response gene forming part of the nuclear factor like 2 (NRF2) pathway, a primary cellular defence against cytotoxic effects of oxidative stress. Curcumin-induced expression of *HMOX1* has been well-characterised in several cellular systems [52–54]. Here we used *HMOX1* regulation to infer and quantitate the intracellular delivery and biological activity of curcumin, curcumin-66γCD$_2$su, and curcumin-66γCD$_2$ur in PC-3 cells. At 12.5 µM, a clear up-regulation of *HMOX1* expression with curcumin alone was observed relative to vehicle control (58-fold, $p < 0.001$; Figure 2.3a). Similar up-regulation (53- or 70-fold) was observed with curcumin encapsulated in 66γCD$_2$su or 66γCD$_2$ur, respectively ($p < 0.001$). Furthermore, at 25.0 µM, both curcumin-66γCD$_2$su and

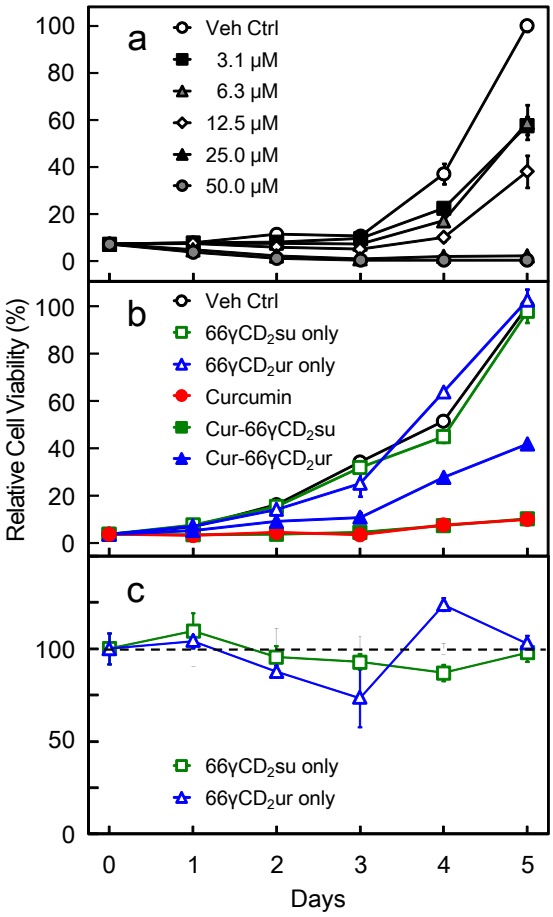

Figure 2.2. Cell viability assays performed using human prostate cancer PC-3 cells. (a) Viable PC-3 cells were treated with indicated concentrations of curcumin over 5 days, and viable cells were counted in the presence of trypan blue, demonstrating that curcumin exhibits dose-dependent anti-proliferative activity. (b) Viable PC-3 cells were counted using trypan blue assays after treatment with 12.5 μM curcumin, curcumin-66γCD_2su, or curcumin-66γCD_2ur over 5 days. (c) Viable PC-3 cells were counted using trypan blue assays and treated with 66γCD_2su or 66γCD_2ur with respect to vehicle control (shown as dashed line), indicating their non-toxic nature ($p > 0.05$).

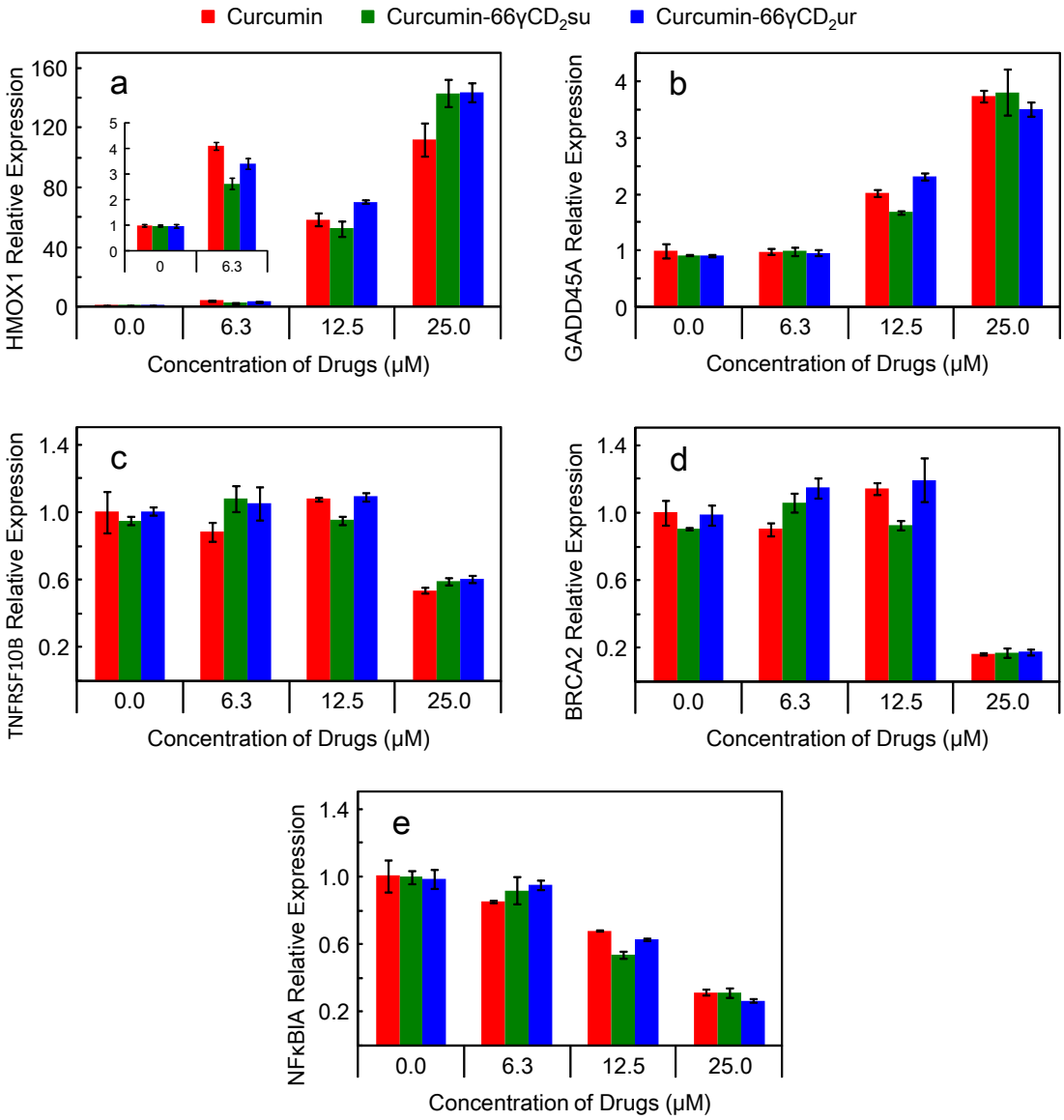

Figure 2.3. Relative expression of (a) *HMOX1*, (b) *GADD45A*, (c) *TNFRSF10B*, (d) *BRCA2*, and (e) *NFκBIA* in PC-3 cells treated with different concentrations of curcumin (red), curcumin-66γCD_2su (green), or curcumin-66γCD_2ur (blue). The gene expression was normalised to those of *GAPDH* and *RPL32*. The 0.0 µM represents vehicle control with 0.05 vol% DMSO (red), 25.0 µM 66γCD_2su (green), and 25.0 µM 66γCD_2ur (blue).

curcumin-66γCD$_2$ur had a significantly greater effect on *HMOX1* up-regulation (140-fold) than curcumin alone (112-fold, $p < 0.001$). *HMOX1* expression did not increase above baseline levels in PC-3 cells treated with either 66γCD$_2$su or 66γCD$_2$ur alone (*i.e.*, 0 µM curcumin; Figure 2.3a and inset), consistent with the results in Figure 2.2. To support this finding further, we investigated four other curcumin target genes [55–62], one of which was up-regulated (*GADD45A*) and three down regulated (*TNFRSF10B*, *BRCA2*, and *NFκBIA*) in response to curcumin treatment. The diamide linked γ-CD dimer encapsulated forms of curcumin were equally as effective as curcumin alone in increasing or decreasing expression of these candidate genes (Figures 2.3b−2.3e), and again 66γCD$_2$su or 66γCD$_2$ur alone did not affect gene expression (Figures 2.3b−2.3e). Together, these results demonstrate that encapsulation with 66γCD$_2$su or 66γCD$_2$ur permits intracellular delivery and biological activity of curcumin.

2.4.3 Qualitative and Quantitative Cellular Uptake Studies of Curcumin

Next, we assessed the amount of curcumin delivered to PC-3 cells qualitatively using confocal fluorescence microscopy. Figure 2.4 shows fluorescence images of PC-3 cells treated with 12.5 µM curcumin, curcumin-66γCD$_2$su or curcumin-66γCD$_2$ur for 1 and 4 days. The fluorescence intensity at 1 day of each treatment was substantially greater than the detection limit (Figure 2.4, upper panels), while the intrinsic fluorescence of untreated cells was negligible (Figures A.3−A.5, panel a, in Appendix A). Irrespective of 66γCD$_2$su or 66γCD$_2$ur encapsulation, curcumin fluorescence was still detectable within cells after single dose treatment at Day 4, with an intensity roughly half of that observed at Day 1, with slightly lower intensities for both treatments with encapsulated curcumin (Figure 2.4, lower panels).

Although fluorescence imaging revealed the intracellular presence of curcumin, the influence of serum proteins on curcumin delivery, specifically the effect of the most abundant protein in FBS, BSA, was not revealed. Therefore, the uptake of curcumin by PC-3 cells 10 and 90 min after treatment was measured using a fluorescent plate reader. The treatments involved using solutions of 12.5 µM curcumin, curcumin-66γCD$_2$su, or curcumin-66γCD$_2$ur in PBS alone or PBS spiked with 4.0 mg/mL BSA, which is the approximate concentration found in 10 % DCC-FBS/PRF RPMI 1640 and 5 times higher than the 12.5 µM diamide linked γ-CD dimers used in our experiments [43–45]. The relative fluorescence intensity of each curcumin solution in the presence of BSA at 10 or 90 min was normalised to that in the ab-

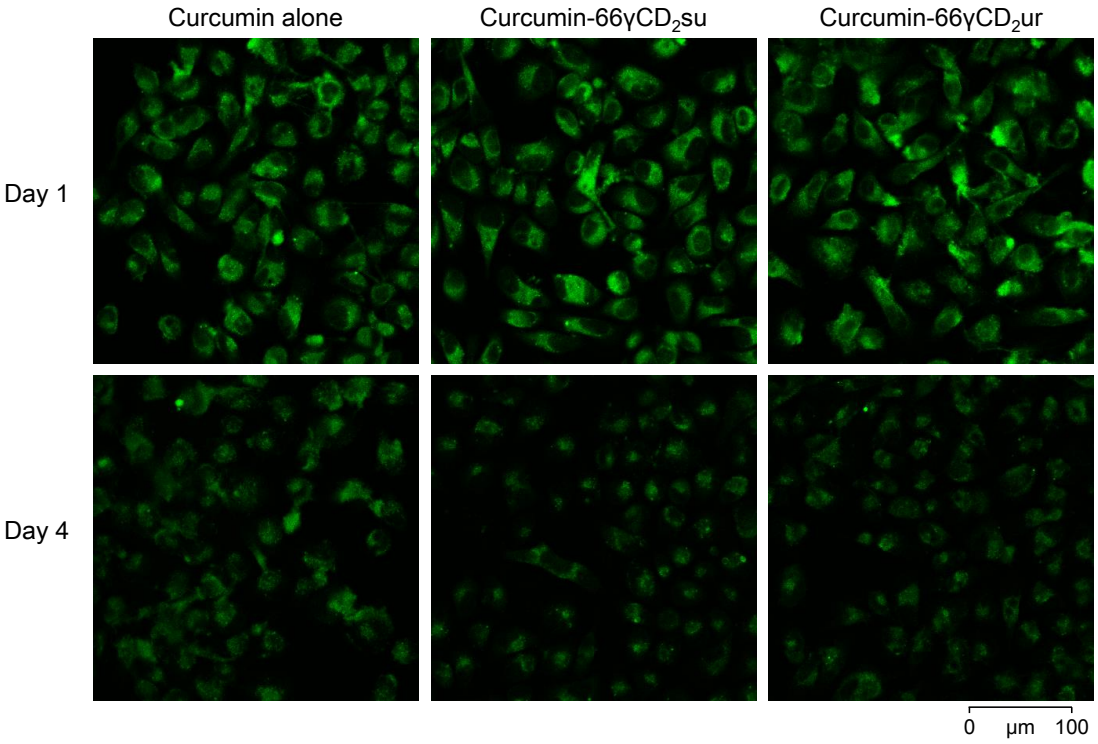

Figure 2.4. Confocal fluorescence images of PC-3 cells treated with 12.5 µM curcumin, curcumin-66γCD$_2$su, and curcumin-66γCD$_2$ur 1 day (top) and 4 days (bottom) after single dose treatment.

sence of BSA (Figure 2.5). Importantly, the relative fluorescence intensity in cells treated with unencapsulated curcumin was 72 % lower when BSA was present in the solution ($p < 0.001$). However, BSA had a minor effect on the relative fluorescence intensity in cells treated with either curcumin-66γCD$_2$su or curcumin-66γCD$_2$-ur (*n.s.*, $p > 0.05$), as shown in Figure 2.5. In addition, the fluorescence intensity of cells treated with curcumin alone in the presence of BSA resulted in a similar level to that of curcumin delivered by either 66γCD$_2$su or 66γCD$_2$ur (Figure A.6 in Appendix A). Furthermore, the treatments were also applied to PC-3 cells in serum-free PBS to determine the amount of curcumin in cells within the time scale that cellular proliferation was negligible. Consistent with first-order binding kinetics, the fluorescent intensity following treatment with curcumin alone reached 50 % of the maximum value within the first 10 min and saturated around 90 min, increasing at a rate constant of $0.050 \pm 0.012\,\mathrm{min}^{-1}$ (Figure A.7 in Appendix A). The maximum fluorescence remained constant over an extended period of time (60–180 min; Figure A.8 in Appendix A). In the presence of either 66γCD$_2$su or 66γCD$_2$ur (Figure A.7 in Appendix A), the curcumin fluorescence intensity increased at a rate constant of

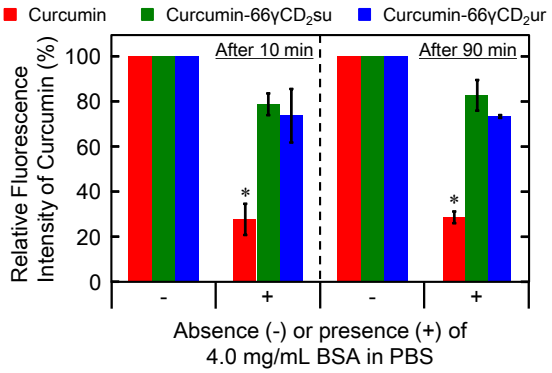

Figure 2.5. Effects of BSA on cellular uptake of curcumin in the absence (−) and presence (+) of either 66γCD$_2$su or 66γCD$_2$ur. PC-3 cells were treated with 12.5 µM of each solution prepared with either PBS alone or PBS spiked with 4.0 mg/mL BSA, for 10 (left) and 90 min (right). The asterisks in the figure represent a statistically significant decrease in fluorescence intensity of curcumin due to the presence of BSA ($p < 0.001$).

$0.076 \pm 0.031\,\text{min}^{-1}$ and $0.029 \pm 0.018\,\text{min}^{-1}$, respectively. The maximum fluorescence intensity of curcumin delivered by either 66γCD$_2$su or 66γCD$_2$ur is $5-9$ times lower than that of curcumin alone.

2.5 Discussion

Curcumin has been shown to have significant medicinal effects including anti-cancer and anti-inflammatory activities [8–11]. However, the poor solubility and stability of curcumin that limit the *in vivo* availability are major problems for the development of curcumin as a therapeutic agent. The association of curcumin with a delivery agent is an approach to address these issues. Our previous study showed effective and significant aqueous stabilisation of curcumin using diamide linked γ-CD dimers, 66γCD$_2$su and 66γCD$_2$ur [16]. Here, we propose the use of 66γCD$_2$su and 66γCD$_2$ur as novel delivery systems for curcumin without perturbing its medicinal efficacy.

We demonstrated that curcumin inhibits the proliferation of PC-3 cells in a dose-dependent manner, which is consistent with previous studies [63, 64]. Importantly, our results reveal that the use of the delivery agents 66γCD$_2$su and 66γCD$_2$ur does not prevent the anti-proliferative effect of curcumin, indicating effective intracellular delivery and biological activity of curcumin. In addition, we demonstrated that 66γ-CD$_2$su and 66γCD$_2$ur alone do not affect cellular proliferation or death, supporting a general non-toxic nature of these delivery agents. This observation is consistent with single γ-CDs being non-toxic [34] and the diamide linker of 66γCD$_2$su and 66γ-CD$_2$ur being hydrolysed enzymatically in the cellular environment [65–68]. It is also important to stress that delivery of curcumin using 66γCD$_2$su and 66γCD$_2$ur here was achieved at a 1 : 1 molar ratio, whereas delivery systems with a much higher cyclodextrin-to-curcumin molar ratios have been reported in previous studies [69–71]. Curcumin delivery using 66γCD$_2$su and 66γCD$_2$ur is therefore more effective and efficient than other cyclodextrin-based delivery systems, and a higher concentration of encapsulated curcumin can be achieved.

Intracellular delivery of curcumin and the negligible effect of 66γCD$_2$su and 66-γCD$_2$ur were observed on the expression of curcumin target genes. The increase or decrease in gene regulation was evident from curcumin treatment and exhibited a strong dependence on the dose of curcumin, which has been shown previously [54]. Our results showed that the gene expression of PC-3 cells treated with 66γCD$_2$su-curcumin or 66γCD$_2$ur-curcumin is also dose-dependent and comparable to curcumin alone, indicating that these delivery agents do not prevent the intracellular efficacy or uptake of curcumin. In addition, we demonstrated that neither 66γCD$_2$su nor 66γ-CD$_2$ur alone has any effect on these curcumin responsive target genes, which further supports their non-toxic nature up to 25.0 μM, consistent with our viability assay results.

Fluorescence imaging and spectroscopic studies provide further, direct evidence of curcumin-cell interaction owing to the sensitivity of the fluorescence properties of curcumin to the polarity of the surrounding environment [22, 72, 73]. For instance, the fluorescence quantum yields of curcumin in BSA and sodium dodecyl sulphate (SDS) micelles, which have hydrophobic characteristics similar to cell membranes, are approximately 2–5 %, while that in a pH 7.4 phosphate buffer solution is negligible [16, 22, 30]. In addition, our previous study showed that curcumin is essentially non-fluorescent in the presence of either 66γCD$_2$su or 66γCD$_2$ur in buffer solution [16]. Our observation of intracellular fluorescence here therefore indicates that curcumin is present in hydrophobic regions, for example, membranes, within the intracellular space. The results can be used to directly assess the delivery of curcumin to PC-3 cells.

Confocal fluorescence images demonstrate a minor difference between the fluorescence intensity of curcumin alone and curcumin delivered by either 66γCD$_2$su or 66γCD$_2$ur, similar to our cellular viability and gene expression results. Together, all of these data indicate efficient intracellular delivery of curcumin by 66γCD$_2$su and 66γCD$_2$ur. Another interesting observation in the confocal fluorescence images is a lower fluorescence level in the nucleus, implying that curcumin is present at a higher concentration in the cytoplasm than the nucleus. This result was also observed in a previous study [74]. Moreover, the slightly lower fluorescence intensity of curcumin delivered by 66γCD$_2$su and 66γCD$_2$ur than curcumin alone at Day 4 is unlikely to arise from lower curcumin levels. This is because nearly identical anti-proliferative effects of curcumin alone and curcumin delivered by 66γCD$_2$su were observed, as shown in Figure 2.2b. It is likely that similar levels of curcumin were present in all cases.

We also considered the role of serum proteins in the cellular uptake of curcumin. It is possible that a significant proportion of curcumin in either 66γCD$_2$su or 66γCD$_2$-ur are bound to serum proteins as the concentration of BSA was substantially higher than that of either 66γCD$_2$su or 66γCD$_2$ur in the medium. Previous studies showed that curcumin (in the absence of 66γCD$_2$su and 66γCD$_2$ur) is captured and stabilised by serum proteins and model membranes [16, 17, 22, 29, 30, 75]. The stabilisation of curcumin by these systems may result in a similar level of anti-proliferative effect and fluorescence intensity of curcumin in the absence of 66γCD$_2$su and 66γCD$_2$ur. To further understand curcumin delivery to PC-3 cells, we performed quantitative curcumin uptake studies.

Our results in Figure 2.5 show that a significant fraction of curcumin binds to BSA in the absence of either 66γCD$_2$su or 66γCD$_2$ur. Previous studies determined that the

binding constants of curcumin to serum proteins are approximately $10^5\,M^{-1}$ [17, 29, 30]. Therefore, the binding of curcumin to the hydrophobic pockets of BSA may be sufficiently strong to prevent curcumin from making contact with cell membranes and thereby inhibit transfer of curcumin by diffusion. In contrast, the intracellular delivery of 66γCD$_2$su- or 66γCD$_2$ur-complexed curcumin appears to be BSA-independent as there is only an insignificant decrease in curcumin uptake between the results with the absence and presence of BSA. This phenomenon is attributable to high binding constants of curcumin to either 66γCD$_2$su or 66γCD$_2$ur, of which are on the order of $10^6\,M^{-1}$ [16]. Here, we propose that curcumin is directly delivered into PC-3 cells by either 66γCD$_2$su or 66γCD$_2$ur as follows. Curcumin may exist in the annuli of either 66γCD$_2$su or 66γCD$_2$ur or be transferred to the hydrophobic pocket of BSA, and/or bind to cell membranes, by diffusion. Our uptake results with and without BSA indicate that a high portion of curcumin remains in the annuli of 66γCD$_2$su and 66γCD$_2$ur rather than being transferred to BSA, in spite of a roughly five times higher BSA concentration. In addition, previous studies suggest a lack of interaction between either β-CD or diamide linked γ-CD dimers and the cell membrane based on SDS model membrane experiments [16, 75]. Hence, the results here strongly suggest that 66γCD$_2$su and 66γCD$_2$ur deliver curcumin directly to the cell membrane, independent of the presence of BSA. Moreover, the fluorescence signal of curcumin alone in the presence of BSA is significantly weaker than that in its presence (Figure A.6 in Appendix A), indicating that BSA reduces curcumin availability. However, the presence of BSA has a negligible effect on the fluorescence signals of curcumin in either 66γCD$_2$su or 66γCD$_2$ur (Figure A.6 in Appendix A), supporting the high entrapment efficiency of the γ-CD dimers.

Our cellular uptake results in the serum-free environment further shows that curcumin and curcumin delivered by 66γCD$_2$su and 66γCD$_2$ur possess similar rate constants for uptake by PC-3 cells, indicating that similar cell membrane diffusion processes are involved for free curcumin and curcumin delivered using either 66γCD$_2$su or 66γCD$_2$ur. In the absence of the diamide linked γ-CD dimers, curcumin is able to partition into the cell membrane by diffusion [16], which results in the maximum amount of curcumin in the cell. In contrast, in the presence of either 66γCD$_2$su or 66γCD$_2$ur, curcumin partitions largely into the diamide linked γ-CD dimers [16], leading to an overall lower level of fluorescence because curcumin in the latter environment is essentially non-fluorescent [16]. However, observable fluorescence signal in addition to similar uptake rate constants illustrates that a moderate level of curcumin is released from 66γCD$_2$su or 66γCD$_2$ur by diffusion.

The advantage of the BSA-independent delivery of curcumin by 66γCD$_2$su and

66γCD$_2$ur is the control of the effective dose of curcumin in cancer treatment. The direct delivery of curcumin to cells raises the possibility of protecting the highly labile curcumin against serum proteins and potentially lipoproteins in the circulatory system for an extended period of time by encapsulation. Furthermore, curcumin forms a more stable complex with 66γCD$_2$su and 66γCD$_2$ur than with BSA [17], and our uptake results suggest a possible gradual increase in intracellular curcumin due to sustained delivery from either 66γCD$_2$su or 66γCD$_2$ur even in the presence of BSA. This phenomenon is consistent with the delayed and reduced effects observed in our cell viability and fluorescence images. Therefore, our delivery agents, 66γCD$_2$su and 66γCD$_2$ur, potentially offer a prolonged delivery of curcumin in cancer therapy, and may therefore protect against rapid hepatic or renal clearance. Finally, while this study is concerned with the delivery of curcumin by 66γCD$_2$su and 66γCD$_2$ur *in vitro*, these agents may also be efficacious to deliver other therapeutic agents in other experimental systems.

A combination of either 66γCD$_2$su or 66γCD$_2$ur with curcumin will be investigated in our future *in vivo* studies to investigate their toxicity and pharmacological profiles, with an ultimate goal of developing curcumin-66γCD$_2$su and curcumin-66-γCD$_2$ur as naturally derived chemotherapeutic drugs or their supplements.

2.6 Conclusions

We report here for the first time the direct intracellular delivery of curcumin using diamide linked γ-CD dimers, 66γCD$_2$su and 66γCD$_2$ur. These delivery agents offer molecular-scale encapsulation of curcumin at concentrations ranging from micromolar to millimolar and a high structural integrity under physiological conditions. While encapsulation of curcumin using either 66γCD$_2$su or 66γCD$_2$ur strongly suppresses it degradation, cellular viability and uptake assays combined with gene expression and fluorescence microscopy reveal that 66γCD$_2$su and 66γCD$_2$ur alone do not produce measurable toxicity on viability or gene expression. The 66γCD$_2$su and 66γCD$_2$ur are both effective means to deliver curcumin into cells, resulting in inhibition of cellular proliferation, while initiating changes in gene expression similar to that exhibited by curcumin alone. Furthermore, the formation of 66γCD$_2$su and 66γCD$_2$ur with curcumin appears to protect curcumin from binding to BSA, which may result in a more efficient intracellular delivery via cell membranes. Together, our results demonstrate the promise of these novel non-toxic molecular-scale agents to deliver curcumin and other highly labile compounds to mammalian cells effectively and therefore may present a more effective means of delivering these agents *in vivo*.

2.7 References

(1) Ferlay, J.; Shin, H.-R.; Bray, F.; Forman, D.; Mathers, C.; Parkin, D. M. Estimates of Worldwide Burden of Cancer in 2008: GLOBOCAN 2008. *Int. J. Cancer* **2010**, *127*, 2893–2917.

(2) Petrylak, D. P.; Tangen, C. M.; Hussain, M. H. A.; Lara, P. J.; Jones, J. A.; Taplin, M. E.; Burch, P. A.; Berry, D.; Moinpour, C.; Kohli, M.; Benson, M. C.; Small, E. J.; Raghavan, D.; Crawford, E. D. Docetaxel and Estramustine Compared with Mitoxantrone and Prednisone for Advanced Refractory Prostate Cancer. *N. Engl. J. Med.* **2004**, *351*, 1513–1520.

(3) Jamieson, E. R.; Lippard, S. J. Structure, Recognition, and Processing of Cisplatin-DNA Adducts. *Chem. Rev.* **1999**, *99*, 2467–2498.

(4) Jung, Y. W.; Lippard, S. J. Direct Cellular Responses to Platinum-Induced DNA Damage. *Chem. Rev.* **2007**, *107*, 1387–1407.

(5) Cheng, A. L.; Hsu, C. H.; Lin, J. K.; Hsu, M. M.; Ho, Y. F.; Shen, T. S.; Ko, J. Y.; Lin, J. T.; Lin, B. R.; Wu, M. S.; Yu, H. S.; Jee, S. H.; Chen, G. S.; Chen, T. M.; Chen, C. A.; Lai, M. K.; Pu, Y. S.; Pan, M. H.; Wang, Y. J.; Tsai, C. C.; Hsieh, C. Y. Phase I Clinical Trial of Curcumin, a Chemopreventive Agent, in Patients with High-Risk or Pre-Malignant Lesions. *Anticancer Res.* **2001**, *21*, 2895–2900.

(6) Aggarwal, B. B.; Kumar, A.; Bharti, A. C. Anticancer Potential of Curcumin: Preclinical and Clinical Studies. *Anticancer Res.* **2003**, *23*, 363–398.

(7) Goel, A.; Kunnumakkara, A. B.; Aggarwal, B. B. Curcumin as "Curecumin": From Kitchen to Clinic. *Biochem. Pharmacol.* **2008**, *75*, 787–809.

(8) Kuttan, R.; Bhanumathy, P.; Nirmala, K.; George, M. C. Potential Anticancer Activity of Turmeric (Curcuma-Longa). *Cancer Lett.* **1985**, *29*, 197–202.

(9) Anand, P.; Sundaram, C.; Jhurani, S.; Kunnumakkara, A. B.; Aggarwal, B. B. Curcumin and Cancer: An "Old-Age" Disease with an "Age-Old" Solution. *Cancer Lett.* **2008**, *267*, 133–164.

(10) Maheshwari, R. K.; Singh, A. K.; Gaddipati, J.; Srimal, R. C. Multiple Biological Activities of Curcumin: A Short Review. *Life Sci.* **2006**, *78*, 2081–2087.

(11) Srimal, R. C.; Dhawan, B. N. Pharmacology of Diferuloyl Methane (Curcumin), A Nonsteroidal Antiinflammatory Agent. *J. Pharm. Pharmacol.* **1973**, *25*, 447–452.

(12) Cole, G. M.; Lim, G. P.; Yang, F.; Teter, B.; Begum, A.; Ma, Q.; Harris-White, M. E.; Frautschy, S. A. Prevention of Alzheimer's Disease: Omega-3 Fatty Acid and Phenolic Anti-Oxidant Interventions. *Neurobiol. Aging* **2005**, *26*, 133–136.

(13) Egan, M. E.; Pearson, M.; Weiner, S. A.; Rajendran, V.; Rubin, D.; Glockner-Pagel, J.; Canny, S.; Du, K.; Lukacs, G. L.; Caplan, M. J. Curcumin, a Major Constituent of Turmeric, Corrects Cystic Fibrosis Defects. *Science* **2004**, *304*, 600–602.

(14) Letchford, K.; Liggins, R.; Burt, H. Solubilization of Hydrophobic Drugs by Methoxy Poly(ethylene glycol)-block-polycaprolactone Diblock Copolymer Micelles: Theoretical and Experimental Data and Correlations. *J. Pharm. Sci.* **2008**, *97*, 1179–1190.

(15) Kaminaga, Y.; Nagatsu, A.; Akiyama, T.; Sugimoto, N.; Yamazaki, T.; Maitani, T.; Mizukami, H. Production of Unnatural Glucosides of Curcumin with Drastically Enhanced Water Solubility by Cell Suspension Cultures of Catharanthus Roseus. *FEBS Lett.* **2003**, *555*, 311–316.

(16) Harada, T.; Pham, D.-T.; Leung, M. H. M.; Ngo, H. T.; Lincoln, S. F.; Easton, C. J.; Kee, T. W. Cooperative Binding and Stabilization of the Medicinal Pigment Curcumin by Diamide Linked γ-Cyclodextrin Dimers: A Spectroscopic Characterization. *J. Phys. Chem. B* **2011**, *115*, 1268–1274.

(17) Leung, M. H. M.; Kee, T. W. Effective Stabilization of Curcumin by Association to Plasma Proteins: Human Serum Albumin and Fibrinogen. *Langmuir* **2009**, *25*, 5773–5777.

(18) Wang, Y. J.; Pan, M. H.; Cheng, A. L.; Lin, L. I.; Ho, Y. S.; Hsieh, C. Y.; Lin, J. K. Stability of Curcumin in Buffer Solutions and Characterization of Its Degradation Products. *J. Pharm. Biomed. Anal.* **1997**, *15*, 1867–1876.

(19) Leung, M. H. M.; Colangelo, H.; Kee, T. W. Encapsulation of Curcumin in Cationic Micelles Suppresses Alkaline Hydrolysis. *Langmuir* **2008**, *24*, 5672–5675.

(20) Mohanty, C.; Acharya, S.; Mohanty, A. K.; Dilnawaz, F.; Sahoo, S. K. Curcumin-Encapsulated MePEG/PCL Diblock Copolymeric Micelles: A Novel Controlled Delivery Vehicle for Cancer Therapy. *Nanomedicine* **2010**, *5*, 433–449.

(21) Tang, H. D.; Murphy, C. J.; Zhang, B.; Shen, Y. Q.; Sui, M. H.; Van Kirk, E. A.; Feng, X. W.; Murdoch, W. J. Amphiphilic Curcumin Conjugate-Forming Nanoparticles as Anticancer Prodrug and Drug Carriers: In Vitro and In Vivo Effects. *Nanomedicine* **2010**, *5*, 855–865.

(22) Wang, Z. F.; Leung, M. H. M.; Kee, T. W.; English, D. S. The Role of Charge in the Surfactant-Assisted Stabilization of the Natural Product Curcumin. *Langmuir* **2010**, *26*, 5520–5526.

(23) Takahashi, M.; Uechi, S.; Takara, K.; Asikin, Y.; Wada, K. Evaluation of an Oral Carrier System in Rats: Bioavailability and Antioxidant Properties of Liposome-Encapsulated Curcumin. *J. Agric. Food Chem.* **2009**, *57*, 9141–9146.

(24) Chen, C.; Johnston, T. D.; Jeon, H.; Gedaly, R.; McHugh, P. R.; Burke, T. G.; Ranjan, D. An In Vitro Study of Liposomal Curcumin: Stability, Toxicity and Biological Activity in Human Lymphocytes and Epstein-Barr Virus-Transform-ed Human B-Cells. *Int. J. Pharm.* **2009**, *366*, 133–139.

(25) Tønnesen, H. H.; Smistad, G.; Agren, T.; Karlsen, J. Studies on Curcumin and Curcuminoids. 23. Effects of Curcumin on Liposomal Lipid-Peroxidation. *Int. J. Pharm.* **1993**, *90*, 221–228.

(26) Mathur, A. B.; Gupta, V. Silk Fibroin-Derived Nanoparticles for Biomedical Applications. *Nanomedicine* **2010**, *5*, 807–820.

(27) Yallapu, M. M.; Gupta, B. K.; Jaggi, M.; Chauhan, S. C. Fabrication of Curcumin Encapsulated PLGA Nanoparticles for Improved Therapeutic Effects in Metastatic Cancer Cells. *J. Colloid Interface Sci.* **2010**, *351*, 19–29.

(28) Das, R. K.; Kasoju, N.; Bora, U. Encapsulation of Curcumin in Alginate-Chitosan-Pluronic Composite Nanoparticles for Delivery to Cancer Cells. *Nano-medicine* **2010**, *6*, 153–160.

(29) Sahu, A.; Kasoju, N.; Bora, U. Fluorescence Study of the Curcumin-Casein Micelle Complexation and Its Application as a Drug Nanocarrier to Cancer Cells. *Biomacromolecules* **2008**, *9*, 2905–2912.

(30) Barik, A.; Priyadarsini, K. I.; Mohan, H. Photophysical Studies on Binding of Curcumin to Bovine Serum Albumin. *Photochem. Photobiol.* **2003**, *77*, 597–603.

(31) Esmaili, M.; Ghaffari, S. M.; Moosavi-Movahedi, Z.; Atri, M. S.; Sharifizadeh, A.; Farhadi, M.; Yousefi, R.; Chobert, J. M.; Haertle, T.; Moosavi-Movahedi, A. A. Beta Casein-Micelle as a Nano Vehicle for Solubility Enhancement of Curcumin; Food Industry Application. *LWT–Food Sci. Technol.* **2011**, *44*, 2166–2172.

(32) Yazdi, S. R.; Corredig, M. Heating of Milk Alters the Binding of Curcumin to Casein Micelles, A Fluorescence Spectroscopy Study. *Food Chem.* **2012**, *132*, 1143–1149.

(33) Yang, L.; Alexandridis, P. Physicochemical Aspects of Drug Delivery and Release from Polymer-Based Colloids. *Curr. Opin. Colloid Interface Sci.* **2000**, *5*, 132–143.

(34) gamma cyclodexrin., Food and Drug Administration, `http://www.accessdata.fda.gov/scripts/fcn/fcnDetailNavigation.cfm?rpt=grasListing&id=46`.

(35) beta cyclodexrin., Food and Drug Administration, `http://www.accessdata.fda.gov/scripts/fcn/fcnDetailNavigation.cfm?rpt=grasListing&id=74`.

(36) alpha cyclodexrin., Food and Drug Administration, `http://www.accessdata.fda.gov/scripts/fcn/fcnDetailNavigation.cfm?rpt=grasListing&id=155`.

(37) Szejtli, J. Introduction and General Overview of Cyclodextrin Chemistry. *Chem. Rev.* **1998**, *98*, 1743–1753.

(38) Hirayama, F.; Uekama, K. Cyclodextrin-Based Controlled Drug Release System. *Adv. Drug Deliver. Rev.* **1999**, *36*, 125–141.

(39) Thompson, D. O. Cyclodextrins - Enabling excipients: Their Present and Future Use in Pharmaceuticals. *Crit. Rev. Ther. Drug* **1997**, *14*, 1–104.

(40) Pham, D. T.; Ngo, H. T.; Lincoln, S. F.; May, B. L.; Easton, C. J. Synthesis of C6(A)-to-C6(A) and C3(A)-to-C3(A) Diamide Linked γ-Cyclodextrin Dimers. *Tetrahedron* **2010**, *66*, 2895–2898.

(41) Marrocco, D.; Tilley, W. D.; Bianco-Miotto, T.; Evdokiou, A.; Scher, H. I.; Rifkind, R. A.; Marks, P. A.; Richon, V. M.; Butler, L. M. Suberoylanilide Hydroxamic Acid (Vorinostat) Represses Androgen Receptor Expression and Acts Synergistically with an Androgen Receptor Antagonist to Inhibit Prostate Cancer Cell Proliferation. *Mol. Cancer Ther.* **2007**, *6*, 51–60.

(42) Uliasz, T. F.; Hewett, S. J. A Microtiter Trypan Blue Absorbance Assay for the Quantitative Determination of Excitotoxic Neuronal Injury in Cell Culture. *J. Neurosci. Methods* **2000**, *100*, 157–163.

(43) Hayakawa, H.; Umehara, K.; Myrvik, Q. Oxidative Responses of Rabbit Alveolar Macrophages: Comparative Priming Activities of MIF/MAF, Sera, and Serum Components. *J. Leukoc. Biol.* **1989**, *45*, 231–238.

(44) Granato, A.; Gores, G.; Vilei, M. T.; Tolando, R.; Ferraresso, C.; Muraca, M. Bilirubin Inhibits Bile Acid Induced Apoptosis in Rat Hepatocytes. *Gut* **2003**, *52*, 1774–1778.

(45) Ueda, A.; Shimomura, M.; Ikeda, M.; Yamaguchi, R.; Tanishita, K. Effect of Glycocalyx on Shear-Dependent Albumin Uptake in Endothelial Cells. *Am. J. Physiol. Heart Circ. Physiol.* **2004**, *287*, H2287–H2294.

(46) Bang, Y. J.; Kim, S. J.; Danielpour, D.; Oreilly, M. A.; Kim, K. Y.; Myers, C. E.; Trepel, J. B. Cyclic-AMP Induces Transforming Growth-Factor-Beta-2 Gene-Expression and Growth Arrest in the Human and Rogen-Independent Prostate Carcinoma Cell Line PC-3. *Proc. Nat. Acad. Sc. U. S.* **1992**, *89*, 3556–3560.

(47) Bang, Y. J.; Pirnia, F.; Fang, W. G.; Kang, W. K.; Sartor, O.; Whitesell, L.; Ha, M. J.; Tsokos, M.; Sheahan, M. D.; Nguyen, P.; Niklinski, W. T.; Myers, C. E.; Trepel, J. B. Terminal Neuroendocrine Differentiation of Human Prostate Carcinoma Cells in Response to Increased Intracellular Cyclic AMP. *Proc. Nat. Acad. Sc. U. S.* **1994**, *91*, 5330–5334.

(48) Calvert, R. C.; Shabbir, M.; Thompson, C. S.; Mikhailidis, D. P.; Morgan, R. J.; Burnstock, G. Immunocytochemical and Pharmacological Characterisation of P2-Purinoceptor-Mediated Cell Growth and Death in PC-3 Hormone Refractory Prostate Cancer Cells. *Anticancer Res.* **2004**, *24*, 2853–2859.

(49) Jiang, Q.; Wong, J.; Fyrst, H.; Saba, J. D.; Ames, B. N. g-Tocopherol or Combinations of Vitamin E Forms Induce Cell Death in Human Prostate Cancer Cells by Interrupting Sphingolipid Synthesis. *Proc. Nat. Acad. Sc. U. S.* **2004**, *101*, 17825–17830.

(50) Paschka, A. G.; Butler, R.; Young, C. Y. F. Induction of Apoptosis in Prostate Cancer Cell Lines by the Green Tea Component, (−)-Epigallocatechin-3-gallate. *Cancer Lett.* **1998**, *130*, 1–7.

(51) Rose, D. P.; Connolly, J. M. Effects of Fatty Acids and Eicosanoid Synthesis Inhibitors on the Growth of 2 Human Prostate Cancer Cell Lines. *Prostate* **1991**, *18*, 243–254.

(52) Thangapazham, R. L.; Shaheduzzaman, S.; Kim, K. H.; Passi, N.; Tadese, A.; Vahey, M.; Dobi, A.; Srivastava, S.; Maheshwari, R. K. Androgen Responsive and Refractory Prostate Cancer Cells Exhibit Distinct Curcumin Regulated Transcriptome. *Cancer Biology & Therapy* **2008**, *7*, 1429–1437.

(53) McNally, S. J.; Harrison, E. M.; Ross, J. A.; Garden, O. J.; Wigmore, S. J. Curcumin Induces Heme Oxygenase 1 through Generation of Reactive Oxygen Species, p38 Activation and Phosphatase Inhibition. *International Journal of Molecular Medicine* **2007**, *19*, 165–172.

(54) Motterlini, R.; Foresti, R.; Bassi, R.; Green, C. J. Curcumin, an Antioxidant and Anti-Inflammatory Agent, Induces Heme Oxygenase-1 and Protects Endothelial Cells against Oxidative Stress. *Free Radic. Biol. Med.* **2000**, *28*, 1303–1312.

(55) Aggarwal, B. B. Prostate Cancer and Curcumin - Add Spice to Your Life. *Cancer Biol. Ther.* **2008**, *7*, 1438–1442.

(56) Thangapazham, R. L.; Shaheduzzaman, S. M.; Kim, K. H.; Passi, N.; Dobi, A.; Srivastava, S.; Maheshwari, R. Androgen Responsive and Refractory Prostate Cancer Cells Exhibit Distinct Curcumin Regulated Transcriptome. *J. Urol.* **2008**, *179*, 190–191.

(57) Ravindran, J.; Subbaraju, G. V.; Ramani, M. V.; Sung, B. Y.; Aggarwal, B. B. Bisdemethylcurcumin and Structurally Related Hispolon Analogues of Curcumin Exhibit Enhanced Prooxidant, Anti-Proliferative and Anti-Inflammatory Activities In Vitro. *Biochem. Pharmacol.* **2010**, *79*, 1658–1666.

(58) Shankar, S.; Chen, Q.; Sarva, K.; Siddiqui, I.; Srivastava, R. K. Curcumin Enhances the Apoptosis-Inducing Potential of TRAIL in Prostate Cancer Cells: Molecular Mechanisms of Apoptosis, Migration and Angiogenesis. *J. Mol. Signal.* **2007**, *2*, 1–14.

(59) Bachmeier, B. E.; Mirisola, V.; Romeo, F.; Generoso, L.; Esposito, A.; Dell'Eva, R.; Blengio, F.; Killian, P. H.; Albini, A.; Pfeffer, U. Reference Profile Correlation Reveals Estrogen-Like Trancriptional Activity of Curcumin. *Cell. Physiol. Biochem.* **2010**, *26*, 471–482.

(60) Chirnomas, D.; Taniguchi, T.; de la Vega, M.; Vaidya, A. P.; Vasserman, M.; Hartman, A. R.; Kennedy, R.; Foster, R.; Mahoney, J.; Seiden, M. V.; D'Andrea, A. D. Chemosensitization to Cisplatin by Inhibitors of the Fanconi Anemia/BRCA Pathway. *Mol. Cancer Ther.* **2006**, *5*, 952–961.

(61) Hour, T.-C.; Chen, J.; Huang, C.-Y.; Guan, J.-Y.; Lu, S.-H.; Pu, Y.-S. Curcumin Enhances Cytotoxicity of Chemotherapeutic Agents in Prostate Cancer Cells by Inducing p21WAF1/CIP1 and C/EBPβ Expressions and Suppressing NF-κB Activation. *Prostate* **2002**, *51*, 211–218.

(62) Mukhopadhyay, A.; Bueso-Ramos, C.; Chatterjee, D.; Pantazis, P.; Aggarwal, B. B. Curcumin Downregulates Cell Survival Mechanisms in Human Prostate Cancer Cell Lines. *Oncogene* **2001**, *20*, 7597–7609.

(63) Syrovets, T.; Gschwend, J. E.; Buchele, B.; Laumonnier, Y.; Zugmaier, W.; Genze, F.; Simmet, T. Inhibition of IκB Kinase Activity by Acetyl-boswellic Acids Promotes Apoptosis in Androgen-Independent PC-3 Prostate Cancer Cells In Vitro and In Vivo. *J. Biol. Chem.* **2005**, *280*, 6170–6180.

(64) Mukerjee, A.; Vishwanatha, J. K. Formulation, Characterization and Evaluation of Curcumin-Loaded PLGA Nanospheres for Cancer Therapy. *Anticancer Res.* **2009**, *29*, 3867–3875.

(65) Janda, K. D.; Schloeder, D.; Benkovic, S. J.; Lerner, R. A. Induction of an Antibody that Catalyzes the Hydrolysis of an Amide Bond. *Science* **1988**, *241*, 1188–1191.

(66) Jencks, W. P., *Catalysis in Chemistry and Enzymology*; Dover Publications: McGraw-Hill: New York, 1969.

(67) Satterth, A. C.; Jencks, W. P. Mechanism of Aminolysis of Acetate Esters. *J. Am. Chem. Soc.* **1974**, *96*, 7018–7031.

(68) Fersht, A., *Enzyme Structure and Mechanism*; W H Freeman & Co (Sd): W. H. Freeman & Company: London, 1985.

(69) Dhule, S. S.; Penfornis, P.; Frazier, T.; Walker, R.; Feldman, J.; Tan, G.; He, J.; Alb, A.; John, V.; Pochampally, R. Curcumin-Loaded γ-Cyclodextrin Liposomal Nanoparticles as Delivery Vehicles for Osteosarcoma. *Nanomedicine* **2012**, *8*, 440–451.

(70) Yadav, V. R.; Prasad, S.; Kannappan, R.; Ravindran, J.; Chaturvedi, M. M.; Vaahtera, L.; Parkkinen, J.; Aggarwal, B. B. Cyclodextrin-Complexed Curcumin Exhibits Anti-Inflammatory and Anti-Proliferative Activities Superior to those of Curcumin through Higher Cellular Uptake. *Biochem. Pharmacol.* **2010**, *80*, 1021–1032.

(71) Yallapu, M. M.; Jaggi, M.; Chauhan, S. C. β-Cyclodextrin-Curcumin Self-Assembly Enhances Curcumin Delivery in Prostate Cancer Cells. *Colloids Surf., B.* **2010**, *79*, 113–125.

(72) Chignell, C. F.; Bilskj, P.; Reszka, K. J.; Motten, A. G.; Sik, R. H.; Dahl, T. A. Spectral and Photochemical Properties of Curcumin. *Photochem. Photobiol.* **1994**, *59*, 295–302.

(73) Khopde, S. M.; Indira Priyadarsini, K.; Palit, D. K.; Mukherjee, T. Effect of Solvent on the Excited-State Photophysical Properties of Curcumin. *Photochem. Photobiol.* **2000**, *72*, 625–631.

(74) Anand, P.; Nair, H. B.; Sung, B. K.; Kunnumakkara, A. B.; Yadav, V. R.; Tekmal, R. R.; Aggarwal, B. B. Design of Curcumin-Loaded PLGA Nanoparticles Formulation with Enhanced Cellular Uptake, and Increased Bioactivity In Vitro and Superior Bioavailability In Vivo. *Biochem. Pharmacol.* **2010**, *79*, 330–338.

(75) Garcia-Rio, L.; Mendez, M.; Paleo, A. R.; Sardina, F. J. New Insights in Cyclodextrin: Surfactant Mixed Systems from the Use of Neutral and Anionic Cyclodextrin Derivatives. *J. Phys. Chem. B* **2007**, *111*, 12756–12764.

Chapter 3

Ultrafast Spectroscopy and Excited-State Dynamics

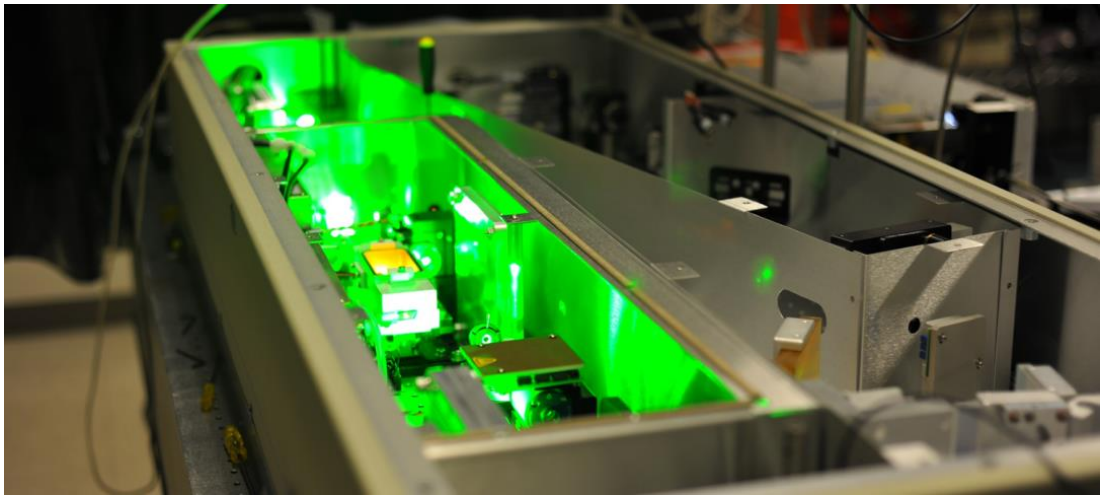

3.1 Introduction to Ultrafast Spectroscopy

The effectiveness of curcumin against melanoma has been demonstrated in previous studies [1–3], in addition to the medicinal effects described in Chapter 1. Some of the therapeutic effects of curcumin are induced by photo-excitation. Hence, investigations on excited-state dynamics of curcumin offer insight into the photo-therapeutic effects of curcumin. However, conventional spectroscopic techniques are unable to reveal ultrafast processes in the excited states which occur in femto- to nanoseconds (10^{-15}–10^{-9} s). The ultrafast spectroscopic techniques employed in our laboratory possess the ability to reveal electronic and molecular processes in the excited states. This chapter describes the experimental setups, time-resolved spectroscopy, and ultrafast photophysical processes.

3.1.1 Femtosecond Laser Pulses

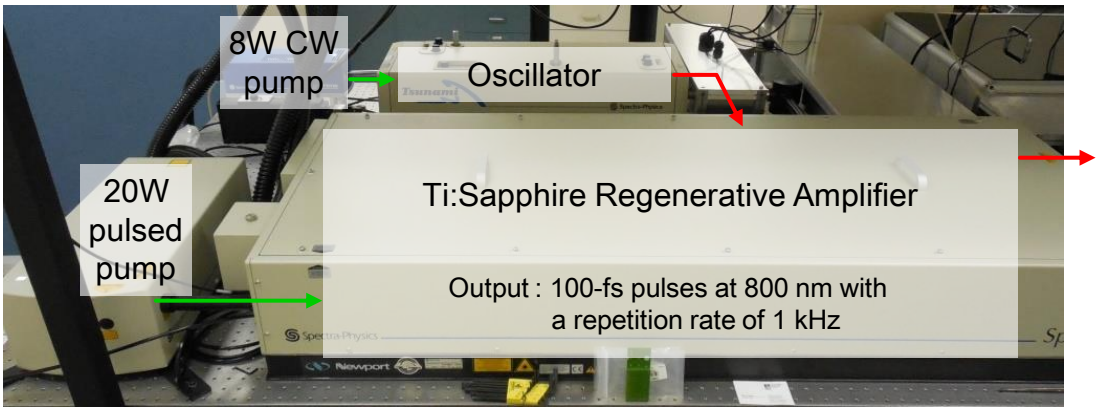

Figure 3.1. Picture of the femtosecond pulsed laser setup which consists of a 8-W Millennia Pro pump laser at 532 nm, a mode-locked Ti:sapphire oscillator, a 20-W Empower pump laser at 527 nm, and a Ti:sapphire regenerative amplifier. The output are 100-fs pulses at 800 nm with a repetition rate of 1 kHz.

Figure 3.1 shows the overall setup of our femtosecond pulsed laser source. Millennia Pro (Spectra-Physics) is an 8-W continuous wave (CW) diode-pumped solid state (DPSS) laser. The monochromatic diode at 808 nm overlaps with the absorption band of neodymium ions (Nd_3^+) in a neodymium-doped yttrium vanadate (Nd:YVO_4) crystal, which results in emission at 1064 nm. The 1064-nm light is focused onto the lithium triborate (LBO) doubling crystal with non-critical phase-match. The resultant 532-nm light is guided into an oscillator.

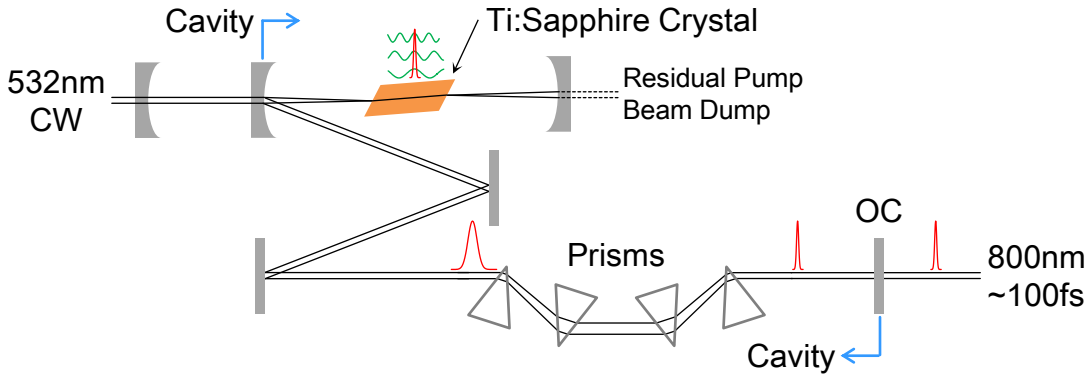

Figure 3.2. Schematic overview of a mode-locked Ti:sapphire oscillator. CW and OC stand for continuous wave and output coupler, respectively.

The *Tsunami* (Spectra-Physics) is a mode-locked titanium-doped sapphire (Ti:sapphire) oscillator (Figure 3.2). A mode locking technique is important for generation of ultrashort pulses (Figure 3.3). The 532-nm light from Millennia Pro excites the Ti:sapphire crystal, inducing stimulated emission with a wavelength of 600–1000 nm within the laser cavity which is defined by an output coupler and a high reflector with a separation of L. The frequencies or modes of this emission are shown as wave forms in Figure 3.3. These modes are phase-matched or locked to establish a standing wave, which results in generation of an ultrashort pulse train. Separation of pulses and repetition rate are defined by the cavity length, L, as,

$$\text{Repetition Rate} = \frac{1}{\text{Pulse Separation}} = \frac{c}{2L} \tag{3.1}$$

where c is the speed of light. With the 80 MHz *Tsunami* oscillator, the cavity optics are separated by $L = 187.5$ cm, and the separation of two adjacent pulses is 12.5 ns. In addition, the bandwidth ($\Delta\lambda$) of the Ti:sapphire emission is important to establish the ultrashort pulse duration (Δt) as described by transform limit [4],

$$\Delta t \geqslant K\frac{\lambda^2}{\Delta\lambda \times c} \tag{3.2}$$

where $K = 0.441$ by assuming Gaussian-shaped pulses, and c is the speed of light. For instance, with an emission spectrum centred at $\lambda = 800$ nm and a bandwidth of 200 nm, the full width at half maximum (FWHM) as pulse duration can be as short as 5 fs.

However, pulse propagation through the optics in the oscillator causes significant broadening of the pulse owing to group velocity dispersion (GVD). GVD is defined as

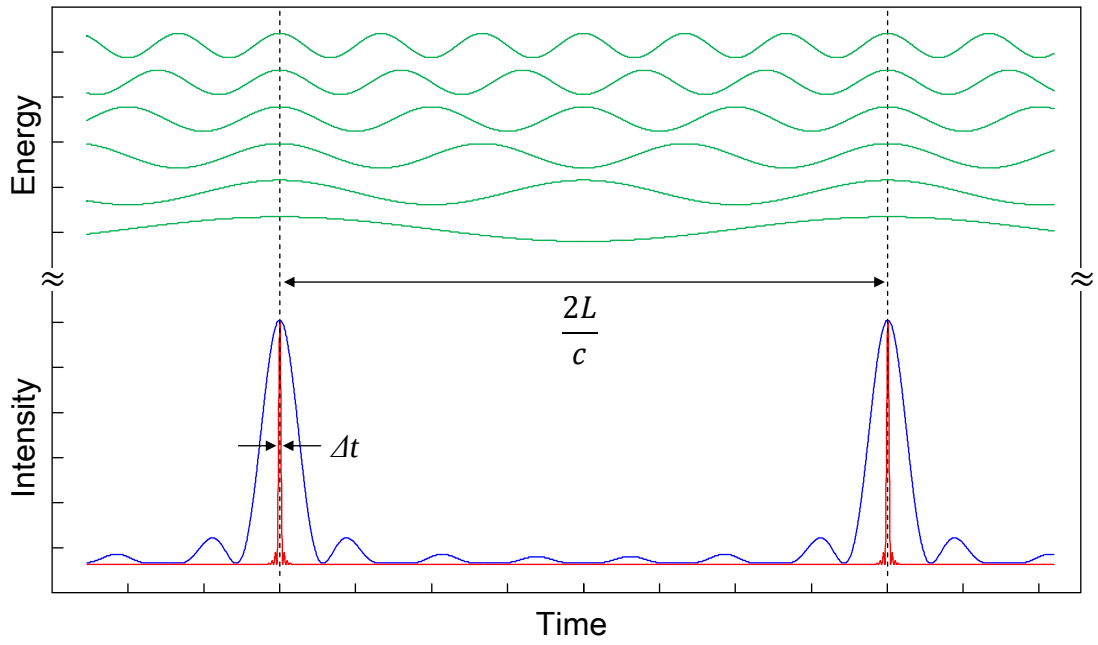

Figure 3.3. Schematic illustration of the mode locking technique in a cavity length, L. Six longitudinal modes from the Ti:sapphire stimulated emission are exemplified in wave forms (green). These modes are phase-matched (dashed line) to form a pulse (blue). Similarly, phase-matching of 100 longitudinal modes forms a sharper pulse (red) which has a duration of Δt. In the *Tsunami*, there are more than 10^5 modes present. The intensity of each pulse is proportional to square of wave form energies. The resultant intensity has an overall pulse shape. The separation of the pulses is determined by $2L/c$, where c is the speed of light.

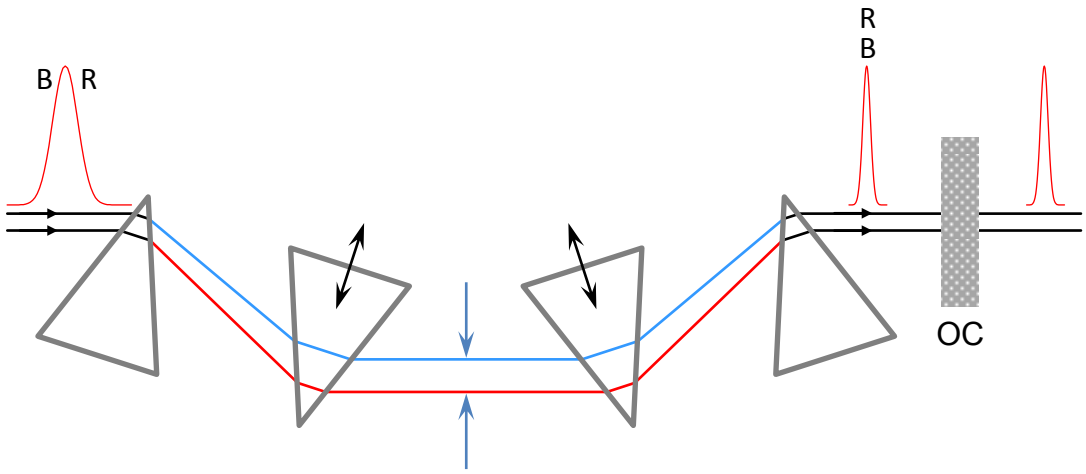

Figure 3.4. Schematic illustration of GVD compensation using four prisms with negative GVD properties. R and B stand for redder and bluer edges of the pulse, respectively. The slit between the second and third prisms is shown in blue arrows. The output coupler (OC) reflects most pulses but transmits those with a high peak power for useful output of the laser.

the difference in group velocity of light in a transparent medium because the refractive index of the medium depends on the wavelength or frequency of light [5]. When a pulse experiences a positive GVD, the redder light travels faster than the bluer light. In addition to GVD, self phase modulation (SPM) of the pulse is also inherent in the Ti:sapphire crystal at high intensities. SPM is due to intensity-dependent refractive index (n) of the crystal as,

$$n = n_0 + n_2 I \tag{3.3}$$

where n_0 and n_2 are the linear and non-linear indices of refraction, respectively, and I is the instantaneous pulse intensity. As a result, the Ti:sapphire crystal also broadens the pulse duration. For the *Tsunami* oscillator, the broadening of the pulse duration due to effects of a positive GVD and SPM is compensated by two prisms in a folded geometry, which is equivalent to four-prism setup, providing a negative GVD, where the bluer light travels a shorter path than the redder light does (Figure 3.4). The pulse propagates through the four prisms and the duration is shortened. The second and third prisms provide adjustment for the pulse duration, and the slit between these prisms selects the peak wavelength of the output. The output coupler is the end of the cavity and transmits pulses with a high peak power for useful output of the laser [5]. Overall, the *Tsunami* mode-locked Ti:sapphire oscillator produces 800-nm pulses with a FWHM of $\sim$ 100 fs at a repetition rate of 80 MHz, which is used for the thesis work.

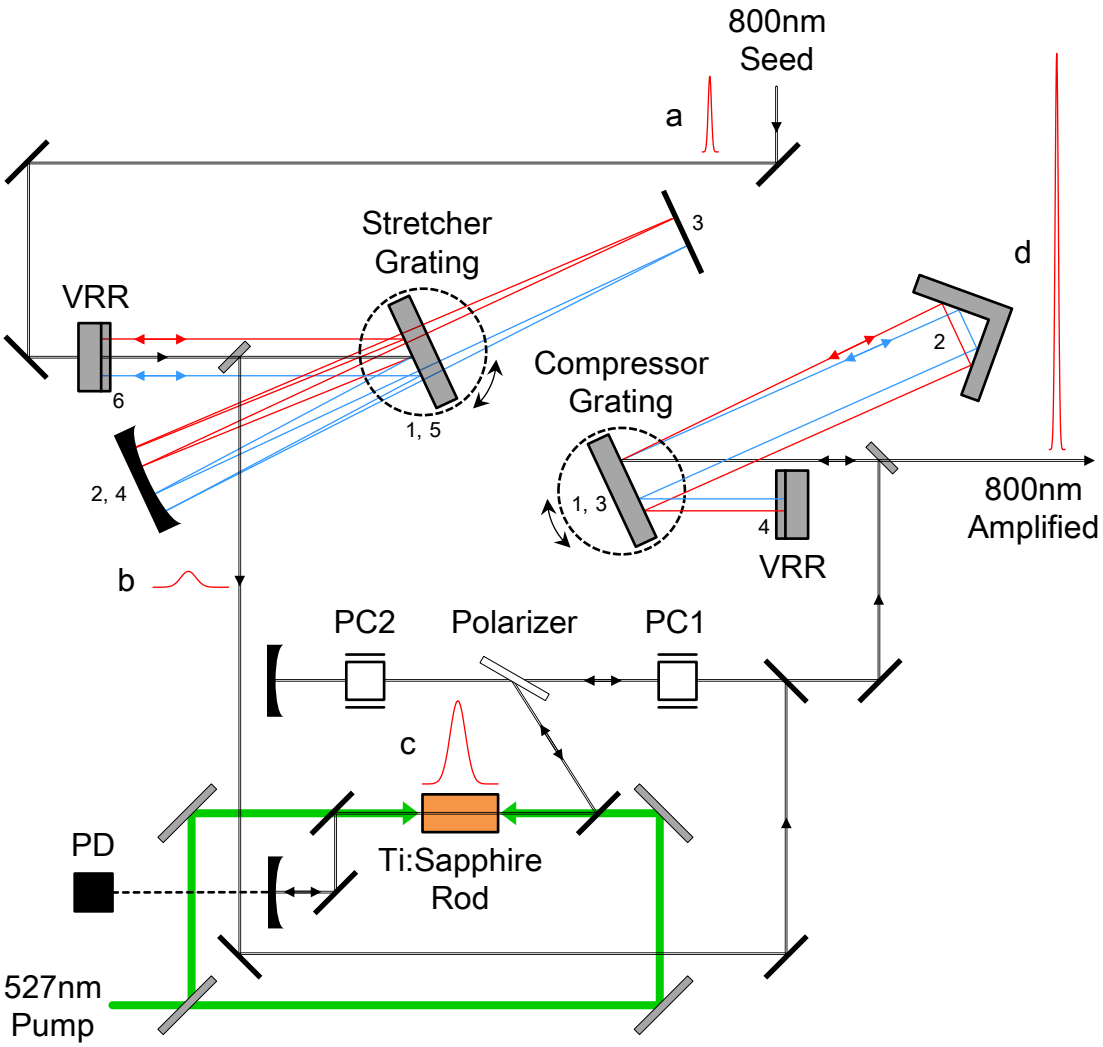

Figure 3.5. Schematic illustration of a Ti:sapphire regenerative amplifier. Pulses (a–d) show their relative changes in pulse duration and power. The numbers in the pulse stretcher and compressor sections represent the sequence of pulse reflection at optics up to vertical retro-reflectors (VRR) during the stretching and compressing processes, respectively. The VRR changes the beam height and the pulses follow the same path in return. PC and PD stand for pockels cell and photodiode detector, respectively.

The output of the oscillator as a seed laser is guided into a Ti:sapphire regenerative amplifier (Spitfire Pro XP, Spectra-Physics, Figure 3.1). Amplification of the seed laser is illustrated in Figure 3.5. Seed pulses from the oscillator (Figure 3.5a) are guided to a pulse stretcher. The pulses experience a positive GVD on the stretcher grating. Note that the redder part of the pulse travels a shorter path than the bluer part. The reflections from the stretcher to the vertical retro-reflector (VRR) are shown as 1–6 in Figure 3.5. The VRR decreases the beam height, and the pulses follow the same path in return but at a lower position. Hence the pulses are stretched further, and the pulse width is increased (Figure 3.5b). This is necessary to avoid damage in optics during the following amplification process. The 20-W Q-switched neodymium-doped yttrium lithium fluoride (Nd:YLF) pulsed pump laser (Empower, Spectra-Physics, Figure 3.1) produces high power 527-nm pulses which induce population inversion in a Ti:sapphire crystal rod. The stretched seed pulses are focused on the Ti:sapphire crystal, which results in amplification of the seed pulse (Figure 3.5c). This amplification is monitored with a photodiode detector (PD, Figure 3.5). Optimally amplified pulses are ejected by changing their polarisation using two pockels cells (PC1 and PC2, Figure 3.5). Finally, the amplified pulses experience a negative GVD on the compressor grating to reduce the pulse width (Figure 3.5d). Note that the bluer part of the pulse travels a shorter path than the redder part. The pulse reflections from the compressor to the vertical retro-reflector (VRR) are shown as 1–4 in Figure 3.5. The VRR increases the beam height, and the pulses follow the same path in return but at a higher position. Overall, the output of the Ti:sapphire regenerative amplifier is 800-nm pulses with a FWHM of 100 fs at a repetition rate of 1 kHz, which are used for time-resolved spectroscopic studies in the thesis work.

3.1.2 Time-resolved Spectroscopy

Time-resolved spectroscopy with 100-fs pulses possesses the ability to show femto- to sub-nanosecond dynamics that are inaccessible with conventional spectroscopic techniques due to their insufficient response time. Typically time-resolved spectroscopic measurements involve two pulses arriving at different time points. Figure 3.6 exemplifies a time-resolved spectroscopic measurement, in which the two pulses are shown in blue and red. The dynamics induced by the blue pulse are of interest (shown as a dashed curve in Figure 3.6). When the red pulse arrives first, only a background signal is measured as the blue pulse has not generated any photo-induced dynamics (Figure 3.6a). Once the blue pulse induces the dynamics of interest, the red pulse measures the effect which is revealed as a solid curve (Figure 3.6b). By delaying the

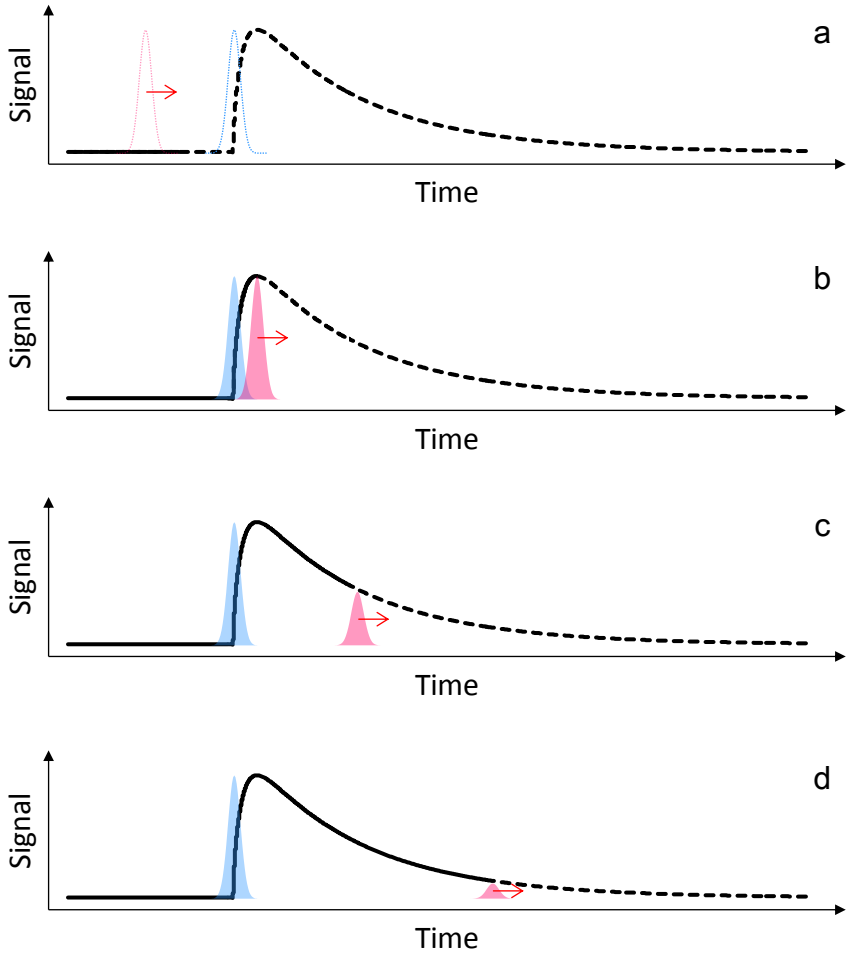

Figure 3.6. Schematic illustration of an example for a time-resolved spectroscopic measurement. Two pulses are shown in blue and red, and the dynamics (shown as a dashed curve) induced by the blue pulse are revealed as a solid curve as measured by the red pulse over time (a–d).

arrival time of the red pulse, the dynamics are resolved over time by the red pulse (Figures 3.6c–d). The resultant decay curve represents the kinetics of photophysical dynamics in the excited state, which are fitted with a multiexponential function,

$$f(t) = \sum_{i=1}^{n} a_i \exp(-t/\tau_i) \tag{3.4}$$

where $\sum_{i=1}^{n} |a_i| = 1$, with the minimum number of exponential terms (n). The fitted function is convoluted with a measured FWHM as a suitable instrument response function. The number of exponential terms (n) indicates the number of processes at time constants (τ_i) and their relative amplitudes (a_i). Overall, two pulsed lasers are used for the basic time-resolved spectroscopic measurements to determine the photophysical dynamics in the excited states. In particular, femtosecond transient absorption spectroscopy and femtosecond fluorescence upconversion spectroscopy are employed in the thesis work.

3.2 Femtosecond Transient Absorption Spectroscopy

3.2.1 Experimental Setup

Femtosecond transient absorption spectroscopy possesses the ability to reveal excited-state dynamics. Figure 3.7 shows the experimental setup of the femtosecond transient absorption spectrometer (Helios, Ultrafast Systems). The 800-nm output from the Ti:sapphire regenerative amplifier (Spitfire Pro XP, Spectra-Physics, Figure 3.1) is split into pump and probe beam lines. The 400-nm pump beam is generated using a 0.5-mm type-I β-barium borate (BBO) crystal (Eksma Optics) and focused onto a sample. The probe beam passes through a delay stage and is used to generate a white light continuum in a 2-mm sapphire crystal. The probe polarisation is oriented at 54.7° with respect to the pump polarisation. This relative angle is called magic angle and necessary to eliminate the effect of depolarisation due to rotational motions of the molecules in the sample. The probe beam is then split into the sample and reference beams with a significantly smaller spot size than the pump at the sample position, which are directed into complementary CMOS detectors for detection in the visible region. Absorption signal or optical density (OD) is defined as follows,

$$\mathrm{OD} = \log(\frac{I_0}{I}) \tag{3.5}$$

where I_0 and I are probe intensities before and after the sample, respectively. The pump beam is modulated at 500 Hz to obtain transient absorption signals,

$$\Delta\mathrm{OD} = \mathrm{OD}_{\mathrm{on}} - \mathrm{OD}_{\mathrm{off}} \tag{3.6}$$

$$= \log(\frac{I_0}{I_{\mathrm{on}}}) - \log(\frac{I_0}{I_{\mathrm{off}}}) \tag{3.7}$$

$$= \log(\frac{I_{\mathrm{off}}}{I_{\mathrm{on}}}) \tag{3.8}$$

where $\mathrm{OD}_{\mathrm{on}}$ and $\mathrm{OD}_{\mathrm{off}}$ represent optical densities with and without the pump, respectively. Similarly, I_{on} and I_{off} represent probe intensities with and without the pump, respectively. Hence, ΔOD is simplified to be independent to the incident probe intensity before the sample (I_0). The reference beam (I_{ref}) is also employed to reduce the fluctuation due to the probe beam instability as,

$$\Delta\mathrm{OD} = \log(\frac{I_{\mathrm{off}}/I_{\mathrm{ref}}}{I_{\mathrm{on}}/I_{\mathrm{ref}}}) \tag{3.9}$$

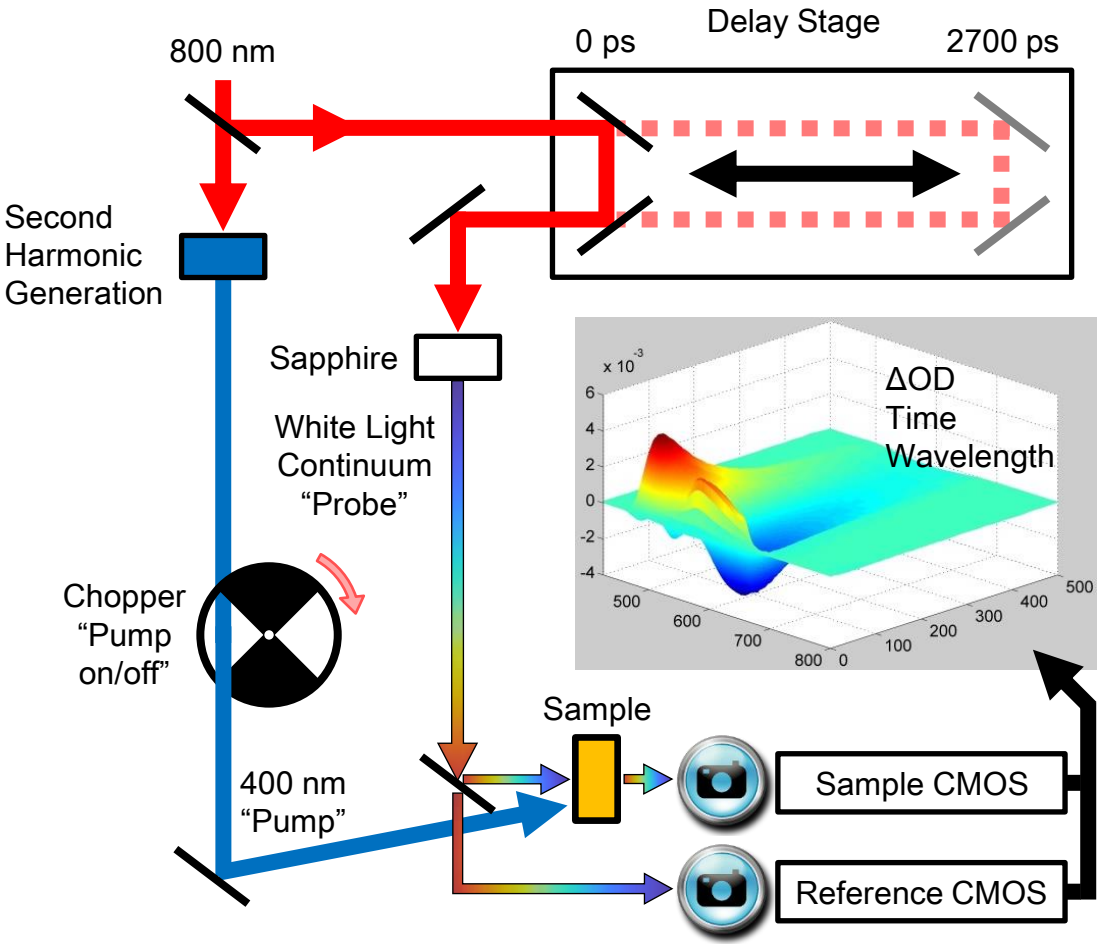

Figure 3.7. Schematic illustration for the experimental setup of the femtosecond transient absorption spectrometer.

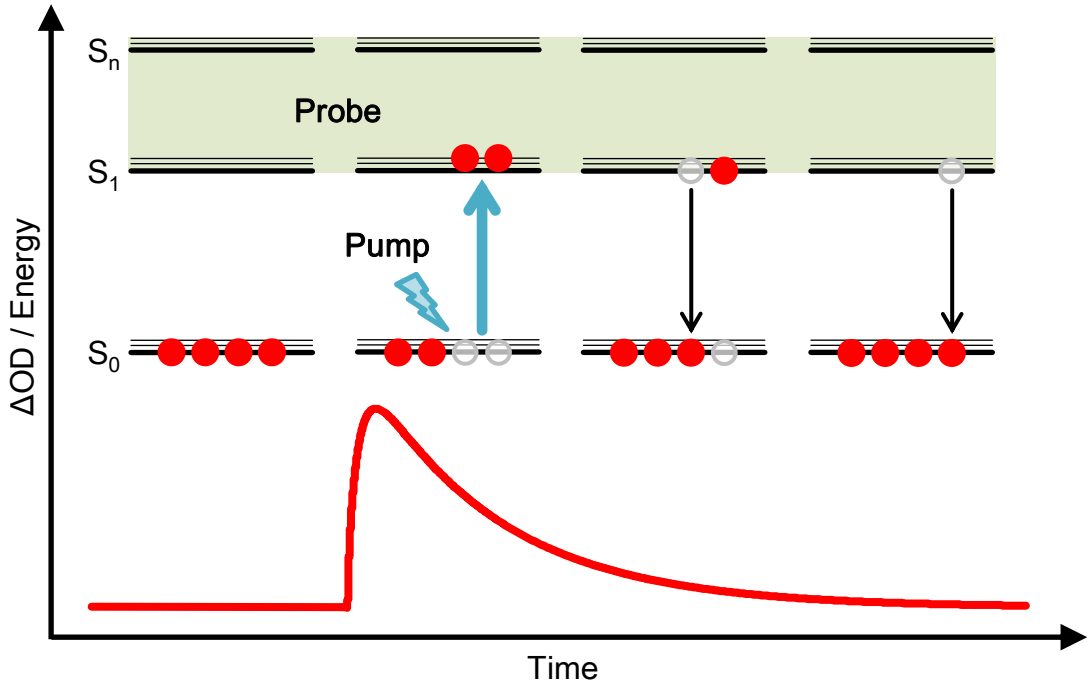

Figure 3.8. Schematic illustration of an excited-state absorption decay. Transient absorption, ΔOD, signals is absorbance of a sample at the first excited state.

The results are obtained as a three-dimensional spectrum with ΔOD, time and wavelength axes. Time-resolved spectra (ΔOD against wavelength) show positive and negative peaks. This thesis focuses on the positive and negative signals as excited-state absorption and stimulated emission of the sample at the first excited state, respectively.

3.2.2 Excited State Absorption

Excited state absorption (ESA) is a transition of a sample from the first electronic excited state to higher states. The pump beam generates excited-state population of the sample, and the measured absorption signals correspond to OD_{on}. When the chopper blocks the pump beam, absorption signals of the ground state population are measured as OD_{off}. Hence, the transient absorption signals, ΔOD, are obtained as ESA signals owing to absorption of the population at the first excited state. As the probe pulse arrives at different time points, the ESA decay is resolved as shown in Figure 3.8. The ESA decay is fitted with a multiexponential function (eq 3.4).

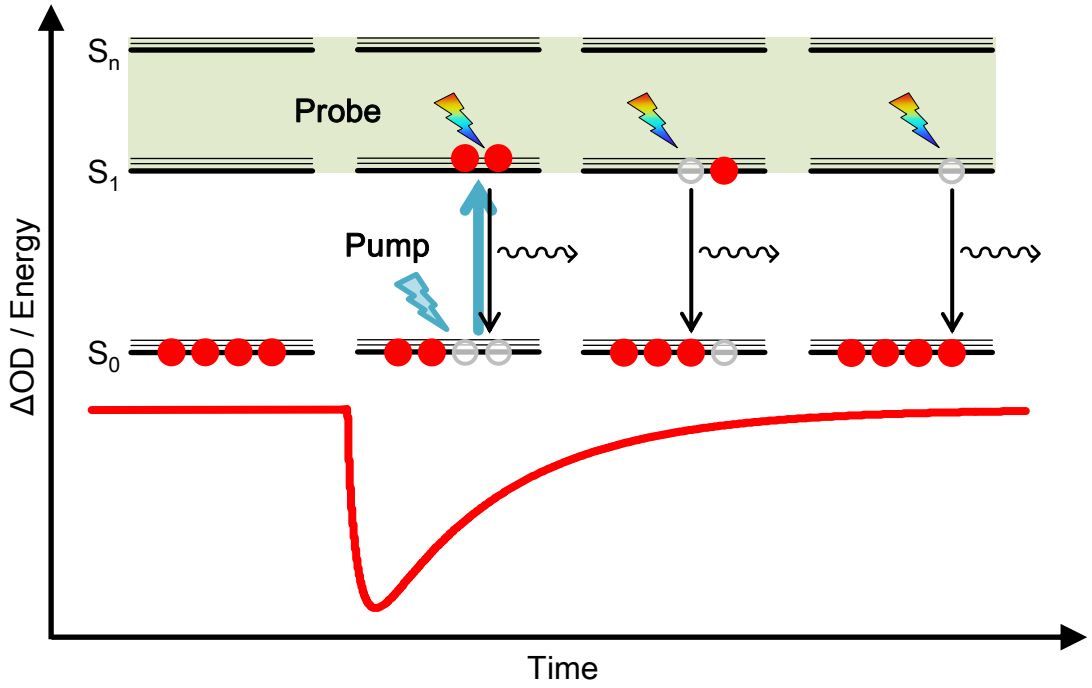

Figure 3.9. Schematic illustration of a stimulated emission decay. Probe pulses cause emission of photons (waved arrow) as a result of depopulation of the excited-state species. Transient absorption, ΔOD, shows negative signals.

3.2.3 Stimulated Emission

Figure 3.9 illustrates the stimulated emission (SE) of a sample. The probe pulse causes depopulation of the first excited-state species by stimulating them to relax to the ground state through emitting a photon. As a result, OD_{on} signals become negative, and transient absorption, ΔOD, exhibits negative signals. The SE spectrum is similar to that of the steady-state fluorescence because of the transition of the population from the first excited state to the ground state. The SE decay is also fitted with a multiexponential function (eq 3.4).

3.2.4 Excited State Absorption Anisotropy

The anisotropy decay reflects the time scale of depolarisation or rotational motions of a sample. The same spectrometer is utilised for the femtosecond transient absorption anisotropy study. The measurements involve collection of two transient absorption signals with the probe polarisation at 0° (parallel, $\Delta OD_{\parallel}$) and 90° (perpendicular, $\Delta OD_{\perp}$) with respect to the pump polarisation, in order to determine the time

dependent anisotropy decay [6],

$$r(t) = \frac{\Delta\mathrm{OD}_{\parallel}(t) - \Delta\mathrm{OD}_{\perp}(t)}{\Delta\mathrm{OD}_{\parallel}(t) + 2\Delta\mathrm{OD}_{\perp}(t)} \tag{3.10}$$

It is fitted with a single exponential function,

$$r(t) = r_0 \exp(-t/\tau^{(r)}) \tag{3.11}$$

where r_0 and $\tau^{(r)}$ are the initial anisotropy value and molecular rotation time, respectively. The theoretical limit of $r_0 = 0.4$ is observed when the pump and probe dipoles are collinear and no depolarisation processes occur within the instrument response function [6].

3.3 Femtosecond Fluorescence Upconversion Spectroscopy

3.3.1 Experimental Setup

Femtosecond fluorescence upconversion spectroscopy possesses the ability to reveal fluorescence relaxation processes. Figure 3.10 shows the schematic experimental setup of the femtosecond transient absorption spectrometer (Halcyone, Ultrafast Systems). The 800-nm output of the Ti:sapphire regenerative amplifier (Spitfire Pro XP, Spectra-Physics) is split into pump and gate beam lines. The 400-nm pump pulses are generated using a 0.5-mm type-I BBO crystal to excite a sample. It is important that the fluorescence decay kinetics show insignificant dependence on the pump power. The fluorescence signal (λ_1) is collected using a plano-convex lens. Then, the gate pulse (at λ_2 = 800 nm) and fluorescence signal are focused onto a 0.4-mm type-I BBO crystal to generate the sum frequency light at λ_3,

$$\frac{1}{\lambda_3} = \frac{1}{\lambda_1} + \frac{1}{\lambda_2} \tag{3.12}$$

The sum frequency signal is detected by a photomultiplier tube attached to a monochromator. The FWHM of the instrument response function is 380 fs which is determined by Raman scattering from neat water.

3.3.2 Fluorescence Lifetime and Solvation Dynamics

The fluorescence decay is fitted with a multiexponential function (eq 3.4). Fluorescence lifetime, $\langle\tau\rangle$, is calculated as,

$$\langle\tau\rangle = \sum_{i=1}^{n} |a_i|\tau_i \tag{3.13}$$

where a_i and τ_i are defined above. More importantly, each exponential term indicates a relaxation process from the first excited state. Possible relaxation processes of curcumin are described in Chapters 4 and 6. However, this chapter focuses on ultrafast relaxation owing to solvation dynamics.

Figure 3.11 illustrates a schematic diagram of solvation dynamics of water molecules. The dipole moment of a probe molecule is extended at the first excited state owing to its electronic transition induced by photo-excitation. Water molecules, which also possess a dipole moment, need to reorganise to accompany the dipole change of the

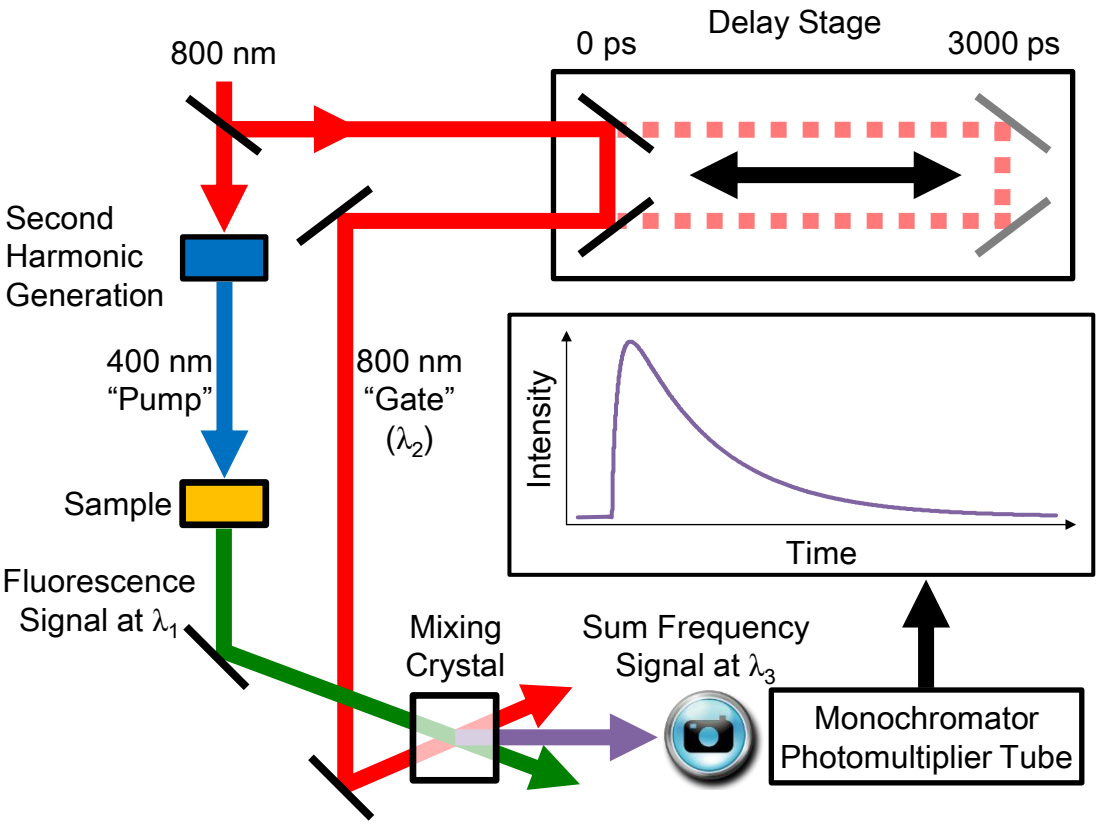

Figure 3.10. Schematic illustration for the experimental setup of the femtosecond fluorescence upconversion spectrometer.

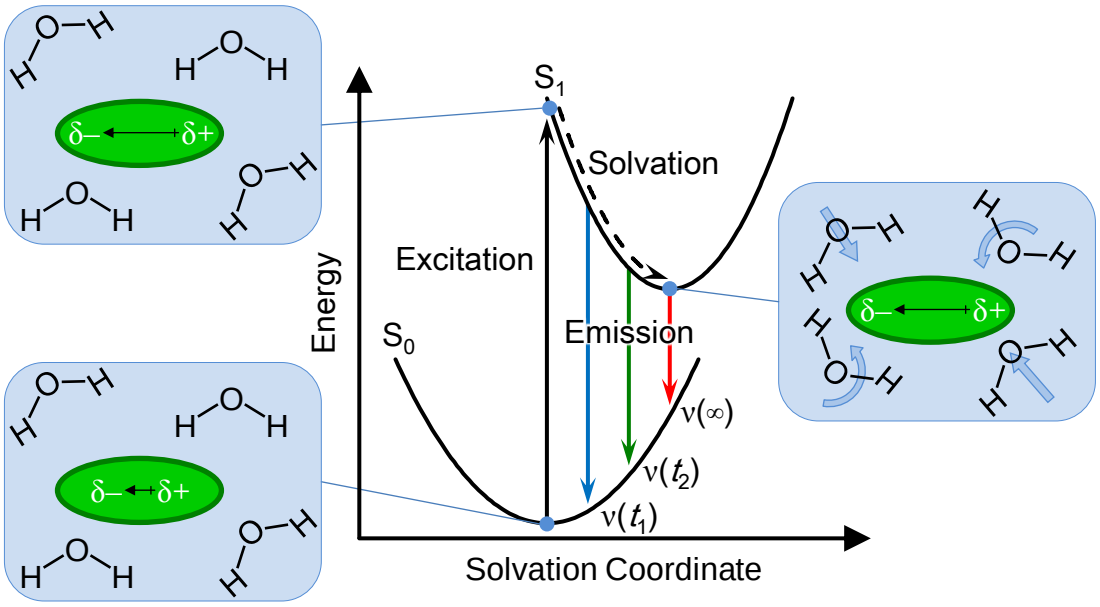

Figure 3.11. Schematic illustration for solvation dynamics of water molecules in response to the dipole change of a probe molecule (green oval) induced by photo-excitation (black arrow). Non-radiative relaxation due to solvent reorganisation is shown as a dashed arrow. Fluorescence emissions are shown as blue, green and red arrows at frequencies, $\nu(t_1)$, $\nu(t_2)$ and $\nu(\infty)$, respectively. Note that water molecules are reorganised to accompany the dipole change of the probe molecule within the first excited (S_1) state.

excited probe molecule. This reorganisation of water molecules is solvation. The probe molecules are solvated over time within the first excited state, followed by undergoing radiative relaxations to the ground state. Therefore, fluorescence decay kinetics are different depending on emission wavelengths. These decay profiles at a range of wavelengths can be used to reconstruct the time-resolved fluorescence spectra [7], which show a spectral red shift over time (t). At a later time point ($t \rightarrow \infty$), the time-resolved spectrum becomes the steady-state fluorescence spectrum. Peak frequencies of those time-resolved fluorescence spectra ($\nu(t)$) are quantified by means of the solvation correlation function,

$$C(t) = \frac{\nu(t) - \nu(\infty)}{\nu(0) - \nu(\infty)} \tag{3.14}$$

where $\nu(0)$ and $\nu(\infty)$ denote the peak frequencies of emission spectra at time zero and infinity. The zero-time fluorescence spectrum is approximated using that of a probe molecule in hexane, according to the method of Fee and Maroncelli [7, 8]. The $\nu(\infty)$

is the peak frequency of the steady-state fluorescence spectrum. Using this method, previous studies have shown that the ultrafast solvation dynamics of bulk water occur in < 1 ps [7, 9, 10]. Chapter 6 of this thesis shows the first solvation dynamics of water in a hydrogel system using curcumin as a probe, and the obtained results are compared with other aqueous systems.

3.4 References

(1) Chan, W.-H.; Wu, H.-J. Anti-Apoptotic Effects of Curcumin on Photosensitized Human Epidermal Carcinoma A431 Cells. *J. Cell. Biochem.* **2004**, *92*, 200–212.

(2) Koon, H. K.; Leung, A. W. N.; Yue, K. K. M.; Mak, N. K. Photodynamic Effect of Curcumin on NPC/CNE2 Cells. *J. Environ. Pathol. Toxicol. Oncol.* **2006**, *25*, 205–216.

(3) Park, K.; Lee, J.-H. Photosensitizer Effect of Curcumin on UVB-Irradiated HaCaT Cells through Activation of Caspase Pathways. *Oncol. Rep.* **2007**, *17*, 537–540.

(4) *Femtosecond Laser Pulses*, 2nd Ed; Rullière, C., Ed.; 1439-2674; Springer New York: 2005.

(5) Paschotta, R., *Encyclopedia of Laser Physics and Technology*, 1st Ed; Wiley-VCH: 2008; Vol. 2.

(6) Lakowicz, J. R., *Principles of Fluorescence Spectroscopy*, 3rd Ed; Springer London, Limited: 2009.

(7) Maroncelli, M.; Fleming, G. R. Picosecond Solvation Dynamics of Coumarin-153 - The Importance of Molecular Aspects of Solvation. *J. Chem. Phys.* **1987**, *86*, 6221–6239.

(8) Fee, R.; Maroncelli, M. Estimating the Time-Zero Spectrum in Time-Resolved Emission Measurements of Solvation Dynamics. *Chem. Phys.* **1994**, *183*, 235–247.

(9) Jimenez, R.; Fleming, G. R.; Kumar, P. V.; Maroncelli, M. Femtosecond Solvation Dynamics of Water. *Nature* **1994**, *369*, 471–473.

(10) Pal, S.; Peon, J.; Zewail, A. Biological Water at the Protein Surface: Dynamical Solvation Probed Directly with Femtosecond Resolution. *Proc. Natl. Acad. Sci. U. S. A.* **2002**, *99*, 1763–1768.

Chapter 4

Femtosecond Transient Absorption Spectroscopy of the Medicinal Agent Curcumin in Diamide Linked γ-Cyclodextrin Dimers

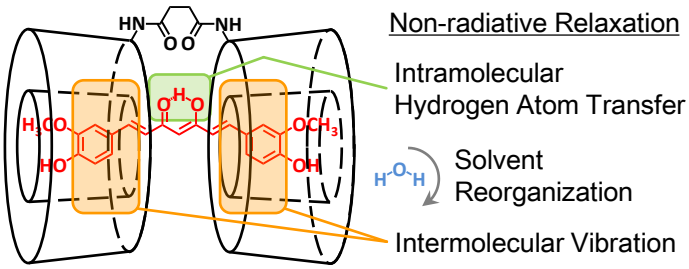

Statement of Authorship

By signing the Statement of Authorship, each author certifies that their stated contribution to the following publication is accurate and that permission in granted for the publication to be included in this thesis.

- Harada, T.; McTernan, H. L.; Pham, D.-T.; Lincoln, S. F.; Kee, T. W., Femtosecond Transient Absorption Spectroscopy of the Medicinal Agent Curcumin in Diamide Linked γ-Cyclodextrin Dimers. *J. Phys. Chem. B* **2015**, 119, 2425-2433 (Published in September 2014). Adapted with permission from this journal article. Copyright (2015) American Chemical Society.

Author Contributions

Name of First Author (Candidate)	Takaaki Harada
Contribution to the Paper	Sample preparations, data acquisition and analysis, and preparation and editing for manuscript
Signature	
Date	17/07/2014

Name of Co-Author	Hamish L. McTernan
Contribution to the Paper	Synthesis of samples
Signature	
Date	02/10/2014

Name of Co-Author	Duc-Truc Pham
Contribution to the Paper	Synthesis of samples
Signature	
Date	21/08/2014

Name of Co-Author	Stephen F. Lincoln
Contribution to the Paper	Supervision of the candidate and editing manuscript
Signature	
Date	02/10/2014

(Continued.)

Name of Co-Author	Tak W. Kee
Contribution to the Paper	Supervision of the candidate, data analysis, editing manuscript, and acted as corresponding author
Signature	
Date	02/10/2014

4.1 Abstract

Curcumin is a biologically active polyphenol and a yellow pigment extracted from turmeric. Our previous study has shown effective encapsulation of curcumin using diamide linked γ-cyclodextrin dimers, namely 66γCD$_2$su and 66γCD$_2$ur, through co-operative 1:1 host-guest complexation. In this study, the excited state dynamics of curcumin complexed with either 66γCD$_2$su or 66γCD$_2$ur in water are investigated using femtosecond transient absorption spectroscopy. Both 66γCD$_2$su-curcumin and 66γCD$_2$ur-curcumin complexes in water show only an excited-state absorption (ESA) band at 530 nm without any stimulated emission (SE) signals, indicating non-radiative decays as the major relaxation pathways. The ESA dynamics of 66γCD$_2$su-curcumin are similar to those of 66γCD$_2$ur-curcumin, consisting of a rapid growth component and three decay components. The growth component, which has a time constant of 0.25–0.41 ps, is assigned to solvent reorganisation. The relatively fast decay components with time constants of 9.3–21.8 ps show significant deuterium isotope effect, consistent with the presence of excited-state intramolecular hydrogen atom transfer (ESIHT) of curcumin. The small-amplitude and slow decay components may be attributed to the dynamics of complexed curcumin and molecular motions due to flexibility of 66γCD$_2$su and 66γCD$_2$ur. In addition, transient absorption anisotropy measurements reveal slow rotational motions of 66γCD$_2$su-curcumin and 66γCD$_2$ur-curcumin complexes. The overall results show that complexation in 66γCD$_2$su and 66γCD$_2$ur has pronounced effects on the photophysics of curcumin.

4.2 Introduction

Curcumin (Figure 4.1a) is a naturally occurring yellow polyphenol present in the rhizomes of the spice plant *Curcuma longa*, commonly known as turmeric [1, 2]. It constitutes 77 % of curcuminoids, which are composed of a group of curcumin analogues, in company with demethoxycurcumin (17 %) and bisdemethoxycurcumin (3 %) [3]. Another curcuminoid, cyclocurcumin, which is also present but at a much lower level, [4] was recently studied [5]. The dominant conformation of curcumin is the keto-enol form in polar solvents (Figure 4.1a) [1, 2]. Recent research on curcumin has shown its medicinal effects including anti-cancer [6–10], anti-Alzheimer's disease [11–13], anti-cystic fibrosis [14, 15], and anti-inflammation properties [16]. However, the poor aqueous stability and solubility of curcumin limit bioavailability and hence hinder applications of curcumin as an effective therapeutic drug [17–19]. Therefore, molecular assemblies as delivery systems, which include micelles [20–23], globular proteins [24, 25], polymer nanoparticles [26, 27], micelle-like aggregates and hydrogels [28], and cyclodextrins [29, 30], have been developed and investigated to improve the availability of curcumin *in vivo*.

Cyclodextrins (CDs) are naturally occurring cyclic oligosaccharides with either 6 (α), 7 (β), or 8 (γ) glucopyranoside units. Figure 4.1b shows the structure of γ-CD. The hydrophobic interior of CDs has the ability to encapsulate a hydrophobic molecular species, while the hydrophilic exterior allows the CD-drug host-guest complexes to be suspended in water, which is attractive for delivering a hydrophobic drug [31, 32]. However, this approach is limited to small molecule drugs due to the limited cavity size of CDs [33]. In order to further improve the CD-based drug delivery systems, a diamide linker between two CDs has been introduced to promote cooperative binding to large molecular guests [34–36]. Our previous study has shown a strong 1:1 cooperative binding of diamide linked γ-CD dimers, namely 66$\gamma$$CD_2$su and 66$\gamma$-$CD_2$ur, to curcumin (Figures 4.1c and 4.1d), which results in a remarkable aqueous stability of curcumin under physiological conditions [29].

Our recent study has also reported the use of 66$\gamma$$CD_2$su and 66$\gamma$$CD_2$ur as curcumin delivery systems to cancer cells [6], and other studies have shown that curcumin has a range of photo-therapeutic effects on melanoma cells [37–39]. There is a growing interest in understanding the photophysical processes of curcumin [40–47]. Thus far, femtosecond transient absorption spectroscopy and fluorescence upconversion spectroscopy have shown that the dominant relaxation pathway of curcumin is excited-state intramolecular hydrogen atom transfer (ESIHT) [40–45]. The ESIHT process is influenced by polar solvents including methanol, DMSO, and acetone due

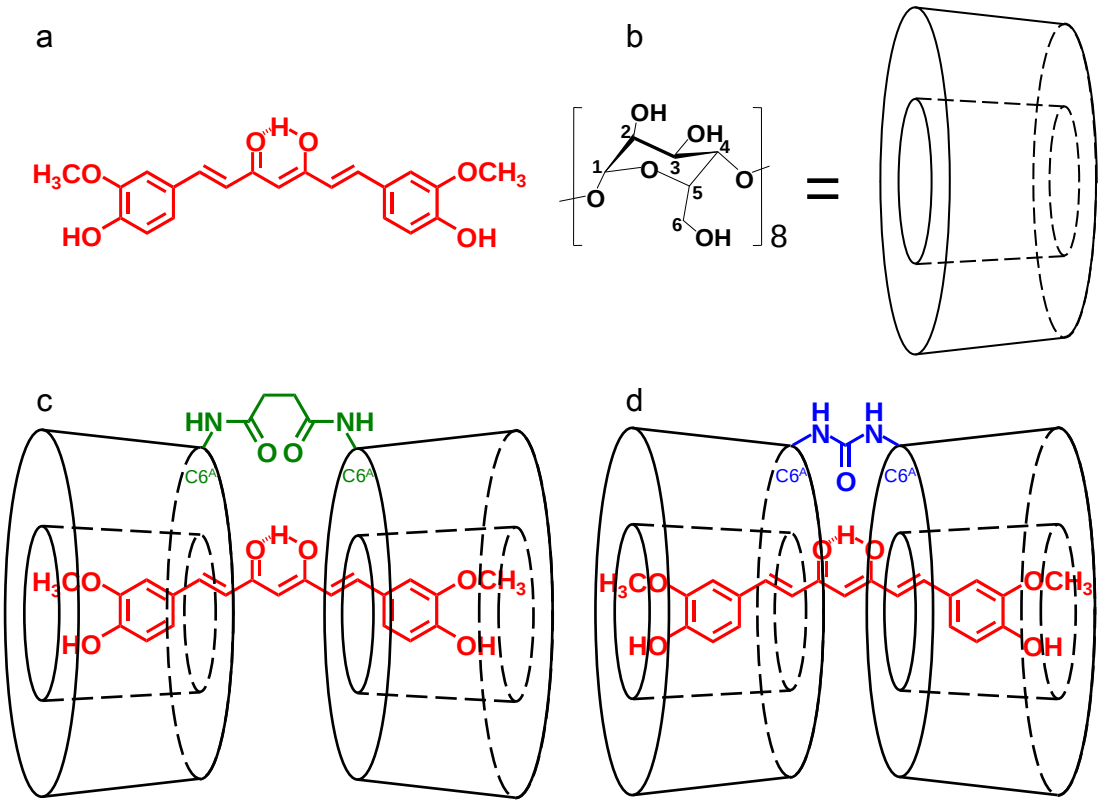

Figure 4.1. Structures of (a) curcumin, (b) γ-CD, and curcumin complexed with (c) 66γCD_2su and (d) 66γCD_2ur.

to solvent-curcumin interactions. Although there have been reports of a relatively fast ESIHT of curcumin in non-polar solvent systems [43, 44, 47], it is still highly unlikely that the observed ESIHT occurs in a direct manner, possibly due to the presence of trace quantities of water in these solvents. Previous work on 3-hydroxyflavone showed that trace amounts of hydrogen-bonding substances can have a significant effect on ESIHT [48]. Furthermore, Schwartz et al. showed that even with rigorous purification of methylcyclohexane traces of hydrogen-bonding impurities (*e.g.*, H_2O) are still present, affecting ESIHT of 3-hydroxyflavone [49]. Nevertheless, the study by Schwartz et al. revealed that ESIHT of 3-hydroxyflavone occurs with a time constant of 240 fs in a highly purified and dried environment [49]. This work provided the first insight into the ultrafast time scale for a direct ESIHT. Interestingly, a very recent study by Mohammed et al. showed that ESIHT of 1,8-dihydroxy-9,10-anthraquinone (DHAQ) involves a direct hydrogen atom transfer from an enol to a keto group in a wide range of solvents [50]. The results suggest that ESIHT of DHAQ occurs within the first 150 fs of the dynamics. Therefore, it follows that a direct ESIHT of curcumin should occur with a similar time constant to those of 3-hydroxyflavone and DHAQ.

In addition to the time scale of ESIHT, there have been some debates on whether the excited-state hydrogen atom transfer reaction of curcumin is intramolecular or intermolecular in nature in polar protic solvents [41, 42, 47]. While Adhikary et al. proposed an intramolecular pathway [41, 42], Ghosh et al. suggested intermolecular hydrogen-bonding of curcumin with the polar protic solvent as an excited-state hydrogen atom transfer mechanism [47]. Although it appears that there are two different pathways, these two proposals are in fact very similar, if not identical. This is because the intramolecular pathway proposed by Adhikary et al. actually involves interactions of curcumin with the polar protic solvent, which is consistent with the conclusions drawn by Kasha and Maroncelli on the ESIHT reactions of 3-hydroxyflavone and 7-azaindole, respectively [48, 51]. Therefore, rather than having two different mechanisms for excited-state hydrogen atom transfer, there is in fact a consensus in the field that interactions with polar protic solvents play an important role in ESIHT of curcumin.

Here, we report the excited-state photo-dynamics of curcumin complexed by the cyclodextrin dimers, 66γCD_2su and 66γCD_2ur, for the first time. The steady-state absorption and fluorescence spectra show that curcumin is non-fluorescent when it is complexed by 66γCD_2su or 66γCD_2ur. Femtosecond transient absorption spectroscopy reveals excited state absorption of curcumin complexed by 66γCD_2su or 66-γCD_2ur in water, without any stimulated emission signals. The non-radiative decay processes involve ESIHT of curcumin, reorganisation of water molecules within the cavity of 66γCD_2su and 66γCD_2ur, and other processes including dynamics of complexed curcumin and molecular motions due to flexibility of the γ-CD moieties of 66γCD_2su and 66γCD_2ur. Time-resolved anisotropy results show that the rotational motions of curcumin complexed by 66γCD_2su and 66γCD_2ur occur on a significantly longer time scale than that of curcumin in a polar organic solvent. Overall, the femtosecond transient absorption results provide insight into the photophysical properties of curcumin when it is complexed by 66γCD_2su and 66γCD_2ur.

4.3 Experimental Section

4.3.1 Materials

Curcumin (1,7-bis(4-hydroxy-3-methoxyphenyl)hepta-1,6-diene-3,5-dione) was obtained from LKT Laboratories (purity $> 98\,\%$). A previous study showed that curcumin with this purity was still comparable to that with a 70 % purity [42], and hence the 2 % impurities were unlikely to affect our spectroscopic measurements. Methanol (MeOH, HPLC grade, 99.7 %) from Scharlau was used as received, and deuterated water (D_2O) and methanol (MeOD-d_4) were purchased from Cambridge Isotope Laboratories (D, 99.9 %). Water (H_2O) was obtained from a Millipore Milli-Q NANOpure water system. The pH of H_2O and pD of D_2O were approximately 7. The $C6^A$-to-$C6^A$ diamide linked γ-cyclodextrin dimers, *N,N'*-bis(6^A-deoxy-γ-cyclodextrin-6^A-yl) succinamide (66γCD_2su), and *N,N'*-bis(6^A-deoxy-γ-cyclodextrin-6^A-yl) urea (66-γCD_2ur), were synthesised using literature methods [36]. Briefly, the native γ-CDs were substituted with 4-toluenesulfonylchloride for activation at the $C6^A$ position, which yielded 6^A-*O*-(4-methylbenzenesulfonyl)-γ-cyclodextrin (6γCDTs). For the synthesis of 66γCD_2su, the reaction between 6γCDTs and ammonium bicarbonate produced 6^A-amino-6^A-deoxy-γ-cyclodextrin, 6γ$CDNH_2$, which was then dimerised by the reaction with bis(4-nitrophenyl) succinate as the linker. For the synthesis of 66γCD_2ur, the reaction between 6γCDTs and sodium azide produced 6^Aazido-6^A-deoxy-γ-cyclodextrin, 6γCDN_3, which was then dimerised by reaction with carbon dioxide as the linker.

4.3.2 Steady-State UV-Visible Absorption and Fluorescence Spectroscopic Studies

UV-visible absorption spectra of 1 μM curcumin complexed with either 66γCD_2su or 66γCD_2ur in a 1:1 ratio in H_2O or D_2O in a 1-cm quartz cuvette were recorded from 300 nm to 700 nm using a Cary 5000 UV-Vis/NIR spectrophotometer (Varian). Similarly, UV-visible absorption spectra of 1 μM curcumin in either MeOH or MeOD-d_4 were acquired from 300 nm to 700 nm. Fluorescence spectra of these solutions were subsequently recorded from 415 nm to 700 nm using a Cary Eclipse Fluorescence spectrophotometer (Varian) with the excitation and emission slit widths set at 5 nm. The excitation wavelength for these experiments was set at 400 nm. The reported spectra were averaged over 5 scans at a scan rate of 600 nm/min.

4.3.3 Femtosecond Transient Absorption Spectroscopic Studies

Solutions of 80 µM curcumin complexed with either 66γCD$_2$su or 66γCD$_2$ur at a 1:1 ratio in H_2O or D_2O were used in the transient absorption spectroscopic studies. Similarly, a curcumin concentration of 80 µM was used in MeOH or MeOD-d_4. All the measurements were acquired using a quartz cuvette with a 2-mm path length. Less than 10 % of curcumin photo-degradation was observed after each set of data acquisition.

The laser system used for the femtosecond transient absorption experiments consisted of a Ti:sapphire mode-locked oscillator (Spectra-Physics, Tsunami), which seeded a Ti:sapphire regenerative amplifier (Spectra-Physics, Spitfire Pro XP) pumped by a 20 W Q-switched Nd:YLF laser (Spectra-Physics, Empower). The output of the amplifier was centred at 800 nm with a repetition rate of 1 kHz and pulse duration of 100 fs, which was then split into pump and probe beam lines. The 400-nm pump pulses were generated using a type-I BBO crystal (Eksma Optics), which was modulated at 500 Hz and then focused onto the sample with a spot size of 710 µm and pulse energy of 720 nJ. The probe beam passed through a delay stage and was used to generate a white light continuum in a 2-mm sapphire crystal. The probe passed through a beam splitter to produce the sample and reference beams with a spot size of 50 µm at the sample position. The sample and reference beams were then directed into complementary CMOS detectors for detection in the visible region. The probe polarisation was oriented at magic angle (54.7°) with respect to the pump polarisation. In all the measurements, a full width at half maximum (FWHM) of 100 fs was used for data analysis.

The same laser system was utilised for the femtosecond transient absorption anisotropy study. The measurement involved collecting two transient absorption signals with the probe polarisation at 0° (parallel, $I_{\parallel}$) and 90° (perpendicular, $I_{\perp}$) with respect to the pump polarisation, in order to determine the time dependent anisotropy $r(t)$ (see eq 4.1). In this study, a concentration of 160 µM was used for 66γCD$_2$su or 66γCD$_2$ur while the concentration of curcumin was kept at 80 µM curcumin to minimise the probability of multiple curcumin molecules binding to a single diamide linked γ-CD dimer.

4.4 Results and Discussion

4.4.1 Steady-State Absorption and Fluorescence Spectra of Curcumin Complexed in 66γCD$_2$su and 66γCD$_2$ur

The steady-state absorption and fluorescence spectra of the 66γCD$_2$su-curcumin and 66γCD$_2$ur-curcumin complexes are displayed in Figures 4.2a and 4.2b, respectively. The spectral envelopes of the curcumin complexes in H_2O and D_2O are very similar except for a minor blue shift for the D_2O solution. In comparison with H_2O and D_2O solvent systems, Figure 4.2c shows the steady-state UV-visible absorption and fluorescence spectra of curcumin in MeOH (red) and MeOD-d_4 (blue). The absorption peak around 430 nm corresponds to the $\pi - \pi^*$ transition of the keto-enol tautomer of curcumin (Figure 4.1a) [20, 42]. The absorption spectrum of curcumin in MeOD-d_4 exhibits a very small blue shift without observable spectral changes [52]. The absorption peak around 420 nm and spectral envelope of 66γCD$_2$su-curcumin and 66γCD$_2$ur-curcumin are similar to those of curcumin in MeOH, which are shown as a gray dashed spectrum in Figures 4.2a and 4.2b. This result indicates that the keto-enol tautomer of curcumin is present in the 66γCD$_2$su-curcumin and 66γCD$_2$-ur-curcumin complexes, as shown in Figures 1c and 1d [29].

Additionally, the absorption spectra of both 66γCD$_2$su-curcumin and 66γCD$_2$ur-curcumin complexes show no 350-nm spectral shoulder, indicating a lack of significant water-curcumin interactions [20, 24, 29]. However, the water-curcumin interactions are still sufficiently strong such that the 66γCD$_2$su-curcumin and 66γCD$_2$-ur-curcumin complexes exhibit very weak fluorescent signals (Figures 4.2a and 4.2b) [29]. At the same curcumin concentration, the fluorescence spectrum of curcumin in MeOD-d_4 exhibits a higher intensity than that of curcumin in MeOH, while their spectral envelopes remain similar (Figure 4.2c) [52]. The fluorescence intensities of 66γCD$_2$su-curcumin and 66γCD$_2$ur-curcumin in D_2O are also higher than those in H_2O. It is clear that the fluorescence intensity and hence the fluorescence quantum yield of curcumin is sensitive to the hydrogen/deuterium (H/D) exchange of curcumin.

It has been shown previously that the enolic hydrogen of curcumin undergoes H/D exchange in deuterated protic solvents and changes the fluorescence quantum yields of curcumin [52]. A previous time-resolved fluorescence spectroscopic study has concluded that ESIHT is a major photophysical process of curcumin in polar protic solvents [42]. The higher fluorescence quantum yield of curcumin in MeOD-d_4 than that in MeOH is due to a longer fluorescence lifetime as a result of the deuterium

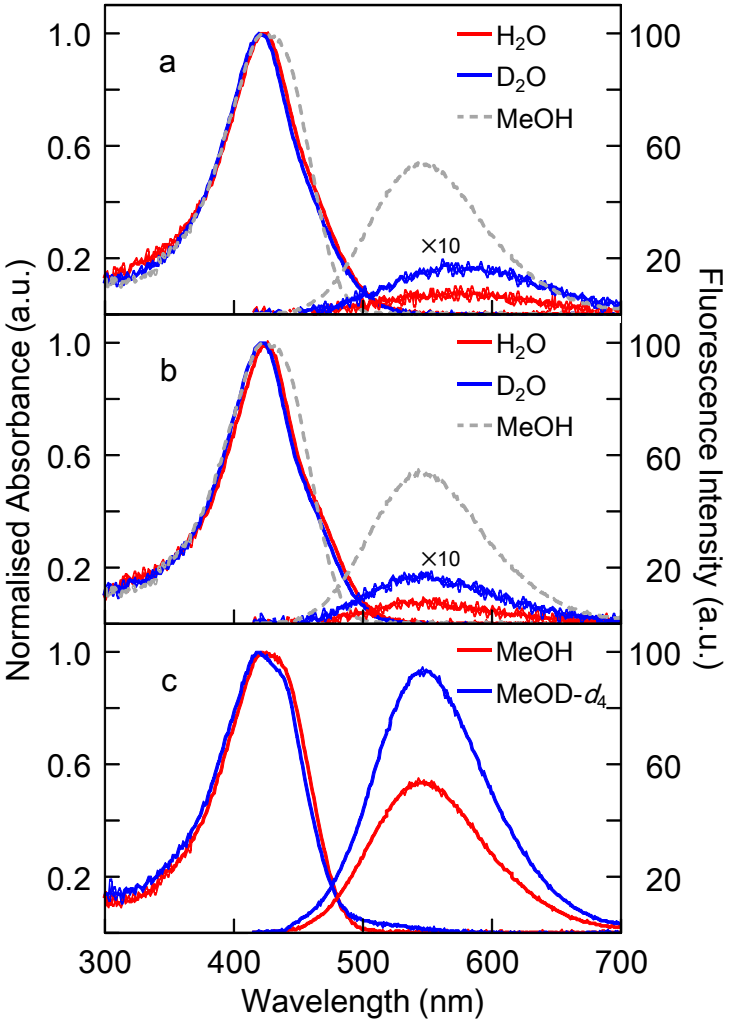

Figure 4.2. Steady-state absorption and fluorescence spectra of curcumin complexed with (a) 66γCD_2su and (b) 66γCD_2ur in H_2O (red) and D_2O (blue), and (c) curcumin in MeOH (red) and MeOD-d_4 (blue), respectively. The gray dashed spectra in panel (a) and (b) represent steady-state absorption and fluorescence spectra of curcumin in MeOH as a reference. The fluorescence spectra of 66γCD_2su-curcumin or 66γ-CD_2ur-curcumin complexes in H_2O or D_2O were multiplied by ten for illustration purposes.

isotope effect [42, 52]. Although, time-resolved fluorescence spectroscopy has been very useful in previous work, it is inapplicable to 66γCD$_2$su-curcumin and 66γCD$_2$ur-curcumin due to their non-fluorescent nature [29]. Hence, in this study, transient absorption spectroscopy was used to offer insight into the excited state dynamics of the 66γCD$_2$su-curcumin and 66γCD$_2$ur-curcumin complexes.

4.4.2 Femtosecond Transient Absorption of Curcumin Complexed in 66γCD$_2$su and 66γCD$_2$ur

Femtosecond transient absorption spectroscopy has been employed for investigations of the excited state dynamics of curcumin in different systems [40, 47]. Here we report the first femtosecond transient absorption study on curcumin solely complexed in 66γCD$_2$su and 66γCD$_2$ur, in a 1:1 host:guest ratio in the aqueous environment. Figures 4.3a and 4.3b show the transient absorption spectra of the 66γCD$_2$su-curcumin complex in H_2O and D_2O, respectively, with several probe delay times, ranging from 0.1 ps to 200 ps. The excited state absorption (ESA) band of curcumin complexed in 66γCD$_2$su in H_2O at 0.1 ps shows a 500-nm peak, but the 530-nm ESA signal becomes pronounced at > 1 ps. Figures 4.3a and 4.3b show that the transient absorption dynamics of 66γCD$_2$su-curcumin in H_2O are faster than those in D_2O, which is discussed below. A similar behaviour in the transient absorption spectra are also present when curcumin is complexed with 66γCD$_2$ur in H_2O or D_2O, as shown in Figures 4.3c and 4.3d, respectively.

Figures 4.3e and 4.3f show the transient absorption spectra of curcumin in MeOH and MeOD-d_4, respectively, with several probe delay times ranging from 0.1 ps to 200 ps. Curcumin in MeOH exhibits a rapid ESA peak around 600 nm at 0.1 ps, which is followed by the appearance of another ESA peak around 500 nm and a stimulated emission (SE) signal around 540 nm at 1 ps. These early time ESA and SE peaks of curcumin in MeOH were also observed in a previous study [40]. The ESA at 600 nm rapidly evolves into SE between 10 ps and 200 ps. The SE signal observed at 540 nm becomes a part of the ESA band centred at 500 nm around 10 ps. This band reaches a maximum ΔOD value around 30 ps and decreases thereafter.

There are three notable differences between the transient absorption spectra of *complexed* and *free* curcumin. First, the transient absorption spectra of 66γCD$_2$su-curcumin and 66γCD$_2$ur-curcumin complexes only exhibit ESA signals within the time window of investigation. The transient absorption spectrum of curcumin in MeOH and MeOD-d_4 at 30 ps are shown in Figures 4.3a–4.3d as gray dashed spectra to highlight the absence of SE signals of curcumin complexed in 66γCD$_2$su and

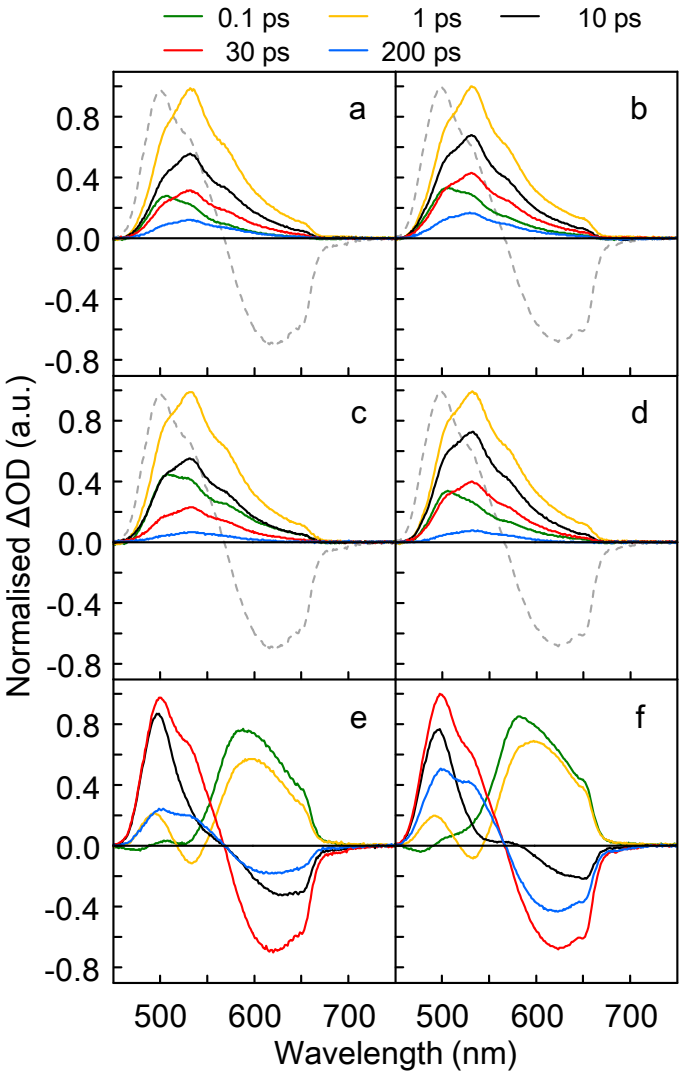

Figure 4.3. Transient absorption spectra of 66γCD_2su-curcumin complex in (a) H_2O and (b) D_2O, those of 66γCD_2ur-curcumin complex in (c) H_2O and (d) D_2O, and those of curcumin in (e) MeOH and (f) MeOD-d_4, at different time delays. Each set of spectra is normalised to the maximum ΔOD signal of the sample. The gray dashed spectrum in panel (a−d) represents transient absorption spectra of curcumin in either MeOH (panel (e)) or MeOD-d_4 (panel (f)) at 30 ps as a reference.

66γCD_2ur. The absence of SE signals for the 66γCD_2su-curcumin or 66γCD_2ur-curcumin complexes is consistent with the very weak fluorescence signals, as shown in Figures 4.2a and 4.2b. Second, there is an apparent difference in the maximum ESA peak position between complexed and free curcumin. Curcumin complexed in either 66γCD_2su or 66γCD_2ur only shows an ESA peak at 530 nm. In contrast, the ESA maximum of free curcumin appears at 500 nm. However, the ESA and SE signals of free curcumin overlap between 450 nm and 700 nm such that the overall ESA maximum of free curcumin appears at 500 nm. Finally, the ESA signals of the 66γCD_2su-curcumin or 66γCD_2ur-curcumin complexes evolve faster than that of curcumin in methanol, as is discussed below.

4.4.3 Excited State Dynamics of Curcumin Complexed in 66γ-CD_2su and 66γCD_2ur

Figures 4.4a and 4.4b show the 500-nm ESA signals of curcumin complexed with 66γCD_2su and 66γCD_2ur, respectively, in H_2O (red) and D_2O (blue) as a function of pump-probe delay time. The 500-nm ESA signals of 66γCD_2su-curcumin and 66γ-CD_2ur-curcumin complexes were fitted with a quad-exponential function consisting of a growth component (τ_1) and three decay components (τ_2, τ_3, and τ_4), which are summarised in Table 4.1. The ESA signals of 66γCD_2su-curcumin complex in H_2O and D_2O show a rapid growth component with a time constant (τ_1) of 0.25 ps with an amplitude of approximately ~ 40 % of the maximum signal amplitude. Comparable results were obtained for the 66γCD_2ur-curcumin complex (Table 4.1). There are three decay components characterised by time constants, τ_2, τ_3, and τ_4, for the ESA signals of both the 66γCD_2su-curcumin and 66γCD_2ur-curcumin complexes (Table 4.1). The time constants τ_2 are approximately 9.3 ps (39 %) and 14.6 ps (34 %) for the 66γCD_2su-curcumin complex in H_2O and D_2O, respectively. For the 66γCD_2-ur-curcumin complex in H_2O and D_2O solvent systems, the time constants τ_2 are 12.7 ps (55 %) and 21.8 ps (53 %), respectively. The time constants τ_3 and τ_4 are fixed to 109 ps and 1200 ps, respectively [53], which are discussed below.

The rapid growth components τ_1 of the ESA signal for both 66γCD_2su-curcumin and 66γCD_2ur-curcumin complexes are assigned to reorganisation of H_2O and D_2O [41, 53, 54], which is consistent with the Stokes shift observed in the steady-state spectra (Figures 4.2a and 4.2b). Vajda et al. have investigated the dynamics of water molecules inside the γ-CD cavity, and their results indicate the presence of significant solute-solvent interactions inside the γ-CD cavity, occurring within 1 ps [53]. Therefore, the interactions between curcumin and water molecules inside 66γCD_2su

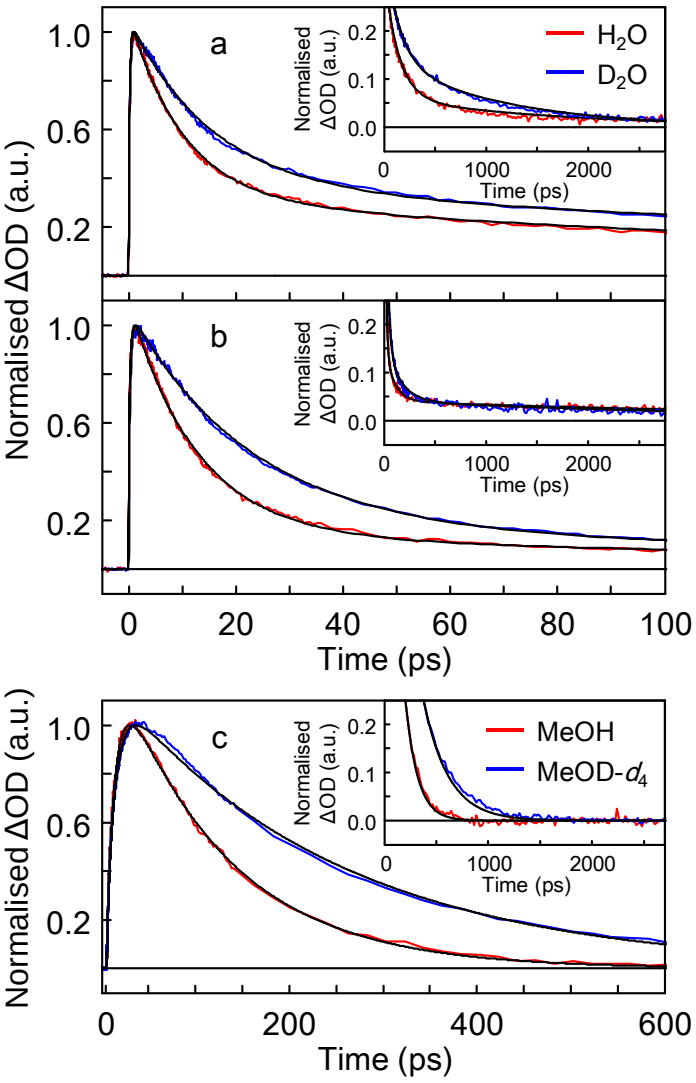

Figure 4.4. Normalised excited state absorption signals of (a) 66γCD_2su-curcumin and (b) 66γCD_2ur-curcumin complexes in H_2O (red) and D_2O (blue), and (c) those of curcumin in MeOH (red) and MeOD-d_4 (blue), at 500 nm. The insets show the signals at later times. Note the time scales of panels (a) and (b) are different from that of panel (c).

and 66γCD_2ur cavities are expected. The presence of water-curcumin interactions is consistent with the non-fluorescent nature of 66γCD_2su-curcumin and 66γCD_2ur-curcumin complexes [29], and the results from a previous molecular dynamics study on these complexes [55]. The process with a time constant of τ_2 is the dominant relaxation process and shows a deuterium isotope effect of 1.6 for 66γCD_2su-curcumin and 1.7 for 66γCD_2ur-curcumin. This relaxation is attributable to ESIHT, which is in agreement with previous studies on curcumin in protic solvents including methanol [41, 42]. The substantial contribution of the decay component τ_2 (approximately 35–55 %) indicates that ESIHT is an important photophysical process of excited state curcumin complexed with 66γCD_2su and 66γCD_2ur. However, the resultant deuterium isotope effect of τ_2 is less than 2, indicating that other relaxation processes may occur at similar time-scales to ESIHT. The relative amplitude of the ESIHT component is lower for 66γCD_2su-curcumin (37%) than 66γCD_2ur-curcumin (54%), as shown in Table 4.1. The difference in relative amplitude is likely to be related to the difference in the hydrogen bonding interactions of curcumin in these assemblies. A recent computational study suggested a significant level of hydrogen bonding between curcumin and the diamide linker of 66γCD_2ur [55]. However, this interaction is absent between curcumin and 66γCD_2su due to the high flexibility of the diamide linker. The long decay time constants τ_3 and τ_4 are present in the ESA decay without showing any deuterium isotope effect. These small-amplitude and slow relaxation processes may involve motions of complexed curcumin and the γ-CD moieties of 66γCD_2su and 66γCD_2ur due to their flexibility. A previous study has shown that the limited cavity size of γ-CD leads to the appearance of small-amplitude and slow relaxation processes, including diffusive motions of the guest molecule, reorientation of highly constrained water molecules within the γ-CD cavity, or fluctuations of the γ-CD molecule [53]. In the same study, the time constants of 109 ps and 1200 ps were assigned to these molecular motions [53]. Here, we fixed τ_3 and τ_4 to these values as these molecular motions are expected to be present in both 66γCD_2su-curcumin and 66γCD_2ur-curcumin complexes. Similar results have also been reported in other studies [56, 57]. Moreover, a recent computational study has shown the presence of water molecules and diffusive motions of curcumin within the γ-CD cavities of 66γCD_2su and 66γCD_2ur [55]. In addition, our previous 2D NOESY ^{1}H NMR spectroscopic results show the intermolecular alkyl hydrogen-hydrogen interactions between curcumin and the γ-CD moieties of 66γCD_2su and 66γCD_2ur [29]. In short, the slow relaxation dynamics of 66γCD_2su-curcumin and 66γCD_2ur-curcumin complexes may be derived from fluctuations of the γ-CD moieties, reorientation of constrained water molecules, diffusive motions of curcumin within the γ-CD cavities, and/or alkyl

hydrogen-hydrogen vibrational motions between curcumin and the γ-CD moieties.

Figure 4.4c shows the time-dependent 500-nm ESA signals of free curcumin in MeOH (red) and MeOD-d_4 (blue), which decay slower than those of curcumin complexed in 66γCD_2su and 66γCD_2ur. The 500-nm ESA signals of curcumin in MeOH and MeOD-d_4 are fitted with a tri-exponential function with two growth components and a single decay component, which are shown in Table 4.1. The two growth components with time constants, τ_1 of 1.17 ps (6 %) and τ_2 of 9.4 ps (43 %), are in agreement with previous studies [40, 47]. The growth components in the ESA signals of curcumin in MeOD-d_4 result in time constants τ_1 of 1.81 ps (7 %) and τ_2 of 10.6 ps (42 %), which are similar to those for curcumin in MeOH. These time constants for curcumin in either MeOH or MeOD-d_4 are assigned to reorganisation of solvent molecules. In addition to the growth components, the ESA signals of curcumin in MeOH show a single decay component with a time constant τ_3 of 116 ps (51 %), as previously reported [40, 47]. The decay component in the ESA signal of curcumin in MeOD-d_4 results in a time constant, τ_3, of 231 ps, showing a significant deuterium isotope effect of 2.0. This decay component is related to ESIHT, as previously investigated using femtosecond fluorescence upconversion spectroscopy [41, 42]. Furthermore, the ESIHT process is influenced by polar solvent molecules, including methanol, due to significant solvent-curcumin interactions, resulting in a longer time constant of free curcumin in MeOH than that of curcumin complexed in 66γCD_2su and 66γCD_2ur.

Overall, the non-radiative relaxation processes of curcumin complexed in 66γ-CD_2su and 66γCD_2ur are determined to be solvent reorganisation, ESIHT, and other slow dynamics. For free curcumin in MeOH and MeOD-d_4, solvent reorganisation and ESIHT are the non-radiative relaxation processes. In all cases, the ESIHT is a major relaxation process and it plays an important role in the photophysical properties of curcumin.

4.4.4 Anisotropy of Curcumin Complexed in 66γCD_2su and 66γ-CD_2ur

To gain further insight into the dynamics of curcumin, the rotational motions of curcumin complexed in 66γCD_2su and 66γCD_2ur were investigated and compared with that of free curcumin in methanol. Transient absorption anisotropy involves measurements of two transient absorption signals with the probe polarisation at 0° (parallel, $I_{\parallel}$) and 90° (perpendicular, $I_{\perp}$) with respect to the pump polarisation. The

Table 4.1. Transient absorption kinetic parameters of curcumin in different systems at 500 nm[a].

Host	Solvent	a_1[b]	τ_1 (ps)	a_2[b]	τ_2 (ps)	a_3	τ_3[c] (ps)	$\langle\tau\rangle$[d] (ps)
66γCD$_2$su	H_2O	−0.42	0.25	0.39	9.3	0.14	109	126
66γCD$_2$su	D_2O	−0.44	0.25	0.34	14.6	0.14	109	210
66γCD$_2$ur	H_2O	−0.38	0.33	0.55	12.7	0.04	109	83
66γCD$_2$ur	D_2O	−0.36	0.41	0.53	21.8	0.08	109	103
–	MeOH	−0.06	1.17	−0.43	9.4	0.51	116	116
–	MeOD-d_4	−0.07	1.81	−0.42	10.6	0.51	231	231

[a] The transient absorption kinetics were fitted with the multiexponential function, $f(t) = \sum_{i=1}^{n} a_i \, exp(-t/\tau_i)$, where $\sum_{i=1}^{n} |a_i| = 1$, with the minimum number of exponential terms (n). The relative error values of the parameters are approximately 10 % from three independent measurements.

[b] The negative amplitude signifies a growth component.

[c] The τ_3 and τ_4 values are fixed to 109 ps and 1200 ps, respectively, for curcumin complexed in 66γCD$_2$su and 66γCD$_2$ur [53]. See text for details.

[d] $\langle\tau\rangle$ is defined as $(\sum_{j=1}^{k} a_j\tau_j)/\sum_{j=1}^{k} a_j$ for the decay components (k).

Table 4.2. Time-resolved transient absorption anisotropy decay parameters of curcumin in different systems at 500 nm[a].

Host	Solvent	r_0	$\tau^{(r)}$ (ps)	$\tau^{(r)}_{DSE}$ [b] (ps)
66γCD$_2$su	H_2O	0.33 ± 0.01	> 1200	$869 - 1189$
66γCD$_2$ur	H_2O	0.32 ± 0.01	> 1200	$869 - 998$
–	MeOH	0.34 ± 0.01	249 ± 13	375

[a] The transient absorption anisotropy decays were fitted to $r(t) = r_0\ exp(-t/\tau^{(r)})$.
[b] Debye-Stokes-Einstein equation at 293 K (refer to eq 4.3).

polarisation anisotropy function, $r(t)$, is defined as follows.

$$r(t) = \frac{I_{\parallel}(t) - I_{\perp}(t)}{I_{\parallel}(t) + 2I_{\perp}(t)} \tag{4.1}$$

The anisotropy decay, $r(t)$, is fitted using a single exponential function,

$$r(t) = r_0\ exp(-t/\tau^{(r)}) \tag{4.2}$$

where r_0 and $\tau^{(r)}$ are the initial anisotropy value and molecular rotation time, respectively.

Figures 4.5a and 4.5b show the anisotropy decays of 66γCD$_2$su-curcumin and 66γCD$_2$ur-curcumin in H_2O, respectively. The 66γCD$_2$su-curcumin and 66γCD$_2$ur-curcumin in H_2O show $r_0 = 0.33 \pm 0.01$ and 0.32 ± 0.01, respectively. The deviation from the theoretical limit of 0.4 in both cases may be due to rapid energy transfer from curcumin to either 66γCD$_2$su or 66γCD$_2$ur and/or to the surrounding solvent molecules. It is clear from Figures 4.5a and 4.5b that $\tau^{(r)}$ of 66γCD$_2$su-curcumin and 66γCD$_2$ur-curcumin in H_2O are significantly longer than the time window available for polarisation anisotropy measurements. The $\tau^{(r)}$ value of > 1200 ps produces a reasonable fit to $r(t)$ for these species. In contrast, Figure 4.5c shows the anisotropy decay of curcumin in MeOH, with $r_0 = 0.34 \pm 0.01$ and $\tau^{(r)} = 249 \pm 13$ ps. These values are in good agreement with those from a previous study [42]. It is clear that rotational motions are present for curcumin in MeOH within the experimental time window. The slow anisotropy decays of 66γCD$_2$su-curcumin and 66γCD$_2$ur-curcumin indicate substantially slower rotational motions than that of curcumin in MeOH, as summarised in Table 4.2.

To understand the difference between the $\tau^{(r)}$ of curcumin in MeOH and in the di-

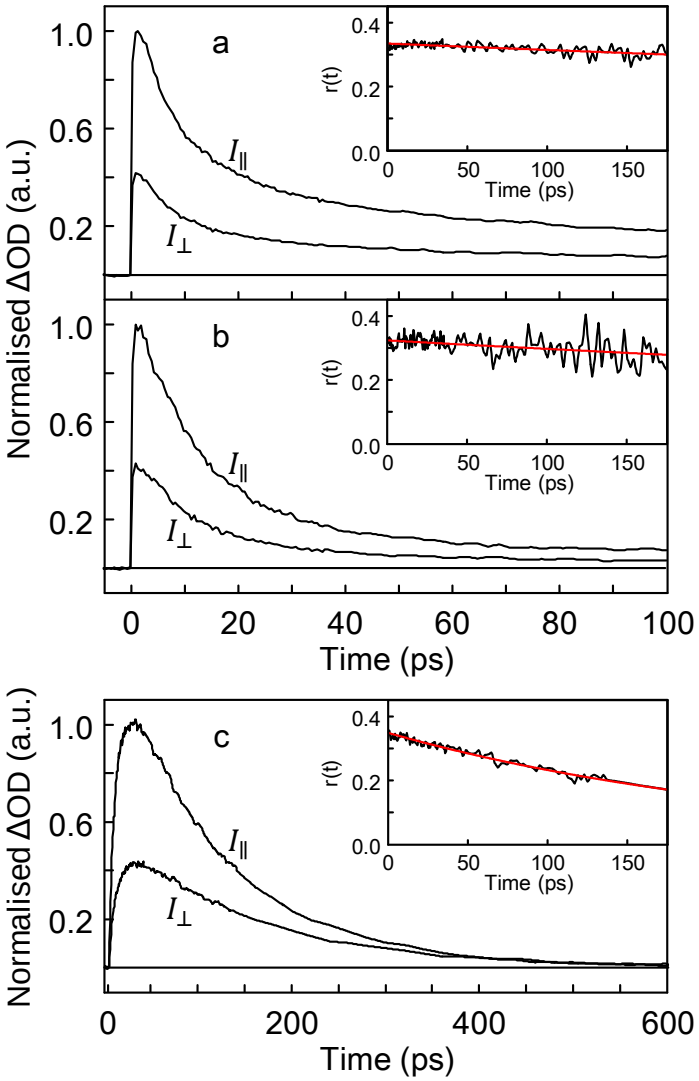

Figure 4.5. Transient absorption anisotropy decays of (a) 66γCD_2su-curcumin in H_2O and (b) 66γCD_2ur-curcumin in H_2O, and (c) curcumin in MeOH, at 500 nm. Note the time scales of panels (a) and (b) are different from that of panel (c). The insets show the anisotropy variations in the first 175 ps. Refer to the eq 4.1 for the definitions of $I_{\parallel}(t)$ and $I_{\perp}(t)$.

amide linked γ-CD dimers, we turn to the Debye-Stokes-Einstein relation to estimate the rotational time constant.

$$\tau_{DSE}^{(r)} = V\eta/k_BT \tag{4.3}$$

The symbols V, η, k_B and T are the hydrodynamic volume of the species under investigation, the viscosity of the medium, the Boltzmann constant and the temperature in Kelvin, respectively. With the use of $\eta_{MeOH} = 5.90 \times 10^{-4}$ Pa s at 293 K and a hydrodynamic radius of 0.85 nm for curcumin [58], $\tau_{DSE}^{(r)}$ of curcumin in MeOH is 375 ps, which is in general agreement with the experimentally determined $\tau^{(r)}$ of ~ 250 ps. Similarly, with the use of the lengths of the succinamide and urea linkers and the dimensions of γ-CD [33], the hydrodynamic volumes of 66γCD$_2$su and 66γCD$_2$ur are estimated to be $(3.50\text{–}4.79) \times 10^{-27}$ m^3 and $(3.50\text{–}4.02) \times 10^{-27}$ m^3, respectively, depending on the distances between the γ-CD moieties owing to flexibility of the diamide linkers. Therefore, given that $\eta_{H_2O} = 1.01 \times 10^{-3}$ Pa s at 293 K, the range of $\tau_{DSE}^{(r)}$ values for curcumin complexed in 66γCD$_2$su and 66γCD$_2$ur are 869–1189 ps and 869–998 ps, respectively. These $\tau_{DSE}^{(r)}$ values are also in general agreement with the experimentally determined $\tau^{(r)}$ values of > 1200 ps. These results indicate that the substantially longer $\tau^{(r)}$ of 66γCD$_2$su-curcumin and 66γCD$_2$-ur-curcumin complexes than that of curcumin in MeOH is due to the significantly larger hydrodynamic volumes of these complexes.

4.5 Conclusions

The excited-state dynamics of curcumin complexed by either 66γCD_2su or 66γ-CD_2ur in water are investigated for the first time, using femtosecond transient absorption spectroscopy. Comparisons are made with respect to *free* curcumin in methanol to gain insight into the effects of complexation in 66γCD_2su and 66γCD_2ur. Steady-state absorption and emission spectroscopic studies indicate significant reduction of water-curcumin interactions as a result of complexation in 66γCD_2su and 66γCD_2ur. Both 66γCD_2su-curcumin and 66γCD_2ur-curcumin in water only show an ESA signal at 530 nm without any SE signals, indicating the presence of significant non-radiative relaxation. The ESA dynamics of 66γCD_2su-curcumin and 66γCD_2ur-curcumin are similar, having a rapid growth component and three decay components. The growth component of 0.25–0.41 ps is assigned to rapid reorganisation of solvent molecules. The relatively fast decay components are attributed to relaxation due to ESIHT (9.3–21.8 ps). The small-amplitude and slow decay components are likely to be due to dynamics of complexed curcumin and molecular motions due to flexibility of the γ-CD moieties of 66γCD_2su and 66γCD_2ur. Finally, the transient absorption anisotropy results reveal that the slow rotational motions of 66γCD_2su-curcumin and 66γCD_2-ur-curcumin in comparison with that of curcumin in MeOH are due to their large hydrodynamic volumes.

4.6 References

(1) Leung, M. H. M.; Harada, T.; Kee, T. W. Delivery of Curcumin and Medicinal Effects of the Copper(II)-Curcumin Complexes. *Curr. Pharm. Des.* **2013**, *19*, 2070–2083.

(2) Goel, A.; Kunnumakkara, A. B.; Aggarwal, B. B. Curcumin as "Curecumin": From Kitchen to Clinic. *Biochem. Pharmacol.* **2008**, *75*, 787–809.

(3) Anand, P.; Sundaram, C.; Jhurani, S.; Kunnumakkara, A. B.; Aggarwal, B. B. Curcumin and Cancer: An "Old-Age" Disease with an "Age-Old" Solution. *Cancer Lett.* **2008**, *267*, 133–164.

(4) Kiuchi, F.; Goto, Y.; Sugimoto, N.; Akao, N.; Kondo, K.; Tsuda, Y. Nematocidal Activity of Turmeric - Synergistic Action of Curcuminoids. *Chem. Pharm. Bull.* **1993**, *41*, 1640–1643.

(5) Adhikary, R.; Barnes, C. A.; Trampel, R. L.; Wallace, S. J.; Kee, T. W.; Petrich, J. W. Photoinduced trans-to-cis Isomerization of Cyclocurcumin. *J. Phys. Chem. B* **2011**, *115*, 10707–10714.

(6) Harada, T.; Giorgio, L.; Harris, T. J.; Pham, D.-T.; Ngo, H. T.; Need, E. F.; Coventry, B. J.; Lincoln, S. F.; Easton, C. J.; Buchanan, G.; Kee, T. W. Diamide Linked γ-Cyclodextrin Dimers as Molecular-Scale Delivery Systems for the Medicinal Pigment Curcumin to Prostate Cancer Cells. *Mol. Pharmaceutics* **2013**, *10*, 4481–4490.

(7) Aggarwal, B. B.; Kumar, A.; Bharti, A. C. Anticancer Potential of Curcumin: Preclinical and Clinical Studies. *Anticancer Res.* **2003**, *23*, 363–398.

(8) Duvoix, A.; Blasius, R.; Delhalle, S.; Schnekenburger, M.; Morceau, F.; Henry, E.; Dicato, M.; Diederich, M. Chemopreventive and Therapeutic Effects of Curcumin. *Cancer Lett.* **2005**, *223*, 181–190.

(9) Dorai, T.; Aggarwal, B. Role of Chemopreventive Agents in Cancer Therapy. *Cancer Lett.* **2004**, *215*, 129–140.

(10) Mehta, K.; Pantazis, P.; McQueen, T.; Aggarwal, B. Antiproliferative Effect of Curcumin (Diferuloylmethane) against Human Breast Tumor Cell Lines. *Anticancer. Drugs* **1997**, *8*, 470–481.

(11) Ono, K.; Hasegawa, K.; Naiki, H.; Yamada, M. Curcumin Has Potent Anti-Amyloidogenic Effects for Alzheimer's β-Amyloid Fibrils In Vitro. *J. Neurosci. Res.* **2004**, *75*, 742–750.

(12) Baum, L.; Ng, A. Curcumin Interaction with Copper and Iron Suggests One Possible Mechanism of Action in Alzheimer's Disease Animal Models. *J. Alzheimers Dis.* **2004**, *6*, 367–377.

(13) Begum, A. N.; Jones, M. R.; Lim, G. P.; Morihara, T.; Kim, P.; Heath, D. D.; Rock, C. L.; Pruitt, M. A.; Yang, F.; Hudspeth, B.; Hu, S.; Faull, K. F.; Teter, B.; Cole, G. M.; Frautschy, S. A. Curcumin Structure-Function, Bioavailability, and Efficacy in Models of Neuroinflammation and Alzheimer's Disease. *J. Pharmacol. Exp. Ther.* **2008**, *326*, 196–208.

(14) Egan, M. E.; Pearson, M.; Weiner, S. A.; Rajendran, V.; Rubin, D.; Glockner-Pagel, J.; Canny, S.; Du, K.; Lukacs, G. L.; Caplan, M. J. Curcumin, a Major Constituent of Turmeric, Corrects Cystic Fibrosis Defects. *Science* **2004**, *304*, 600–602.

(15) Cartiera, M. S.; Ferreira, E. C.; Caputo, C.; Egan, M. E.; Caplan, M. J.; Saltzman, W. M. Partial Correction of Cystic Fibrosis Defects with PLGA Nanoparticles Encapsulating Curcumin. *Mol. Pharmaceutics* **2010**, *7*, 86–93.

(16) Lantz, R. C.; Chen, G. J.; Solyom, A. M.; Jolad, S. D.; Timmermann, B. N. The Effect of Turmeric Extracts on Inflammatory Mediator Production. *Phytomedicine* **2005**, *12*, 445–452.

(17) Anand, P.; Kunnumakkara, A. B.; Newman, R. A.; Aggarwal, B. B. Bioavailability of Curcumin: Problems and Promises. *Mol. Pharmaceutics* **2007**, *4*, 807–818.

(18) Letchford, K.; Liggins, R.; Burt, H. Solubilization of Hydrophobic Drugs by Methoxy Poly(ethylene glycol)-block-polycaprolactone Diblock Copolymer Micelles: Theoretical and Experimental Data and Correlations. *J. Pharm. Sci.* **2008**, *97*, 1179–1190.

(19) Kaminaga, Y.; Nagatsu, A.; Akiyama, T.; Sugimoto, N.; Yamazaki, T.; Maitani, T.; Mizukami, H. Production of Unnatural Glucosides of Curcumin with Drastically Enhanced Water Solubility by Cell Suspension Cultures of Catharanthus Roseus. *FEBS Lett.* **2003**, *555*, 311–316.

(20) Wang, Z. F.; Leung, M. H. M.; Kee, T. W.; English, D. S. The Role of Charge in the Surfactant-Assisted Stabilization of the Natural Product Curcumin. *Langmuir* **2010**, *26*, 5520–5526.

(21) Leung, M. H. M.; Colangelo, H.; Kee, T. W. Encapsulation of Curcumin in Cationic Micelles Suppresses Alkaline Hydrolysis. *Langmuir* **2008**, *24*, 5672–5675.

(22) Tønnesen, H. H. Solubility, Chemical and Photochemical Stability of Curcumin in Surfactant Solutions - Studies of Curcumin and Curcuminolds, XXVIII. *Pharmazie* **2002**, *57*, 820–824.

(23) Banerjee, C.; Ghosh, S.; Mandal, S.; Kuchlyan, J.; Kundu, N.; Sarkar, N. Exploring the Photophysics of Curcumin in Zwitterionic Micellar System: An Approach to Control ESIPT Process in the Presence of Room Temperature Ionic Liquids (RTILs) and Anionic Surfactant. *J. Phys. Chem. B* **2014**, *118*, 3669–3681.

(24) Leung, M. H. M.; Kee, T. W. Effective Stabilization of Curcumin by Association to Plasma Proteins: Human Serum Albumin and Fibrinogen. *Langmuir* **2009**, *25*, 5773–5777.

(25) Sahu, A.; Kasoju, N.; Bora, U. Fluorescence Study of the Curcumin-Casein Micelle Complexation and Its Application as a Drug Nanocarrier to Cancer Cells. *Biomacromolecules* **2008**, *9*, 2905–2912.

(26) Mohanty, C.; Sahoo, S. K. The In Vitro Stability and In Vivo Pharmacokinetics of Curcumin Prepared as an Aqueous Nanoparticulate Formulation. *Biomaterials* **2010**, *31*, 6597–6611.

(27) Shaikh, J.; Ankola, D. D.; Beniwal, V.; Singh, D.; Kumar, M. N. V. R. Nanoparticle Encapsulation Improves Oral Bioavailability of Curcumin by at Least 9-fold when Compared to Curcumin Administered with Piperine as Absorption Enhancer. *Eur. J. Pharm. Sci.* **2009**, *37*, 223–230.

(28) Harada, T.; Pham, D.-T.; Lincoln, S. F.; Kee, T. W. The Capture and Stabilization of Curcumin Using Hydrophobically Modified Polyacrylate Aggregates and Hydrogels. *J. Phys. Chem. B* **2014**, *118*, 9515–9523.

(29) Harada, T.; Pham, D.-T.; Leung, M. H. M.; Ngo, H. T.; Lincoln, S. F.; Easton, C. J.; Kee, T. W. Cooperative Binding and Stabilization of the Medicinal Pigment Curcumin by Diamide Linked γ-Cyclodextrin Dimers: A Spectroscopic Characterization. *J. Phys. Chem. B* **2011**, *115*, 1268–1274.

(30) Tønnesen, H.; Másson, M.; Loftsson, T. Studies of Curcumin and Curcuminoids. XXVII. Cyclodextrin Complexation: Solubility, Chemical and Photochemical Stability. *Int. J. Pharm.* **2002**, *244*, 127–135.

(31) Uekama, K.; Hirayama, F.; Irie, T. Cyclodextrin Drug Carrier Systems. *Chem. Rev.* **1998**, *98*, 2045–2076.

(32) Davis, M.; Brewster, M. Cyclodextrin-Based Pharmaceutics: Past, Present and Future. *Nat. Rev. Drug Discovery* **2004**, *3*, 1023–1035.

(33) Szejtli, J. Introduction and General Overview of Cyclodextrin Chemistry. *Chem. Rev.* **1998**, *98*, 1743–1753.

(34) Pham, D. T.; Clements, P.; Easton, C. J.; Papageorgiou, J.; Maya, B. L.; Lincoln, S. F. Complexation of 6-(4'-(toluidinyl)naphthalene-2-sulfonate by β-Cyclodextrin and Linked β-Cyclodextrin Dimers. *New J. Chem.* **2008**, *32*, 712–718.

(35) Pham, D.-T.; Clements, P.; Easton, C. J.; Papageorgiou, J.; May, B. L.; Lincoln, S. F. Dimerisation and Complexation of 6-(4'-t-butylphenylamino)naphthalene-2-sulphonate by β-Cyclodextrin and Linked β-Cyclodextrin Dimers. *Supramol. Chem.* **2009**, *21*, 510–519.

(36) Pham, D. T.; Ngo, H. T.; Lincoln, S. F.; May, B. L.; Easton, C. J. Synthesis of C6(A)-to-C6(A) and C3(A)-to-C3(A) Diamide Linked γ-Cyclodextrin Dimers. *Tetrahedron* **2010**, *66*, 2895–2898.

(37) Chan, W.-H.; Wu, H.-J. Anti-Apoptotic Effects of Curcumin on Photosensitized Human Epidermal Carcinoma A431 Cells. *J. Cell. Biochem.* **2004**, *92*, 200–212.

(38) Koon, H. K.; Leung, A. W. N.; Yue, K. K. M.; Mak, N. K. Photodynamic Effect of Curcumin on NPC/CNE2 Cells. *J. Environ. Pathol. Toxicol. Oncol.* **2006**, *25*, 205–216.

(39) Park, K.; Lee, J.-H. Photosensitizer Effect of Curcumin on UVB-Irradiated HaCaT Cells through Activation of Caspase Pathways. *Oncol. Rep.* **2007**, *17*, 537–540.

(40) Leung, M. H. M.; Pham, D.-T.; Lincoln, S. F.; Kee, T. W. Femtosecond Transient Absorption Spectroscopy of Copper(II)-Curcumin Complexes. *Phys. Chem. Chem. Phys.* **2012**, *14*, 13580–13587.

(41) Adhikary, R.; Carlson, P. J.; Kee, T. W.; Petrich, J. W. Excited-State Intramolecular Hydrogen Atom Transfer of Curcumin in Surfactant Micelles. *J. Phys. Chem. B* **2010**, *114*, 2997–3004.

(42) Adhikary, R.; Mukherjee, P.; Kee, T. W.; Petrich, J. W. Excited-State Intramolecular Hydrogen Atom Transfer and Solvation Dynamics of the Medicinal Pigment Curcumin. *J. Phys. Chem. B* **2009**, *113*, 5255–5261.

(43) Nardo, L.; Paderno, R.; Andreoni, A.; Másson, M.; Haukvik, T.; Tønnesen, H. H. Role of H-bond Formation in the Photoreactivity of Curcumin. *Spectroscopy* **2008**, *22*, 187–198.

(44) Nardo, L.; Andreoni, A.; Bondani, M.; Másson, M.; Tønnesen, H. H. Studies on Curcumin and Curcuminoids. XXXIV. Photophysical Properties of a Symmetrical, Non-Substituted Curcumin Analogue. *J. Photochem. Photobiol. B: Biol.* **2009**, *97*, 77–86.

(45) Mandal, S.; Ghosh, S.; Banik, D.; Banerjee, C.; Kuchlyan, J.; Sarkar, N. An Investigation into the Effect of the Structure of Bile Salt Aggregates on the Binding Interactions and ESIHT Dynamics of Curcumin: A Photophysical Approach to Probe Bile Salt Aggregates as a Potential Drug Carrier. *J. Phys. Chem. B* **2013**, *117*, 13795–13807.

(46) Khopde, S. M.; Indira Priyadarsini, K.; Palit, D. K.; Mukherjee, T. Effect of Solvent on the Excited-State Photophysical Properties of Curcumin. *Photochem. Photobiol.* **2000**, *72*, 625–631.

(47) Ghosh, R.; Mondal, J. A.; Palit, D. K. Ultrafast Dynamics of the Excited States of Curcumin in Solution. *J. Phys. Chem. B* **2010**, *114*, 12129–12143.

(48) McMorrow, D.; Kasha, M. Intramolecular Excited-State Proton Transfer in 3-Hydroxyflavoney. Hydrogen-Bonding Solvent Perturbations. *J. Phys. Chem.* **1984**, *88*, 2235–2243.

(49) Schwartz, B. J.; Peteanu, L. A.; Harris, C. B. Direct Observation of Fast Proton Transfer: Femtosecond Photophysics of 3-Hydroxyflavone. *J. Phys. Chem.* **1992**, *96*, 3591–3598.

(50) Mohammed, O. F.; Xiao, D.; Batista, V. S.; Nibbering, E. T. J. Excited-State Intramolecular Hydrogen Transfer (ESIHT) of 1,8-Dihydroxy-9,10-anthraquinone (DHAQ) Characterized by Ultrafast Electronic and Vibrational Spectroscopy and Computational Modeling. *J. Phys. Chem. A* **2014**, *118*, 3090–3099.

(51) Moog, R. S.; Maroncelli, M. 7-Azaindole in Alcohols: Solvation Dynamics and Proton Transfer. *J. Phys. Chem.* **1991**, *95*, 10359–10369.

(52) Barik, A.; Goel, N.; Priyadarsini, K.; Mohan, H. Effect of Deuterated Solvents on the Excited State Photophysical Properties of Curcumin. *J. Photosci.* **2004**, *11*, 95–99.

(53) Vajda, S.; Jimenez, R.; Rosenthal, S.; Fidler, V.; Fleming, G.; Castner, E. Femtosecond to Nanosecond Solvation Dynamics in Pure Water and Inside the γ-Cyclodextrin Cavity. *J. Chem. Soc. Faraday Trans.* **1995**, *91*, 867–873.

(54) Jimenez, R.; Fleming, G. R.; Kumar, P. V.; Maroncelli, M. Femtosecond Solvation Dynamics of Water. *Nature* **1994**, *369*, 471–473.

(55) Wallace, S. J.; Kee, T. W.; Huang, D. M. Molecular Basis of Binding and Stability of Curcumin in Diamide-Linked γ-Cyclodextrin Dimers. *J. Phys. Chem. B* **2013**, *117*, 12375–12382.

(56) Roy, D.; Mondal, S. K.; Sahu, K.; Ghosh, S.; Sen, P.; Bhattacharyya, K. Temperature Dependence of Anisotropy Decay and Solvation Dynamics of Coumarin 153 in γ-Cyclodextrin Aggregates. *J. Phys. Chem. A* **2005**, *109*, 7359–7364.

(57) Sen, P.; Roy, D.; Mondal, S. K.; Sahu, K.; Ghosh, S.; Bhattacharyya, K. Fluorescence Anisotropy Decay and Solvation Dynamics in a Nanocavity: Coumarin 153 in Methyl β-Cyclodextrins. *J. Phys. Chem. A* **2005**, *109*, 9716–9722.

(58) Zsila, F.; Bikadi, Z.; Simonyi, M. Circular Dichroism Spectroscopic Studies Reveal pH Dependent Binding of Curcumin in the Minor Groove of Natural and Synthetic Nucleic Acids. *Org. Biomol. Chem.* **2004**, *2*, 2902–2910.

Chapter 5

The Capture and Stabilisation of Curcumin Using Hydrophobically Modified Polyacrylate Aggregates and Hydrogels

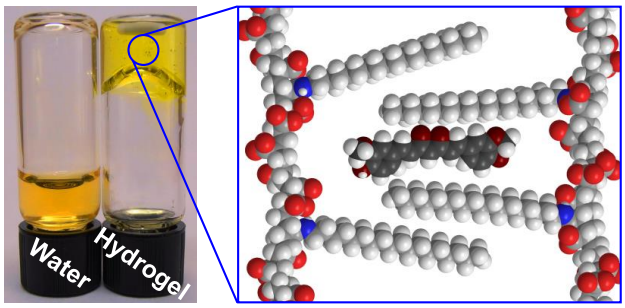

Statement of Authorship

By signing the Statement of Authorship, each author certifies that their stated contribution to the following publication is accurate and that permission in granted for the publication to be included in this thesis.

- Harada, T.; Pham, D.-T.; Lincoln, S. F.; Kee, T. W., The Capture and Stabilization of Curcumin Using Hydrophobically Modified Polyacrylate Aggregates and Hydrogels. *J. Phys. Chem. B* **2014**, 118, 9515–9523 (Published in July 2014). Adapted with permission from this journal article. Copyright (2014) American Chemical Society.

Author Contributions

Name of First Author (Candidate)	Takaaki Harada
Contribution to the Paper	Synthesis and preparation of samples, data acquisition and analysis, and preparation and editing for manuscript
Signature	
Date	17/07/2014

Name of Co-Author	Duc-Truc Pham
Contribution to the Paper	Synthesis of samples
Signature	
Date	21/08/2014

Name of Co-Author	Stephen F. Lincoln
Contribution to the Paper	Supervision of the candidate and editing manuscript
Signature	
Date	02/10/2014

(Continued.)

Name of Co-Author	Tak W. Kee
Contribution to the Paper	Supervision of the candidate, data analysis, editing manuscript, and acted as corresponding author
Signature	
Date	02/10/2014

5.1 Abstract

Hydrophobically modified polyacrylates are shown to suppress the degradation of the medicinal pigment curcumin under physiological conditions. In aqueous solution, the 3 % octadecyl randomly substituted polyacrylate, PAAC18, forms micelle-like aggregates at a concentration of < 1 wt% and a hydrogel at > 1 wt%. Under both conditions, PAAC18 shows a remarkable ability to suppress the degradation of curcumin at pH 7.4 and 37 °C such that its degradation half-life is increased by 1600–2000 folds. The suppression of degradation is attributed to hydrophobic interactions between curcumin and the octadecyl substituents of PAAC18 within the micelle-like aggregates and the hydrogel, as indicated by 2D NOESY ^{1}H NMR spectroscopy. UV-visible absorption titration results are consistent with the interaction of curcumin with five octadecyl substituents on average, which appears to substantially exclude water and greatly decrease the curcumin degradation rate. Dynamic light scattering and zeta potential measurements show the average hydrodynamic diameters of the PAAC18 aggregates to be 0.86–1.15 µm with a negative surface charge. In contrast to the octadecyl substitution, the 3 % dodecyl randomly substituted polyacrylate, PAAC12, shows a negligible effect on slowing the degradation of curcumin, consistent with the dodecyl substituents being insufficiently long to capture curcumin in an adequately hydrophobic environment. These observations indicate the potential for PAAC18 to act as a model drug delivery system.

5.2 Introduction

Curcuminoids are a group of naturally occurring pigments extracted from the rhizomes of *Curcuma longa*, commonly known as turmeric [1, 2]. The most abundant active agent is curcumin (Figure 5.1a), which constitutes 77 % of curcuminoids [3]. Other major curcuminoids include demethoxycurcumin and bisdemethoxycurcumin, which compose 17 % and 3 %, respectively [3]. The medicinal effects of curcumin have been demonstrated for cancer [4–8], inflammation [8, 9], Alzheimer's disease [10–12], and cystic fibrosis [13, 14]. As a result, clinical trials are either underway or have been completed with an aim to develop curcumin as a therapeutic agent [15–18]. However, there are two key challenges that have hindered the development of curcumin as a readily usable drug. These are the low aqueous solubility of curcumin which limits its availability *in vivo* [19, 20], and its susceptibility to hydrolysis and fragmentation which result in substantial degradation within 15 minutes [21–23]. Seeking to address these problems, recent studies have explored a number of delivery systems which include micelles [24–28], plasma proteins [22, 29, 30], cyclodextrins [21, 31, 32], and polymer nanoparticles [33–35].

An attractive approach is to capture and deliver curcumin in hydrogels, which have been utilised in pharmaceutical and biomedical fields including drug delivery and tissue engineering [36–41]. Hydrogels possess the ability to hold large quantities of water and biological fluids by forming three-dimensional networks [42]. Polyacrylate is an attractive starting material for hydrogel construction because of its well-established applications in drug delivery and tissue engineering [43–46]. The synthesis and characterisation of the 3 % octadecyl and dodecyl randomly substituted polyacrylates, PAAC18 and PAAC12, respectively (Figure 5.1b) were reported in previous studies [47–49]. In aqueous solution, hydrophobic interactions between the alkyl substituents of these polyacrylates result in intra- and inter-strand associations, depending on the polyacrylate concentration in weight percent (wt%) as follows. Aqueous solutions of PAAC18 at 0.5 wt% exhibit a low viscosity [48, 49], suggesting the formation of micelle-like aggregates due to the dominant presence of intra-strand associations. Increasing the PAAC18 concentration up to 1 wt% results in a gradual increase in viscosity [48, 49], showing a greater propensity to form cross-linking between different strands. At a concentration > 1 wt%, PAAC18 aqueous solutions form a hydrogel. Similarly, > 2.7 wt% PAAC12 aqueous solutions form a hydrogel [48]. Thus, the spontaneous cross-linking between polyacrylate strands conveniently allows a variation of viscosity up to the formation of hydrogels as concentration is varied.

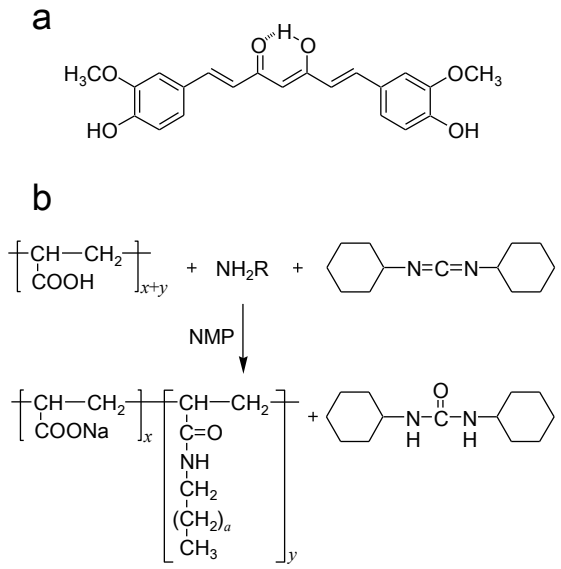

Figure 5.1. (a) The keto-enol form of curcumin. (b) The synthetic scheme for the random substitution of polyacrylate with either octadecyl or dodecyl substituents to give PAAC18 and PAAC12, respectively, where NMP is 1-methyl-2-pyrrolidone and R represents either the octadecyl ($a = 16$) or dodecyl ($a = 10$) substituent. The degree of random substitution is presented as $x : y = 97 : 3$ for 3 % substitution and $x : y = 90 : 10$ for 10 % substitution.

In this study, we investigate the capture of curcumin by hydrophobically modified polyacrylates in aqueous solutions. Both the micelle-like aggregates and hydrogels formed by PAAC18 show a remarkable ability to increase the solubility of curcumin and suppress its degradation under physiological conditions, while PAAC12 shows little effect. A strong binding of curcumin by the octadecyl substituents is revealed by UV-visible absorption titration studies and a similar binding is shown to occur by 2D NOESY ^{1}H NMR spectroscopy. Dynamic light scattering studies reveal average hydrodynamic diameters of 0.86–1.15 µm for the PAAC18 micelle-like aggregates, of which zeta potential results show to have negatively charged surfaces.

5.3 Experimental Section

5.3.1 Materials

Curcumin (1,7-bis(4-hydroxy-3-methoxyphenyl)hepta-1,6-diene-3,5-dione) was obtained from LKT Laboratories (purity 98%). Methanol (AR grade, 99.5%), dimethyl sulphoxide (DMSO, ACS grade), sodium dihydrogen phosphate monohydrate ($NaH_2PO_4 \cdot H_2O$, AR grade) and disodium hydrogen phosphate dihydrate ($Na_2HPO_4 \cdot 2\,H_2O$, AR grade) from Merck Pty Ltd were used as received, and D_2O and DMSO-d_6 were purchased from Cambridge Isotope Laboratories (D, 99.9%). Polyacrylic acid (Mw = 250,000, Mw/Mn $\approx$ 2) was obtained from Sigma Aldrich as a 35 wt% aqueous solution and freeze dried to constant weight. Dodecylamine (99%), octadecylamine (99%), 1-methyl-2-pyrrolidone (NMP) (99.5%) and dicyclohexylcarbodiimide (DCC) (99%) were used as received from Sigma Aldrich. Sodium hydroxide (NaOH) pellets (AR grade, 97.0%) from Ajax Finechem were used to make a 40 % NaOH solution with water deionised using a Millipore Milli-Q NANOpure system. The 50 mM phosphate buffer solution at pH 7.4 ([$NaH_2PO_4 \cdot H_2O$] = 0.156 %w/v and [$Na_2HPO_4 \cdot 2\,H_2O$] = 1.04 %w/v) was also prepared in deionised water.

5.3.2 Syntheses of Hydrophobically Modified Polyacrylates

The 3 % octadecyl and dodecyl randomly substituted polyacrylates, namely PAAC-18 and PAAC12, respectively, were prepared and characterised as previously described [48, 49]. Briefly, octadecylamine and DCC solutions in NMP were added to a solution of polyacrylic acid in NMP with vigorous stirring. After 48 h at 60 °C, the solution was cooled to room temperature, and a 40 % NaOH aqueous solution was added to induce precipitation of the polyacrylate product. After washing and filtering the precipitate with NMP at 60 °C and methanol at room temperature, the crude PAAC18 was dialysed (molecular weight cut-off of 7500 Da) against deionised water for five days. The solution in the dialysis tube was then freeze dried and PAAC18 was obtained as a white solid. A similar method in which dodecylamine replaced octadecylamine was used to synthesise PAAC12. The 10 % octadecyl and dodecyl randomly substituted polyacrylates, 10%-PAAC18 and 10%-PAAC12, respectively, were also synthesised by methods similar to those described above except that the amounts of octadecylamine and dodecylamine used were proportionately increased. The degrees of substitution for the substituted polyacrylates were determined from ^{1}H NMR spectra as described previously [48, 49].

5.3.3 UV-Visible Absorption Spectra of Curcumin in Aqueous Solutions of PAAC18, PAAC12 and 10%-PAAC12, and the Half-Lives of Curcumin Degradation

All UV-visible absorption measurements were carried out in solutions made up in 50 mM phosphate buffer solutions at pH 7.4 and temperature was kept at 37 °C. The concentrations of PAAC18 were 0.3 wt%, 1.0 wt% and 2.0 wt%, those of PAAC12 were 1.0 wt% and 2.9 wt%, and that of 10%-PAAC12 was 0.5 wt%. Solutions of 10%-PAAC18 became cloudy as a result of precipitation and were not further studied. For the experiments in which the curcumin half-lives , $t_{1/2}$, were determined, the samples were prepared by adding $\sim 4\,\mu L$ of curcumin stock (5.4 mM in methanol) to either 700 µL of buffer solution alone or solutions of PAAC18, PAAC12 or 10%-PAAC12 to give a curcumin concentration of 30 µM. Absorption spectra were acquired from these solutions in 0.2-cm quartz cells thermostated at 37 °C using a Varian Cary 5000 UV-Vis/NIR spectrophotometer. In the experiments where degradation of curcumin occurred in phosphate buffer solution alone or in the presence of 1.0 wt% PAAC12, the UV-visible absorption spectra were collected over 30 min at 1-min intervals in the wavelength range of 300–700 nm. For the experiments where degradation of curcumin was much slower in the presence of PAAC18 (at 0.3 wt%, 1.0 wt% or 2.0 wt%), 10%-PAAC12 (at 0.5 wt%) and PAAC12 (at 2.9 wt%), the UV-visible absorption spectra were collected over 18 h at 60-min intervals in the wavelength range of 300–700 nm. In addition, evolution of absorbance around 350 nm which is attributed to generation of curcumin degradation products was analysed by normalising it to the peak absorbance around 430 nm to show the release kinetics of curcumin from PAAC18, PAAC12 and 10%-PAAC12 (Figure B.2 in Appendix B) [21–23].

5.3.4 Binding Constant of the PAAC18-Curcumin Complex

The binding constant, K_n, for the PAAC18-curcumin complex, $(C18)_n$-Cur, was determined from the UV-visible absorbance changes (equation 5.1 below), which occurred on addition of aliquots in the range of 2–5 µL of the 2.5-mM curcumin stock solution in DMSO in a stepwise fashion to 700 µL of a 0.3 wt% PAAC18 aqueous solution in three separate titrations, in which curcumin concentrations ranged from 8 µM to 248 µM in 50 mM phosphate buffer at pH 7.4, at 37 °C. Thus, the DMSO concentration was kept to < 10 %v/v in the PAAC18 solution to minimise any effect of DMSO on the binding of curcumin with the octadecyl substituents of PAAC18, for each titration. Each titration was carried out in a 0.2-cm path-length quartz cell over

45 min during which time curcumin degradation was insignificant and no precipitation of either curcumin or PAAC18 occurred. The binding constants were determined by best-fitting an algorithm derived through equations 5.2−5.6 (discussed below) for the variation of molar absorbance at 0.5-nm intervals over the wavelength range 400–500 nm with the ratio of the total octadecyl substituent concentration of PAAC18 to the total curcumin concentration, $[C18]_n$/[Cur], as the average number of octadecyl substituents binding to each curcumin, n, was varied from 1 to 10 using a non-linear least-squares program (HypSpec) [50, 51].

5.3.5 2D NOESY ^{1}H NMR Spectra of Curcumin in PAAC18 and 10%-PAAC12

The 2D NOESY ^{1}H NMR spectra were recorded with a Varian-Inova 600 spectrometer operating at 599.602 MHz using a standard pulse sequence with a mixing time of 300 ms and acquisition time of 150 ms with 8 repetitions. The first sample was prepared by adding 6.4 µL of a 40 mg/mL stock solution of curcumin in DMSO-d_6 to 700 µL of a 1.0 wt% solution of PAAC18 in D_2O to achieve a curcumin concentration of 1.0 mM, which resulted in an approximately 1 : 3 molar ratio of curcumin to the octadecyl substituents of PAAC18. It is noted that the curcumin concentration in the NMR study is about 30 times higher than that used in the UV-visible absorption study. The second sample was prepared by adding 6.4 µL of a 80 mg/mL stock solution of curcumin in DMSO-d_6 to 700 µL of a 1.0 wt% solution of 10%-PAAC12 in D_2O, which resulted in an approximately 1 : 7 molar ratio of curcumin to the dodecyl substituents of 10%-PAAC12. The rate of degradation of curcumin in the presence of PAAC12 was too rapid for spectra of adequate reliability to be collected.

5.3.6 3D Molecular Illustration and Molecular Size Estimation of Curcumin in PAAC18 and PAAC12

The chemical structures of curcumin, PAAC18 and PAAC12 were energy-minimised and illustrated using CS Chem3D Ultra MM2 protocol [52]. The 3D molecular illustration of curcumin in PAAC18 is shown in the table of content graphic. The size of curcumin was calculated using the distance between methoxy carbon atoms. Furthermore, assuming that the octadecyl substituent is present as a straight chain, its length was calculated using the distance between the terminal carbon atoms. Similarly, the length of a straight dodecyl substituent was calculated.

5.3.7 Dynamic Light Scattering and Zeta Potential Measurements on PAAC18, PAAC12 and 10%-PAAC12

Hydrodynamic diameters and zeta potentials of PAAC18, PAAC12 and 10%-PAAC12 were determined using a Malvern ZetaSizer Nano S. The instrument settings were automatically set by Malvern dispersion technology software with a 633-nm laser. Hydrodynamic diameter and zeta potential measurements were made on degassed aqueous solutions of either 0.3 wt% and 1.0 wt% PAAC18, 1.0 wt% PAAC12, and 0.5 wt% 10%-PAAC12 alone or in the presence of 30 µM curcumin in low volume disposable cuvettes. Zeta potential measurements were made on these solutions alone in disposable zeta potential cuvettes (DTS1060). The ionic strength varied over the range of approximately 30 mM to 60 mM, depending upon the weight percent of the polyacrylate solution. The refractive index (RI) of each polyacrylate solution was assumed to be similar to that of a sodium dodecyl sulphate (SDS) micellar solution (material RI = 0.11 and water dispersant RI = 1.33) due to their structural similarities. The width of a distribution for hydrodynamic diameter is represented as a standard deviation (SD). Hydrodynamic diameter measurements for a 2.0 wt% PAAC18 solution showed inconsistent results due to a combination of the instrument hydrodynamic diameter detection limit of 6 µm and its unsuitability for measurements of viscous solutions.

5.4 Results and Discussion

5.4.1 Degradation of Curcumin in Phosphate Buffer and Stabilisation Effects of Hydrophobically Modified Polyacrylates

High levels of the aqueous stability of curcumin are important to its availability *in vivo*. The rapid changes in the absorption spectra of curcumin in a pH 7.4 phosphate buffer solution at 37 °C over 30 min are shown in Figure 5.2a. The decay at the maximum absorbance at 427 nm with a half-life of 0.04 ± 0.01 h (Table 5.1) is shown in the inset of Figure 5.2a. This result, together with the growth of the absorbance around 350 nm, is consistent with the degradation of curcumin [21–23]. Previous studies have shown that degradation of curcumin by hydrolysis and fragmentation led to possible formation of *trans*-6-(4'-hydroxy-3'-methoxyphenyl)-2,4-dioxo-5-hexenal (*half*-curcumin), ferulic acid, feruloyl methane and vanillin [23, 53].

The time-dependent UV-visible absorption spectra of curcumin in 0.3 wt% PAAC18 over 18 h are shown in Figure 5.2b. The shape of the initial absorption spectrum is similar to that of curcumin in a sodium dodecyl sulphate (SDS) micellar solution and polar organic solvents including methanol and DMSO [25, 28], which suggests a similarity between the hydrophobic micro-environments in these solvents and that of PAAC18. Suppression of rapid curcumin degradation was characterised by an estimated half-life of 71.6 ± 4.0 h in the 0.3 wt% PAAC18 solution, which is ≥ 1600 times longer than that in the absence of PAAC18 (0.04 ± 0.01 h, Table 5.1). The time-dependent UV-visible absorption spectra of curcumin in 1.0 wt% and 2.0 wt% PAAC18 solutions are shown in Figures 5.2c and 5.2d, respectively. Curcumin degradation is also decreased in these hydrogels as shown by estimated half-lives of 74.0 ± 9.2 h and 98.6 ± 16.2 h, respectively, which are 1700–2000 times longer than that observed in the absence of PAAC18 (0.04 ± 0.01 h, Table 5.1). It is interesting that the degradation of curcumin in the presence of PAAC18 also contains useful information regarding release of curcumin from these aggregates and hydrogels. We argue that degradation occurs when curcumin is released from PAAC18 to the aqueous environment owing to hydrolysis and fragmentation, as mentioned above. As a consequence, the rate of curcumin release can be inferred from the rate of curcumin degradation. The results are shown in Figure B.2 (Appendix B).

To gain insight into the effect of the alkyl substituent length on the stabilisation of curcumin degradation, the 3 % dodecyl substituted polyacrylate, PAAC12, was also investigated. A previous study has shown that the viscosities of PAAC12 aqueous

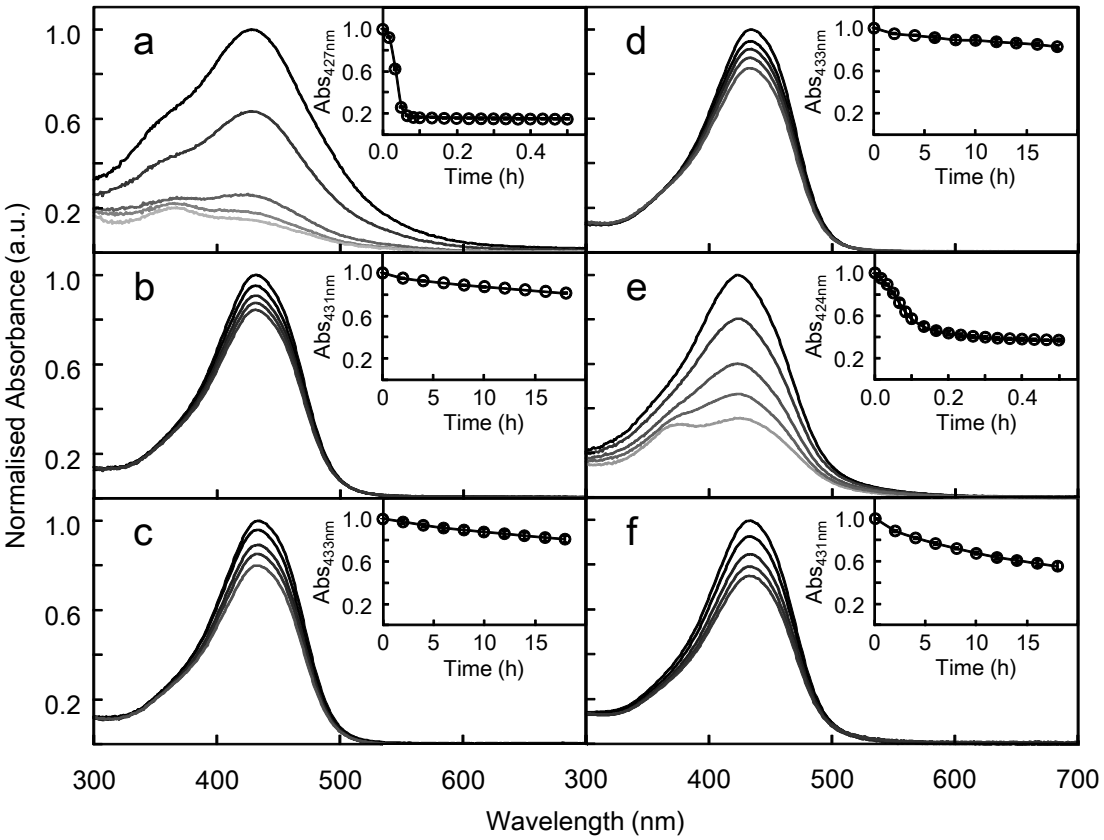

Figure 5.2. Time-dependent UV-visible absorption spectra of 30 µM curcumin in (a) pH 7.4 phosphate buffer solution, those in PAAC18 at (b) 0.3 wt%, (c) 1.0 wt% and (d) 2.0 wt%, and those in (e) PAAC12 at 1.0 wt% and (f) 10%-PAAC12 at 0.5 wt%, at 37 °C. Spectra were recorded for 0.5 h in the panels (a) and (e) and 18 h in the panels (b−d) and (f). The insets show the decays of the absorption maxima due to degradation of curcumin, which are fitted to a mathematical function to estimate values of half-lives. A 0.5 wt% solution of 10%-PAAC12 possesses the equivalent number of substituent carbons to 1.0 wt% PAAC18. Note that only selected data are shown for clarity purposes.

Table 5.1. Modified polyacrylate concentrations, half-life ($t_{1/2}$) of curcumin degradation, hydrodynamic diameters and zeta potential of micelle-like aggregates and fluid hydrogels of PAAC18, PAAC12 and 10%-PAAC12.

Polyacrylate	[Curcumin] (μM)	$t_{1/2}$ (h)[a]	Diameter ± SD (μm)[b,c]	Zeta potential (mV)[c]
–	30	0.04 ± 0.01	–	–
0.3wt% PAAC18	–	–	0.86 ± 0.14	-70 ± 6
0.3wt% PAAC18	30	71.6 ± 4.0	0.98 ± 0.22	–
1.0wt% PAAC18	–	–	1.12 ± 0.17	-73 ± 5
1.0wt% PAAC18	30	74.0 ± 9.4	1.15 ± 0.22	–
2.0wt% PAAC18	–	–	>6[d]	–
2.0wt% PAAC18	30	98.6 ± 16.2	>6[d]	–
1.0wt% PAAC12	–	–	1.40 ± 0.29	-70 ± 7, -35 ± 5
1.0wt% PAAC12	30	0.07 ± 0.02	1.35 ± 0.38	–
0.5wt% 10%-PAAC12	–	–	1.42 ± 0.44	-64 ± 6
0.5wt% 10%-PAAC12	30	22.3 ± 4.0	2.26 ± 0.92	–

[a] In aqueous 50 mM phosphate buffer at pH 7.4 and 37 °C.

[b] Mean hydrodynamic diameter and standard deviation (SD) of a distribution.

[c] At 25 °C (ionic strength of 30–60 mM).

[d] Meaningful data was not obtained for 2.0 wt% PAAC18 solutions due to the instrument detection limit of 6 μm and its unsuitability for use with viscous samples.

solutions at 1.0 wt% ($\sim 2 \times 10^{-3}$ Pa s) and 2.9 wt% ($\sim 8 \times 10^{-3}$ Pa s) are similar to those of PAAC18 solutions at 0.5 wt% and 1.0 wt%, respectively [49], which infers that similar levels of cross-linking between polyacrylate strands are present. Thus, PAAC12 at these concentrations should exhibit similar abilities to suppress curcumin degradation. However, the time-dependent UV-visible absorption spectra showed that solutions of PAAC12 at 1.0 wt% and 2.9 wt% are ineffective in inhibiting curcumin degradation, as shown in Figure 5.2e (0.07 ± 0.01 h, Table 5.1) and Figure B.1 in Appendix B, respectively. These results indicate that the alkyl substituent must be sufficiently long to capture curcumin to suppress its degradation. The effect of 10%-PAAC12 solution at 0.5 wt% was also investigated to give insight into the effect of the degree of polyacrylate substitution on the aqueous stabilisation of curcumin. At this concentration, 10%-PAAC12 possesses the same number of substituent carbons as does PAAC18 solution at 1.0 wt%. The time-dependent UV-visible absorption spectra of curcumin in 0.5 wt% 10%-PAAC12 solution show that the rate of curcumin degradation is slowed (Figure 5.2f), which is consistent with a considerable increase of its half-life (22.3 ± 4.0 h, Table 5.1). However, this suppression of curcumin degradation is less than that achieved in 1.0 wt% PAAC18 solution (Figure 5.2c, Table 5.1) despite of the equivalent number of substituent alkyl carbons. This result indicates that the length of the substituent has a more substantial effect on the aqueous stability of curcumin than the effect of the extent of polyacrylate substitution or the concentration of the polyacrylate. Similarly, the rate of release of curcumin from PAAC12 can be inferred from the rate of degradation and the results are shown in Figure B.2 in Appendix B. Overall, the results show the presence of strong interactions between curcumin and the octadecyl substituents of PAAC18.

5.4.2 Binding Constant of the PAAC18-Curcumin Complex

A systematic variation in the molar absorbance maximum of curcumin, ε, and its wavelength, λ, occur as a curcumin stock solution is titrated into an aqueous PAAC18 solution at pH 7.4 and 37 °C (Figure 5.3a), consistent with the binding of curcumin by the octadecyl substituents of PAAC18, as follows. This binding may be represented by eq 5.1 where a group of n octadecyl substituents of PAAC18, $(C18)_n$, binds to a single curcumin molecule, Cur, to form a complex, $(C18)_n$-Cur:

$$(C18)_n + \text{Cur} \rightleftharpoons (C18)_n\text{-Cur} \tag{5.1}$$

The binding constant, K_n, at equilibrium is given by

$$K_n = \frac{[(\mathrm{C18})_n\text{-Cur}]}{[(\mathrm{C18})_n][\mathrm{Cur}]} \tag{5.2}$$

Given that $[(\mathrm{C18})_n]_0$ and $[\mathrm{Cur}]_0$ are the initial concentrations:

$$[\mathrm{Cur}]_0 = [(\mathrm{C18})_n\text{-Cur}] + [\mathrm{Cur}] \tag{5.3}$$

$$[(\mathrm{C18})_n]_0 = [(\mathrm{C18})_n\text{-Cur}] + [(\mathrm{C18})_n] \tag{5.4}$$

It follows that the molar absorbance at a particular wavelength, $\mathrm{A}(\lambda)$, is given by

$$\mathrm{A}(\lambda) = \varepsilon(\lambda)\cdot\ell\cdot[\mathrm{Cur}]_0 \tag{5.5}$$

$$= \varepsilon_{\mathrm{Cur}}(\lambda)\cdot\ell\cdot[\mathrm{Cur}] + \varepsilon_{(\mathrm{C18})_n\text{-Cur}}(\lambda)\cdot\ell\cdot[(\mathrm{C18})_n\text{-Cur}] \tag{5.6}$$

where ε, $\varepsilon_{\mathrm{Cur}}$ and $\varepsilon_{(\mathrm{C18})_n\text{-Cur}}$ are the observed molar absorptivity and the molar absorptivities of Cur and $(\mathrm{C18})_n$-Cur, respectively. The magnitude of K_n was determined by best-fitting an algorithm derived through eqs 5.2–5.6 to the variation of the molar absorbance, A, at 0.5 nm intervals over the range 400–500 nm with the ratio $[(\mathrm{C18})_n]/[\mathrm{Cur}]$ for n = 1–10.

The number of substituents involved in complexation may vary with the total [C18] such that complexations of different stoichiometries arise, but it is not possible to carry out a calculation to determine the exact nature of this variation. Thus, several calculations were carried out for the equilibria shown in eqs 5.1–5.2 where a group of n octadecyl substituents for the complex $(\mathrm{C18})_n$-Cur was varied in the range of $1 \leq n \leq 10$, using the quantities in eqs 5.3–5.4 to derive an algorithm based on eqs 5.5–5.6 to best fit to the absorbance data. The variations of λ_{max} and ε_{max} as increasing the total curcumin concentrations are shown in Figure 5.3a. The variations indicate changes in the complexation of curcumin by the octadecyl substituents of PAAC18. A satisfactory fit could not be obtained for the binding of single octadecyl substituent and single curcumin ($n = 1$), but good fits were obtained for n = 2–10 for which K_n are plotted in Figure 5.3b. (The binding constants, K_n for other n values appear in Table B.1 in Appendix B.) The largest derived binding constant of $(2.1 \pm 0.1) \times 10^4$ M^{-1} corresponds to n = 5, which implies that the most favourable binding involves a single curcumin and five octadecyl substituents of PAAC18 on average. It is probable that there is a small variation of n around n = 5 in a dynamic equilibrium, but the binding model used here does not allow an exploration of this. The binding constant of $(\mathrm{C18})_5$-curcumin complex is comparable to those of curcumin in micellar solutions

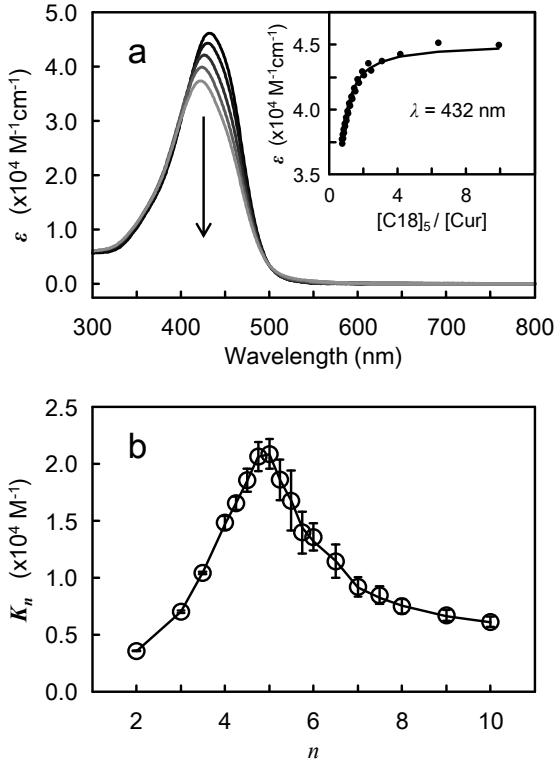

Figure 5.3. (a) Molar absorptivity (ε) as a function of λ for curcumin in titration studies in pH 7.4 phosphate buffer at 37 °C, where the arrow shows that direction of change in λ_{max} and ε with a decrease in $[C18]_5$/[Cur] ratio. The inset shows the variation of ε with $[C18]_5$/[Cur] ratio at 432 nm and the solid line represents the best fit of the algorithm obtained in the range 400–500 nm. (b) Binding constants (K_n) of the $(C18)_n$-curcumin complex as a function of n. Note that only selected data are shown for clarity purposes.

[24, 27]. Moreover, analysis of the results revealed that the molar absorptivity of $(C18)_n$-curcumin complex is $4.47 \times 10^4\ M^{-1}\ cm^{-1}$ at $\lambda_{max} = 432$ nm, while curcumin alone in buffer possesses an ε_{Cur} of $2.20 \times 10^4\ M^{-1}\ cm^{-1}$ at $\lambda_{max} = 427$ nm.

5.4.3 2D NOESY ^{1}H NMR Study of PAAC18-Curcumin Complex

The 2D NOESY ^{1}H NMR spectrum of a 1.0-mM solution of curcumin in a 1.0 wt% solution of PAAC18 in D_2O, shown in Figure 5.4, provides evidence for curcumin binding by the octadecyl substituents of PAAC18. The ^{1}H resonances arising from the curcumin CH protons appear in the range 6.3–7.4 ppm and those of methoxy (OCH_3) protons appear at 3.8 ppm in this solution. These proton peaks are broadened and show upfield shifts by comparison with curcumin alone in either deuterated chloroform or DMSO-d_6 solutions (Table B.2 in Appendix B) [54, 55]. Within the PAAC18 spectrum, the polyacrylate backbone CH and CH_2 resonances appear in the range 1.3–2.4 ppm, while the octadecyl substituent CH_3, CH_2 and N-CH_2 resonances appear at ~ 0.6 ppm, ~ 1.5 ppm and 3.1 ppm, respectively. Strong cross-peaks arise from the through-space interactions of the CH protons of curcumin with the CH_2 and CH_3 protons of the octadecyl substituents of PAAC18 (enclosed in a bold rectangle) and those from interactions between the OCH_3 protons of curcumin and those of the octadecyl substituents of PAAC18 (enclosed in plain rectangles). These results indicate an interaction distance of ≤ 400 pm between these protons. However, no cross-peaks between curcumin and either the octadecyl N-CH_2 protons or the polyacrylate backbone CH and CH_2 protons were observed, which is consistent with the dominant interaction between the octadecyl substituents and curcumin. The 2D NOESY ^{1}H NMR spectrum of a slightly viscous sample of 2.0-mM curcumin in 1.0 wt% 10%-PAAC12 solution shows substantial broadening of the proton resonances of both curcumin and 10%-PAAC12 (Figure B.3 in Appendix B). This result is consistent with decreased transverse proton relaxation times arising from a lengthened tumbling time and a consequently decreased effectiveness of through-space dipolar interactions, resulting in the absence of significant cross-peaks (Figure B.3 in Appendix B). These observations are consistent with the effectiveness of the suppression of curcumin degradation through binding by PAAC18, PAAC12 and 10%-PAAC12 being substantially dependent on the relative lengths of the octadecyl and dodecyl substituents and curcumin which are approximately 2160, 1400 and 1920 pm, respectively. Although increasing the local concentration of the dodecyl substituent in 10%-PAAC12 offsets this disadvantage of the shorter substituent to some extent, curcumin is more likely to be fully encapsulated in hydrophobic do-

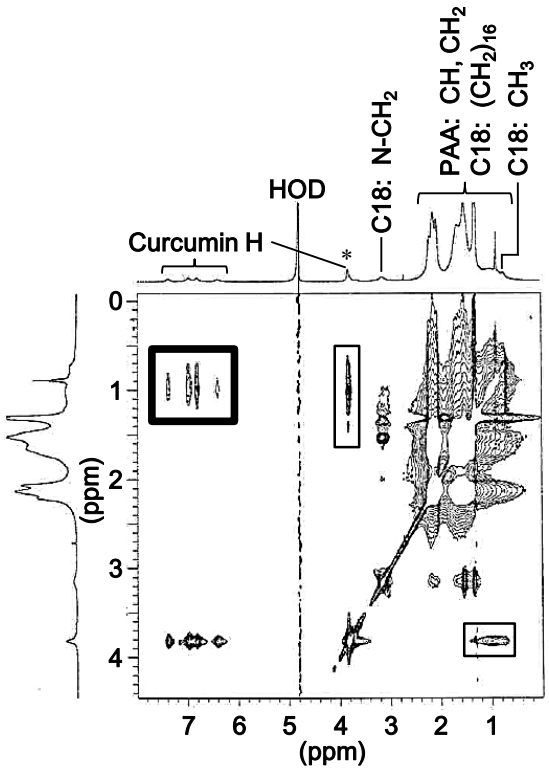

Figure 5.4. 2D NOESY ^{1}H NMR spectrum of 1.0-mM curcumin in a 1.0 wt% PAAC18 solution in D_2O at pD 7. The cross-peaks arising from the interactions between the octadecyl substituent protons and the curcumin CH and CH_3O protons are enclosed in bold and plain rectangles, respectively. The asterisk indicates the curcumin CH_3O resonance.

mains of octadecyl substituent aggregates formed by PAAC18 rather than those of dodecyl substituent aggregates formed by PAAC12.

5.4.4 Hydrodynamic Diameters of PAAC18, PAAC12 and 10%-PAAC12 Micelle-Like Aggregates

It was suggested earlier that PAAC18 and PAAC12 exist as micelle-like aggregates at low concentrations in aqueous solutions due to the presence of intra-polyacrylate cross-links formed by association between either octadecyl or dodecyl substituents [48, 49]. In this study, hydrodynamic diameters and zeta potentials of PAAC18, PAAC12 and 10%-PAAC12 provide insight into the formation of micelle-like aggregates and their differing abilities to suppress the degradation of curcumin (Table 5.1). The 0.3 wt% solution of PAAC18 forms aggregates with a mean hydrodynamic diameter of 0.86 µm (Figure 5.5a). The incorporation of curcumin causes a

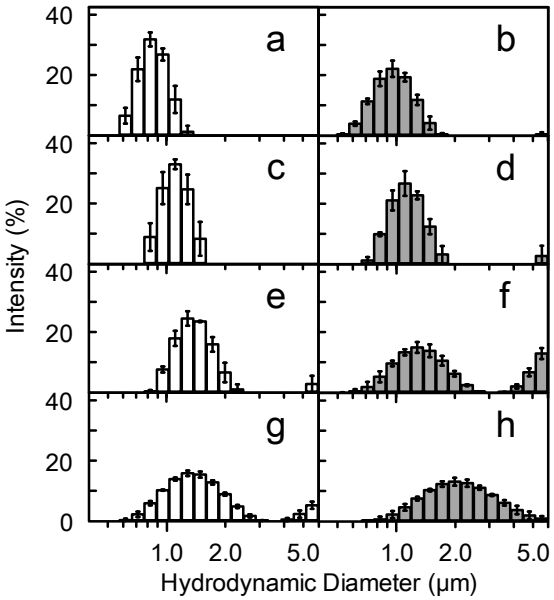

Figure 5.5. Hydrodynamic diameter distributions of (a−b) 0.3 wt% PAAC18, (c−d) 1.0 wt% PAAC18, (e−f) 1.0 wt% PAAC12, and (g−h) 0.5 wt% 10%-PAAC12 aqueous solutions, in the absence (unfilled) and presence (filled) of 30 μM curcumin.

small change in the hydrodynamic diameter of the micelle-like aggregates to 0.98 μm and an increase in the width of the distribution (as its standard deviation) from 0.14 μm to 0.22 μm, as shown in Figure 5.5b. Similarly, Figures 5.5c and 5.5d show that the mean diameter of the PAAC18 micelle-like aggregates is 1.12 μm at 1.0 wt% and that the addition of curcumin causes a negligible change (Table 5.1). These results suggest that the increased concentration of PAAC18 allows more extensive cross-linking among octadecyl substituents and an increase in aggregate size. Thus, the octadecyl intra-strand associations of PAAC18 are sufficiently strong to maintain the micelle-like structure of the hydrophobic substituents in the presence of curcumin. A more viscous solution of 2.0 wt% PAAC18, however, produced inconsistent size distributions (data not shown), probably due to a high level of inter-strand cross-linking resulting in large aggregates with hydrodynamic diameter over the detection limit of 6 μm, consistent with the formation of a hydrogel network.

Figure 5.5e shows that a solution of PAAC12 at 1.0 wt% has a mean hydrodynamic diameter of 1.40 μm, which is larger than those of PAAC18 at 0.3 wt% and 1.0 wt%. This is consistent with the shorter dodecyl substituents forming looser aggregates than do the octadecyl substituents. The incorporation of curcumin increases the width of the distribution from 0.29 μm to 0.38 μm for the smaller aggregate and causes the formation of larger aggregates, as shown in Figure 5.5f. The overall effect

may be that curcumin is more exposed to water, which is consistent with the rapid degradation of curcumin observed under these conditions (Figure 5.2e). Figures 5.5g and 5.5h show that the mean hydrodynamic diameter of the 10%-PAAC12 micelle-like aggregates is 1.42 µm at 0.5 wt% and the presence of curcumin significantly shifts the mean hydrodynamic diameter to 2.26 µm, with a corresponding change in the distribution width from 0.44 µm to 0.92 µm. Thus, addition of curcumin appears to reduce dodecyl intra-strand polyacrylate associations of 10%-PAAC12, resulting in the wider hydrodynamic diameter distribution of the micelle-like aggregates. Nevertheless, the degradation of curcumin is greatly slowed ($t_{1/2}$ = 22.3 h) by comparison with that in PAAC12 at 1.0 wt% ($t_{1/2}$ = 0.07 h) as a consequence of the greater concentration of dodecyl substituents in 10%-PAAC12. These results suggest that the reduced intra-strand associations of dodecyl hydrophobic substituents of PAAC12 and 10%-PAAC12 are related to their lesser ability to suppress curcumin degradation by comparison with PAAC18. It has been shown in previous studies that sodium dodecyl sulphate (SDS) and dodecyl trimethylammonium bromide (DTAB) micelles are effective in stabilising curcumin [25, 28]. However, in this study, PAAC12 exhibits no stabilising effects even though it also has dodecyl groups. It should be noted that the number of dodecyl groups per curcumin in a SDS or DTAB micelle is > 60 [56]. Although a similar ratio of dodecyl groups to curcumin is found in 1.0 wt% PAAC12, it is clear that not all dodecyl groups are involved in binding of curcumin due to the large aggregate size, as shown in Figures 5.5e and 5.5f. It is highly likely that the available dodecyl groups for curcumin binding is significantly less than 60 in 1.0 wt% PAAC12, which contributes to its inability to stabilise curcumin. From these observations, it is clear that the greater ability of the octadecyl substituents to aggregate is the origin of PAAC18 being more effective in suppressing curcumin degradation than PAAC12 and 10%-PAAC12. The smaller hydrodynamic diameters of the micelle-like aggregates of PAAC18 than those of PAAC12 are attributed to the formation of more strongly bound aggregates, which is consistent with the significant decrease in the curcumin degradation rate in the presence of PAAC18 (Figures 5.2b−5.2d).

5.4.5 Zeta Potentials of PAAC18, PAAC12 and 10%-PAAC12 Micelle-Like Aggregates

The zeta potentials determined for the PAAC18, PAAC12 and 10%-PAAC12 systems, which are attributable to the negatively charged polyacrylate carboxylate groups, are shown in Figure 5.6. The high zeta potential values of PAAC18 at 0.3 wt% and 1.0 wt% of -70 ± 6 mV and -73 ± 5 mV, respectively (Table 5.1 and Figures

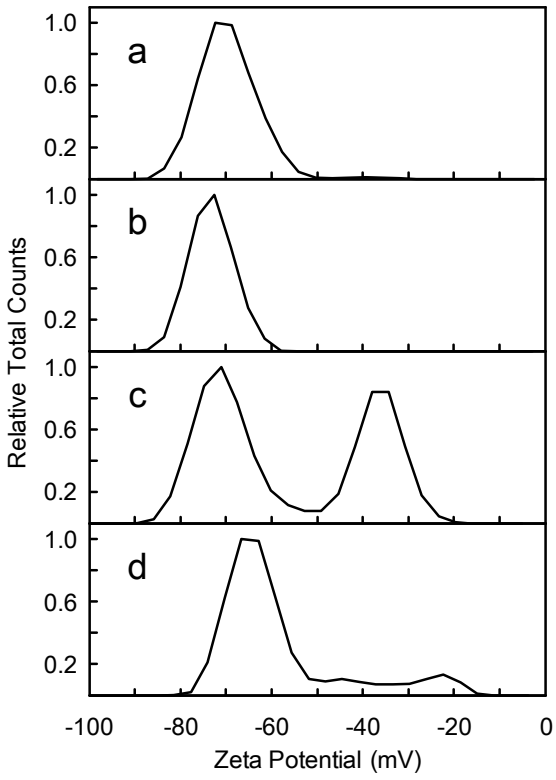

Figure 5.6. Zeta potential measurements of aqueous solutions of PAAC18 at (a) 0.3 wt% and (b) 1.0 wt%, (c) PAAC12 at 1.0 wt%, and (d) 10%-PAAC12 at 0.5 wt%.

5.6a−5.6b), are consistent with the formation of stable colloidal micelle-like aggregates as indicated by no precipitation occurring over 30 days. This is similar to the behaviour of other highly stable colloidal systems of similar zeta potentials [57]. Two zeta potentials of -70 ± 7 mV and -35 ± 5 mV were determined for a PAAC12 solution at 1.0 wt% (Figure 5.6c). The main zeta potential peak of 10%-PAAC12 is located at -64 ± 6 mV, and minor broad peak arises around -40 mV (Figure 5.6d). The zeta potential values of -70 mV and -64 mV for PAAC12 and 10%-PAAC12, respectively, correspond to the micelle-like aggregates, while the smaller zeta potential peaks may be attributable to the presence of non-aggregated substituents of PAAC12 and 10%-PAAC12, which are consistent with their distributions of hydrodynamic diameters (Figures 5.5e and 5.5g). The much greater non-aggregated substituent component for PAAC12 is probably related to its inability to suppress curcumin degradation as shown in Figure 5.2e.

5.5 Conclusions

This study highlights the potential applications of curcumin micelle-like aggregates and hydrogels formed using hydrophobically modified polyacrylates as model curcumin delivery systems. The capture of the medicinal pigment curcumin by the hydrophobically modified polyacrylates, PAAC18 and 10%-PAAC12 helps identify some of the factors which stabilise curcumin in aqueous solution. The length of the octadecyl substituent of PAAC18 and its aggregation with curcumin in both micelle-like aggregates and hydrogels show a remarkable combined ability to suppress its degradation, as indicated by an increase in the curcumin half-life by a factor of 1600–2000. At the molecular level, results from 2D NOESY ^{1}H NMR spectroscopy indicate that the association of curcumin with octadecyl substituents of PAAC18 occurs through hydrophobic interactions, where those from UV-visible absorption titration show that it occurs dominantly through five octadecyl substituents binding curcumin with a $K_5 = (2.1 \pm 0.1) \times 10^4\ \mathrm{M}^{-1}$. These molecular interactions underpin the macroscopic observations of hydrodynamic diameters and zeta potentials which indicate the formation of micelle-like aggregates and hydrogels of PAAC18. The shorter dodecyl substituent of PAAC12 is ineffective in suppressing curcumin degradation. While the more highly substituted 10%-PAAC12 shows an improved stabilisation of curcumin, it is less effective than PAAC18. In conclusion, the octadecyl hydrophobic substituents of PAAC18 possess a significant ability to stabilise curcumin in both micelle-like aggregates and hydrogels under physiological conditions.

5.6 References

(1) Leung, M. H. M.; Harada, T.; Kee, T. W. Delivery of Curcumin and Medicinal Effects of the Copper(II)-Curcumin Complexes. *Curr. Pharm. Des.* **2013**, *19*, 2070–2083.

(2) Sa, G.; Das, T. Anti-Cancer Effects of Curcumin: Cycle of Life and Death. *Cell Division* **2008**, *3*, 1–14.

(3) Anand, P.; Thomas, S. G.; Kunnumakkara, A. B.; Sundaram, C.; Harikumar, K. B.; Sung, B.; Tharakan, S. T.; Misra, K.; Priyadarsini, I. K.; Rajasekharan, K. N.; Aggarwal, B. B. Biological Activities of Curcumin and Its Analogues (Congeners) Made by Man and Mother Nature., English *Biochem. Pharmacol.* **2008**, *76*, 1590–1611.

(4) Hatcher, H.; Planalp, R.; Cho, J.; Tortia, F. M.; Torti, S. V. Curcumin: From Ancient Medicine to Current Clinical Trials. *Cell. Mol. Life Sci.* **2008**, *65*, 1631–1652.

(5) Huang, M. T.; Lou, Y. R.; Ma, W.; Newmark, H. L.; Reuhl, K. R.; Conney, A. H. Inhibitory Effects of Dietary Curcumin on Forestomach, Duodenal, and Colon Carcinogenesis in Mice. *Cancer Res.* **1994**, *54*, 5841–5847.

(6) Rao, C. V.; Rivenson, A.; Simi, B.; Reddy, B. S. Chemoprevention of Colon Carcinogenesis by Dietary Curcumin, A Naturally-Occurring Plant Phenolic Compound. *Cancer Res.* **1995**, *55*, 259–266.

(7) Sharma, O. P. Antioxidant Activity of Curcumin and Related Compounds. *Biochem. Pharmacol.* **1976**, *25*, 1811–1812.

(8) Aggarwal, B. B.; Kumar, A.; Bharti, A. C. Anticancer Potential of Curcumin: Preclinical and Clinical Studies. *Anticancer Res.* **2003**, *23*, 363–398.

(9) Lantz, R. C.; Chen, G. J.; Solyom, A. M.; Jolad, S. D.; Timmermann, B. N. The Effect of Turmeric Extracts on Inflammatory Mediator Production. *Phytomedicine* **2005**, *12*, 445–452.

(10) Lim, G. P.; Chu, T.; Yang, F. S.; Beech, W.; Frautschy, S. A.; Cole, G. M. The Curry Spice Curcumin Reduces Oxidative Damage and Amyloid Pathology in an Alzheimer Transgenic Mouse. *J. Neurosci.* **2001**, *21*, 8370–8377.

(11) Ono, K.; Hasegawa, K.; Naiki, H.; Yamada, M. Curcumin Has Potent Anti-Amyloidogenic Effects for Alzheimer's β-Amyloid Fibrils In Vitro. *J. Neurosci. Res.* **2004**, *75*, 742–750.

(12) Yang, F. S.; Lim, G. P.; Begum, A. N.; Ubeda, O. J.; Simmons, M. R.; Ambegaokar, S. S.; Chen, P. P.; Kayed, R.; Glabe, C. G.; Frautschy, S. A.; Cole, G. M. Curcumin Inhibits Formation of Amyloid β Oligomers and Fibrils, Binds Plaques, and Reduces Amyloid In Vivo. *J. Biol. Chem.* **2005**, *280*, 5892–5901.

(13) Cartiera, M. S.; Ferreira, E. C.; Caputo, C.; Egan, M. E.; Caplan, M. J.; Saltzman, W. M. Partial Correction of Cystic Fibrosis Defects with PLGA Nanoparticles Encapsulating Curcumin. *Mol. Pharmaceutics* **2010**, *7*, 86–93.

(14) Egan, M. E.; Pearson, M.; Weiner, S. A.; Rajendran, V.; Rubin, D.; Glockner-Pagel, J.; Canny, S.; Du, K.; Lukacs, G. L.; Caplan, M. J. Curcumin, a Major Constituent of Turmeric, Corrects Cystic Fibrosis Defects. *Science* **2004**, *304*, 600–602.

(15) Cheng, A. L.; Hsu, C. H.; Lin, J. K.; Hsu, M. M.; Ho, Y. F.; Shen, T. S.; Ko, J. Y.; Lin, J. T.; Lin, B. R.; Wu, M. S.; Yu, H. S.; Jee, S. H.; Chen, G. S.; Chen, T. M.; Chen, C. A.; Lai, M. K.; Pu, Y. S.; Pan, M. H.; Wang, Y. J.; Tsai, C. C.; Hsieh, C. Y. Phase I Clinical Trial of Curcumin, a Chemopreventive Agent, in Patients with High-Risk or Pre-Malignant Lesions. *Anticancer Res.* **2001**, *21*, 2895–2900.

(16) Sharma, R. A.; Euden, S. A.; Platton, S. L.; Cooke, D. N.; Shafayat, A.; Hewitt, H. R.; Marczylo, T. H.; Morgan, B.; Hemingway, D.; Plummer, S. M.; Pirmohamed, M.; Gescher, A. J.; Steward, W. P. Phase I Clinical Trial of oral Curcumin: Biomarkers of Systemic Activity and Compliance. *Clin. Cancer Res.* **2004**, *10*, 6847–6854.

(17) ClinicalTrials.gov, Trial of Curcumin in Advanced Pancreatic Cancer., M.D. Anderson Cancer Center, `http://clinicaltrials.gov/ct2/show/NCT00094445`.

(18) ClinicalTrials.gov, Curcumin in Patients With Mild to Moderate Alzheimer's Disease., `http://clinicaltrials.gov/ct2/show/NCT00099710`.

(19) Kaminaga, Y.; Nagatsu, A.; Akiyama, T.; Sugimoto, N.; Yamazaki, T.; Maitani, T.; Mizukami, H. Production of Unnatural Glucosides of Curcumin with Drastically Enhanced Water Solubility by Cell Suspension Cultures of Catharanthus Roseus. *FEBS Lett.* **2003**, *555*, 311–316.

(20) Letchford, K.; Liggins, R.; Burt, H. Solubilization of Hydrophobic Drugs by Methoxy Poly(ethylene glycol)-block-polycaprolactone Diblock Copolymer Micelles: Theoretical and Experimental Data and Correlations. *J. Pharm. Sci.* **2008**, *97*, 1179–1190.

(21) Harada, T.; Pham, D.-T.; Leung, M. H. M.; Ngo, H. T.; Lincoln, S. F.; Easton, C. J.; Kee, T. W. Cooperative Binding and Stabilization of the Medicinal Pigment Curcumin by Diamide Linked γ-Cyclodextrin Dimers: A Spectroscopic Characterization. *J. Phys. Chem. B* **2011**, *115*, 1268–1274.

(22) Leung, M. H. M.; Kee, T. W. Effective Stabilization of Curcumin by Association to Plasma Proteins: Human Serum Albumin and Fibrinogen. *Langmuir* **2009**, *25*, 5773–5777.

(23) Wang, Y. J.; Pan, M. H.; Cheng, A. L.; Lin, L. I.; Ho, Y. S.; Hsieh, C. Y.; Lin, J. K. Stability of Curcumin in Buffer Solutions and Characterization of Its Degradation Products. *J. Pharm. Biomed. Anal.* **1997**, *15*, 1867–1876.

(24) Iwunze, M. O. Binding and Distribution Characteristics of Curcumin Solubilized in CTAB Micelle. *J. Mol. Liq.* **2004**, *111*, 161–165.

(25) Leung, M. H. M.; Colangelo, H.; Kee, T. W. Encapsulation of Curcumin in Cationic Micelles Suppresses Alkaline Hydrolysis. *Langmuir* **2008**, *24*, 5672–5675.

(26) Tønnesen, H. H. Solubility, Chemical and Photochemical Stability of Curcumin in Surfactant Solutions - Studies of Curcumin and Curcuminolds, XXVIII. *Pharmazie* **2002**, *57*, 820–824.

(27) Sahu, A.; Kasoju, N.; Bora, U. Fluorescence Study of the Curcumin-Casein Micelle Complexation and Its Application as a Drug Nanocarrier to Cancer Cells. *Biomacromolecules* **2008**, *9*, 2905–2912.

(28) Wang, Z. F.; Leung, M. H. M.; Kee, T. W.; English, D. S. The Role of Charge in the Surfactant-Assisted Stabilization of the Natural Product Curcumin. *Langmuir* **2010**, *26*, 5520–5526.

(29) Barik, A.; Mishra, B.; Kunwar, A.; Priyadarsini, K. I. Interaction of Curcumin with Human Serum Albumin: Thermodynamic Properties, Fluorescence Energy Transfer and Denaturation Effects. *Chem. Phys. Lett.* **2007**, *436*, 239–243.

(30) Barik, A.; Priyadarsini, K. I.; Mohan, H. Photophysical Studies on Binding of Curcumin to Bovine Serum Albumin. *Photochem. Photobiol.* **2003**, *77*, 597–603.

(31) Baglole, K. N.; Boland, P. G.; Wagner, B. D. Fluorescence Enhancement of Curcumin upon Inclusion into Parent and Modified Cyclodextrins. *J. Photochem. Photobiol. A* **2005**, *173*, 230–237.

(32) Singh, R.; Tønnesen, H. H.; Vogensen, S. B.; Loftsson, T.; Másson, M. Studies of Curcumin and Curcuminoids. XXXVI. The Stoichiometry and Complexation Constants of Cyclodextrin Complexes as Determined by the Phase-Solubility Method and UV-Vis Titration. *J. Incl. Phenom. Macro.* **2010**, *66*, 335–348.

(33) Mohanty, C.; Sahoo, S. K. The In Vitro Stability and In Vivo Pharmacokinetics of Curcumin Prepared as an Aqueous Nanoparticulate Formulation. *Biomaterials* **2010**, *31*, 6597–6611.

(34) Shaikh, J.; Ankola, D. D.; Beniwal, V.; Singh, D.; Kumar, M. N. V. R. Nanoparticle Encapsulation Improves Oral Bioavailability of Curcumin by at Least 9-fold when Compared to Curcumin Administered with Piperine as Absorption Enhancer. *Eur. J. Pharm. Sci.* **2009**, *37*, 223–230.

(35) Bisht, S.; Feldmann, G.; Soni, S.; Ravi, R.; Karikar, C.; Maitra, A.; Maitra, A. Polymeric Nanoparticle-Encapsulated Curcumin ("Nanocurcumin"): A Novel Strategy for Human Cancer Therapy. *J. Nanobiotechnology* **2007**, *5*, 18.

(36) Agnihotri, S. A.; Mallikarjuna, N. N.; Aminabhavi, T. M. Recent Advances on Chitosan-Based Micro- and Nanoparticles in Drug Delivery. *J. Controlled Release* **2004**, *100*, 5–28.

(37) Dong, L. C.; Yan, Q.; Hoffman, A. S. Controlled Release of Amylase from a Thermal and pH-Sensitive, Macroporous Hydrogel. *J. Controlled Release* **1992**, *19*, 171–177.

(38) Ende, M. T. A.; Peppas, N. A. Transport of Ionizable Drugs and Proteins in Crosslinked Poly(acrylic acid) and Poly(acrylic acid-co-2-hydroxyethyl methacrylate) Hydrogels. 2. Diffusion and Release Studies. *J. Controlled Release* **1997**, *48*, 47–56.

(39) Peppas, N. A.; Hilt, J. Z.; Khademhosseini, A.; Langer, R. Hydrogels in Biology and Medicine: From Molecular Principles to Bionanotechnology. *Adv. Mater.* **2006**, *18*, 1345–1360.

(40) Suh, J. K. F.; Matthew, H. W. T. Application of Chitosan-Based Polysaccharide Biomaterials in Cartilage Tissue Engineering: A Review. *Biomaterials* **2000**, *21*, 2589–2598.

(41) Yan, Q.; Hoffman, A. S. Synthesis of Macroporous Hydrogels with Rapid Swelling and Deswelling Properties for Delivery of Macromolecules. *Polymer* **1995**, *36*, 887–889.

(42) Peppas, N. A.; Bures, P.; Leobandung, W.; Ichikawa, H. Hydrogels in Pharmaceutical Formulations. *Eur. J. Pharm. Biopharm.* **2000**, *50*, 27–46.

(43) Tuntikulwattana, S.; Sinchaipanid, N.; Ketjinda, W.; Williams, D. B.; Mitrevej, A. Fabrication of Chitosan-Polyacrylic Acid Complexes as Polymeric Osmogents for Swellable Micro/Nanoporous Osmotic Pumps. *Drug Dev. Ind. Pharm.* **2011**, *37*, 926–933.

(44) Torrado, S.; Prada, P.; de la Torre, P. M.; Torrado, S. Chitosan-Poly(acrylic) Acid Polyionic Complex: In Vivo Study to Demonstrate Prolonged Gastric Retention. *Biomaterials* **2004**, *25*, 917–923.

(45) Grimm, S.; Giesa, R.; Sklarek, K.; Langner, A.; Gosele, U.; Schmidt, H. W.; Steinhart, M. Nondestructive Replication of Self-Ordered Nanoporous Alumina Membranes via Cross-Linked Polyacrylate Nanofiber Arrays. *Nano Lett.* **2008**, *8*, 1954–1959.

(46) Xie, B. J.; Parkhill, R. L.; Warren, W. L.; Smay, J. E. Direct Writing of Three-Dimensional Polymer Scaffolds using Colloidal Gels. *Adv. Funct. Mater.* **2006**, *16*, 1685–1693.

(47) Wang, K. T.; Iliopoulos, I.; Audebert, R. Viscometric Behaviour of Hydrophobically Modified Poly(sodium acrylate). *Polym. Bull.* **1988**, *20*, 577–582.

(48) Guo, X.; Abdala, A. A.; May, B. L.; Lincoln, S. F.; Khan, S. A.; Prud'homme, R. K. Rheology Control by Modulating Hydrophobic and Inclusion Associations in Modified Poly(acrylic acid) Solutions. *Polymer* **2006**, *47*, 2976–2983.

(49) Wang, J.; Li, L.; Ke, H.; Liu, P.; Zheng, L.; Guo, X.; Lincoln, S. F. Rheology Control by Modulating Hydrophobic and Inclusive Associations of Side-Groups in Poly(acrylic acid). *Asia-Pac. J. Chem. Eng.* **2009**, *4*, 537–543.

(50) Gans, P.; Sabatini, A.; Vacca, A. Investigation of Equilibria in Solution. Determination of Equilibrium Constants with the HYPERQUAD Suite of Programs. *Talanta* **1996**, *43*, 1739–1753.

(51) Protonic Software., `http://www.hyperquad.co.uk/`.

(52) Chem3D Ultra., `http://www.cambridgesoft.com/`.

(53) Tønnesen, H. H.; Karlsen, J. Studies on Curcumin and Curcuminoids. 5. Alkaline-Degradation of Curcumin. *Z. Lebensm. Unters. Forsch.* **1985**, *180*, 132–134.

(54) Anderson, A. M.; Mitchell, M. S.; Mohan, R. S. Isolation of Curcumin from Turmeric. *J. Chem. Educ.* **2000**, *77*, 359–360.

(55) Jayaprakasha, G. K.; Rao, L. J. M.; Sakariah, K. K. Improved HPLC Method for the Determination of Curcumin, Demethoxycurcumin, and Bisdemethoxycurcumin. *J. Agric. Food Chem.* **2002**, *50*, 3668–3672.

(56) Griffiths, P. C.; Paul, A.; Khayat, Z.; Heenan, R. K.; Ranganathan, R.; Grillo, I. A Small-Angle Neutron Scattering Study of Biologically Relevant Mixed Surfactant Micelles Comprising 1,2-Diheptanoyl-*sn*-phosphatidylcholine and Sodium Dodecyl Sulfate or Dodecyltrimethylammonium Bromide. *Soft Matter* **2005**, *1*, 152–159.

(57) Jin, Y.; Ye, F.; Wu, C.; Chan, Y.-H.; Chiu, D. T. Generation of Functionalized and Robust Semiconducting Polymer Dots with Polyelectrolytes. *Chem. Commun.* **2012**, *48*, 3161–3163.

Chapter 6

Ultrafast Dynamics of the Medicinal Pigment Curcumin and Solvation Dynamics of Water in Octadecyl Substituted Polyacrylate Hydrogel

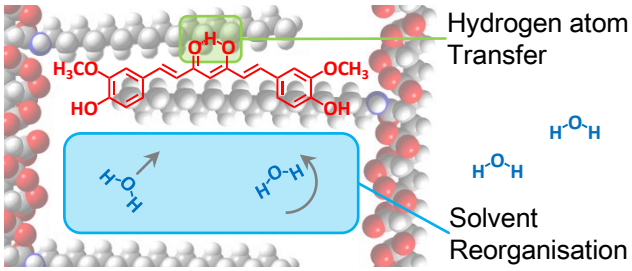

Statement of Authorship

By signing the Statement of Authorship, each author certifies that their stated contribution to the following publication is accurate and included in this thesis.

- Harada, T.; Lincoln, S. F.; Kee, T. W., Ultrafast Dynamics of the Medicinal Pigment Curcumin and Solvation Dynamics of Water in Octadecyl Substituted Polyacrylate Hydrogel. (In preparation).

Author Contributions

Name of First Author (Candidate)	Takaaki Harada
Contribution to the Paper	Sample synthesis and preparations, data acquisition and analysis, and preparation and editing for manuscript
Signature	
Date	17/07/2014

Name of Co-Author	Stephen F. Lincoln
Contribution to the Paper	Supervision of the candidate and editing manuscript
Signature	
Date	02/10/2014

Name of Co-Author	Tak W. Kee
Contribution to the Paper	Supervision of the candidate, data analysis, editing manuscript, and acted as corresponding author
Signature	
Date	02/10/2014

6.1 Abstract

Curcumin is a yellow polyphenol extracted from turmeric. A large number of studies have demonstrated its multiple medicinal effects. These effects, however, are limited due to its poor aqueous stability and solubility. A hydrogel of 3 % octadecyl randomly substituted polyacrylate (PAAC18) has been shown to provide a high aqueous stability for curcumin under physiological conditions. In this work, we study the ultrafast dynamics of water and curcumin in the PAAC18 hydrogel. The steady-state absorption and fluorescence spectra show a large Stokes shift, indicating solvation dynamics of water in the PAAC18 hydrogel in response to the presence of excited-state curcumin. Using femtosecond fluorescence upconversion spectroscopy, we show that the dominant solvation response (0.91 ± 0.23 ps) is a fast inertial motion owing to the presence of bulk-like water in the vicinity of the hydrophobic octadecyl substituents of the PAAC18 hydrogel. The slow translational diffusion response (5.70 ± 0.73 ps) is attributed to the motion of confined water molecules in a three-dimensional cross-linking network of the octadecyl substituents of PAAC18. In addition to solvation dynamics of water in the PAAC18 hydrogel, curcumin shows an excited-state absorption band at 500 nm using femtosecond transient absorption spectroscopy. The dynamics of the excited-state absorption reflect the non-radiative relaxation processes of curcumin, including solvent reorganisation (0.75 ± 0.03 ps) and excited-state intramolecular hydrogen atom transfer (16.6 ± 0.8 ps). Overall, we demonstrate slow diffusion of water in the PAAC18 hydrogel and reveal the photophysical processes of curcumin encapsulated in the PAAC18 hydrogel using ultrafast spectroscopic techniques.

6.2 Introduction

Curcuminoids are a group of naturally existing pigments extracted from turmeric (*Curcuma longa*) [1, 2]. The most abundant polyphenol is curcumin (Schemes 6.1a and 6.1b), which constitutes 77 % of curcuminoids in company with demethoxycurcumin (17 %) and bisdemethoxycurcumin (3 %) [3]. Previously, the medicinal effects of curcumin have been demonstrated in the treatment of inflammation [4, 5], cancer [5–10], Alzheimer's disease [11–13], and cystic fibrosis [14, 15]. As a consequence, clinical trials are either underway or have been completed with an aim to utilise curcumin as a therapeutic drug [16–19]. However, poor aqueous solubility and stability of curcumin hinder its availability *in vivo*. The aqueous solubility of curcumin is approximately 11 µg/L [20, 21], and its low stability results in a rapid degradation within 15 min at pH 7.4 and 37 °C [22, 23]. In order to overcome these two challenges, recent studies have investigated a number of delivery systems, including micelles [24–27], globular proteins [28–30], cyclodextrins [22, 31, 32], and polymer nanoparticles [33–35]. Previously, our work has shown that hydrophobically modified polyacrylate hydrogels have the ability to stabilise curcumin in the aqueous environment [36].

Hydrogels have been utilised in various fields including drug delivery and tissue engineering [37–42]. They possess the ability to hold a large quantity of water by forming a three-dimensional network as a result of polymer cross-linking [43–46]. Previous studies have reported synthesis of 3 % octadecyl randomly substituted polyacrylate, PAAC18 (Scheme 6.1c) [47–49]. PAAC18 forms a micelle-like aggregate at concentrations of < 1 wt% in aqueous systems; however, it becomes a hydrogel at concentrations of > 1 wt% as a result of substantial interstrand associations between octadecyl substituents of PAAC18 [48, 49]. The 1.5 wt% aqueous solution of PAAC18 exhibits a viscosity of approximately 1 Pa s [48, 49], which is $\sim$1000 times higher than that of bulk water. We have shown that the stabilisation effect of PAAC18 as micelle-like aggregates and hydrogels for curcumin is attributed to the host-guest complexation of curcumin with the hydrophobic octadecyl substituents rather than the polyacrylate moiety of PAAC18 [36].

Previous studies have also demonstrated photo-dynamic therapy effects of curcumin for treating melanoma [50–52]. Hence, it is important to understand the photophysical dynamics of curcumin. In previous work, femtosecond transient absorption spectroscopy and fluorescence upconversion spectroscopy have been employed to provide insight into the photophysical processes of excited-state curcumin [53–59]. The dominant relaxation of curcumin is excited-state intramolecular hydrogen atom transfer (ESIHT) in the keto-enol moiety of curcumin (Scheme 6.1a) [53–59].

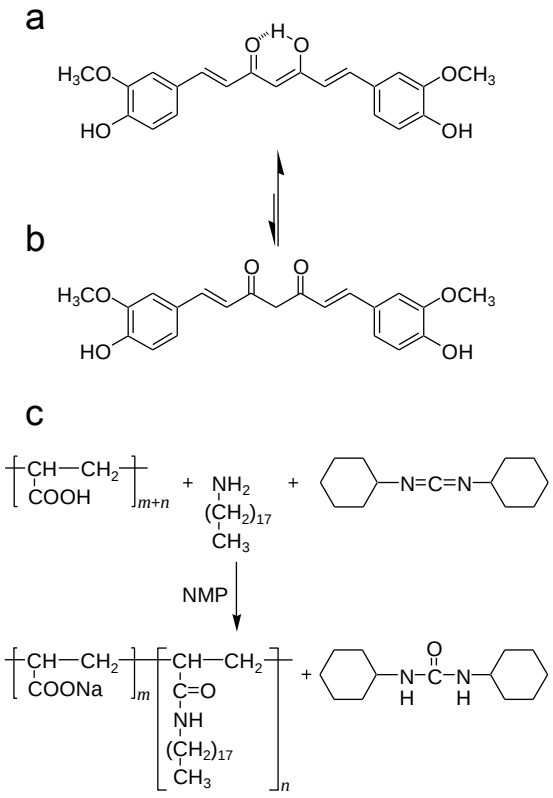

Scheme 6.1. Equilibrium of curcumin between (a) keto-enol and (b) diketo forms. (c) A scheme depicting the synthesis of polyacrylate randomly substituted with octadecylamine to produce PAAC18. NMP is 1-methyl-2-pyrrolidone. The 3 % substitution is represented as the mole ratio $m : n$ of 97 : 3.

Furthermore, solvent reorganisation (solvation) also plays an important role in the excited-state dynamics. Because a significant level of solvent reorganisation occurs in < 1 ps in bulk water [60, 61], it is critical to employ time-resolved spectroscopic techniques with a sufficiently high time resolution. As a result, femtosecond fluorescence upconversion spectroscopy, which has a time resolution of 300–400 fs, has been used to reveal ultrafast dynamics of solvent molecules [59–65]. In addition, previous studies have explored solvation dynamics of water in other aqueous systems including micelles [59, 64], reverse micelles [62, 63], and proteins [64–66]. In these studies, solvation dynamics were observed with an average time constant ranging from 1 to 475 ps. To our knowledge, the dynamics of water molecules in a hydrogel have not been reported in the literature.

Here, we report solvation dynamics of water and the photophysics of excited-state curcumin in the PAAC18 hydrogel. The steady-state absorption and fluorescence spectra of curcumin in the PAAC18 hydrogel show a large Stokes shift. Femtosecond

fluorescence upconversion spectroscopy offers insight into the solvation dynamics of water in the PAAC18 hydrogel by using curcumin as a probe. The solvation correlation function reveals similar solvation dynamics of water in the PAAC18 hydrogel compared with those of confined water in reverse micelles. In addition, the results show the presence of slow dynamics of water in the PAAC18 hydrogel compared with those of bulk water. The excited-state dynamics of curcumin in the PAAC18 hydrogel are also investigated using femtosecond transient absorption spectroscopy. The non-radiative decay processes of curcumin involve solvation, ESIHT and other motions including alkyl hydrogen-hydrogen vibrational motions and diffusive motions of curcumin in the flexible octadecyl substituents of PAAC18. Overall, the ultrafast spectroscopic results in this study reveal the photophysical properties of curcumin and behaviour of the surrounding water molecules in the PAAC18 hydrogel.

6.3 Experimental Section

6.3.1 Materials

Curcumin (1,7-bis(4-hydroxy-3-methoxyphenyl)hepta-1,6-diene-3,5-dione) was obtained from LKT Laboratories (purity $> 98\,\%$). Methanol (AR grade, 99.5 %), dimethyl sulphoxide (DMSO, ACS grade) and hexane (AR grade) from Merck Millipore were used as received. Deuterated water (D_2O) and methanol (MeOD-d_4) were purchased from Cambridge Isotope Laboratories (D, 99.9 %). Polyacrylic acid (Mw = 250,000 g/mol, Mw/Mn $\approx$ 2) was sourced from Sigma Aldrich as a 35 wt% aqueous solution and freeze dried to a constant weight. Octadecylamine (99 %), 1-methyl-2-pyrrolidone (NMP) (99.5 %) and dicyclohexylcarbodiimide (DCC) (99 %) were used as obtained from Sigma Aldrich. Sodium hydroxide (NaOH) pellets (AR grade, 97.0 %) from Ajax Finechem were used to make a 40 % NaOH solution with deionised water from a Millipore Milli-Q NANOpure water system. A 50 mM phosphate buffer solution at pH 7.4 was also prepared with Milli-Q water in this study.

6.3.2 Synthesis of Octadecyl Substituted Polyacrylate Hydrogel

The 3 % octadecyl randomly substituted polyacrylate (PAAC18) was prepared and characterised as previously described [48, 49]. Briefly, octadecylamine and DCC solutions in NMP were added to a solution of polyacrylic acid in NMP with vigorous stirring. After 48 h at 60 °C, the solution was cooled to room temperature, and a 40 % NaOH aqueous solution was added to induce precipitation of the polyacrylate product. After washing and filtering the precipitate with NMP at 60 °C and methanol at room temperature, the crude PAAC18 was dialysed (molecular weight cut-off of 7500 g/mol) against deionised water for 5 days. The solution in the dialysis tube was then freeze dried and PAAC18 was obtained as a white solid. The degree of octadecyl substitution for PAAC18 was determined using ^{1}H NMR spectroscopy as described previously [48, 49]. The PAAC18 solid was dissolved in a 50 mM phosphate buffer solution at pH 7.4 to form a 1.5 wt% PAAC18 hydrogel.

6.3.3 Steady-State UV-Visible Absorption and Fluorescence Spectra of Curcumin in PAAC18 Hydrogel

The 1 µM curcumin solution in either 1.5 wt% PAAC18 hydrogel or hexane in a 1-cm quartz cuvette was prepared with an absorbance of < 0.1 to avoid the inner filter effect. Absorption spectra were recorded in the wavelength range of 300–800 nm

using a Cary 5000 UV-Vis/NIR spectrophotometer (Varian). Fluorescence spectra of the solution were subsequently recorded from 415 nm to 750 nm at a scan rate of 600 nm/min using a Cary Eclipse fluorescence spectrophotometer (Varian) with excitation and emission slit widths of 5 nm. The excitation wavelength was set at 400 nm. The fluorescence spectra were corrected for the wavelength dependence of the lamp spectral intensity and detector response.

6.3.4 Femtosecond Time-Resolved Fluorescence Measurements

Solutions of 100 µM curcumin in 1.5 wt% PAAC18 hydrogel were used in the fluorescence upconversion spectroscopic studies. All the measurements were acquired using a quartz cuvette with a 2-mm path length.

The laser system used for the femtosecond time-resolved fluorescence experiments consisted of a Ti:sapphire mode-locked oscillator (Spectra-Physics, Tsunami), which seeded a Ti:sapphire regenerative amplifier (Spectra-Physics, Spitfire Pro XP) pumped by a 20 W Q-switched Nd:YLF laser (Spectra-Physics, Empower). The output of the amplifier was centred at 800 nm with a repetition rate of 1 kHz and pulse duration of 100 fs, which was then split into pump and gate beam lines. The 400-nm pump pulse was generated using a 0.5-mm type-I BBO crystal with a pulse energy of 50 nJ. No pump pulse energy dependence was observed in the results. The fluorescence signal was collected using a plano-convex lens. Then, the gate pulse and fluorescence signal were focused onto a 0.4-mm type-I BBO crystal to generate the sum frequency light, which was detected by a photomultiplier tube attached to a monochromator. The full width at half maximum (FWHM) of the instrument response function was 380 fs, which was determined by Raman scattering of neat water [67]. Time-resolved fluorescence decays were collected from 470 nm to 590 nm at intervals of 10 nm. Less than 10 % of curcumin photo-degradation was observed after each measurement.

Solvation dynamics of water in the PAAC18 hydrogel were quantified using the solvation correlation function,

$$C(t) = \frac{\nu(t) - \nu(\infty)}{\nu(0) - \nu(\infty)} \tag{6.1}$$

where $\nu(0)$, $\nu(t)$, and $\nu(\infty)$ denote the peak frequencies of the fluorescence spectra at time zero, t, and infinity. The zero-time fluorescence spectrum was approximated using the fluorescence spectrum of curcumin in hexane, according to the method of Fee and Maroncelli [68, 69]. The $\nu(\infty)$ value was taken as the peak frequency of

the steady-state fluorescence spectrum. The $\nu(t)$ values were determined by taking the maxima from the log-normal fits of the time-resolved fluorescence peaks which were re-constructed according to the procedure described by Maroncelli and Fleming using the steady-state fluorescence spectrum and fitting parameters from wavelength-resolved decay traces [69]. Standard deviations of fluorescence maxima are 60 cm^{-1} for the time-resolved fluorescence spectra and 30 cm^{-1} for zero-time and steady-state spectra, which were determined from three independent experiments. These uncertainties were included in error bars for $C(t)$ in addition to the standard deviations of $C(t)$ from three independent experiments. The fractional solvation at 380 fs was calculated using,

$$f_{380\text{ fs}} = 1 - C(t = 380\text{ fs}) \tag{6.2}$$

as described previously [58, 59, 63].

6.3.5 Femtosecond Transient Absorption Spectroscopic Studies

Solutions of 100 µM curcumin in 1.5 wt% PAAC18 hydrogel were used in the transient absorption spectroscopic studies. Similarly, 100 µM curcumin in 1.5 wt% PAAC18 hydrogel solution of neat water and deuterated water were also used in the transient absorption spectroscopic studies to demonstrate a deuterium isotope effect. All the measurements were acquired using a quartz cuvette with a 2-mm path length.

The same 800-nm output of the Ti:sapphire regenerative amplifier (Spectra-Physics, Spitfire Pro XP) was split into the pump and probe beam lines. The 400-nm pump pulse was generated using a 0.5-mm type-I BBO crystal, mechanically chopped at 500 Hz and then focused onto the sample with a spot size of 385 µm and pulse energy of 700 nJ. The probe beam line passed through a delay stage and was used to generate a white light continuum as the broadband probe in a 2-mm sapphire crystal. A 750-nm shortpass filter (optical density 4, 3 mm, Edmund Optics) was placed after the sapphire crystal to separate the probe from the 800-nm seed beam. The probe passed through a beam splitter to produce the sample and reference beams with a spot size of 80 µm at the sample position and pulse energy of < 10 nJ. The sample and reference beams were then directed into complementary CMOS detectors for detection in the visible region. The probe polarisation was oriented at magic angle (54.7°) with respect to the pump polarisation. In all the measurements, the FWHM of 100 fs was used as the instrument response function for data analysis. The error values were determined as standard deviations of three independent measurements. Less than 10 % of curcumin photo-degradation was observed after each set of data acquisition.

6.4 Results and Discussion

6.4.1 Steady-State Absorption and Fluorescence Spectra of Curcumin in PAAC18 Hydrogel

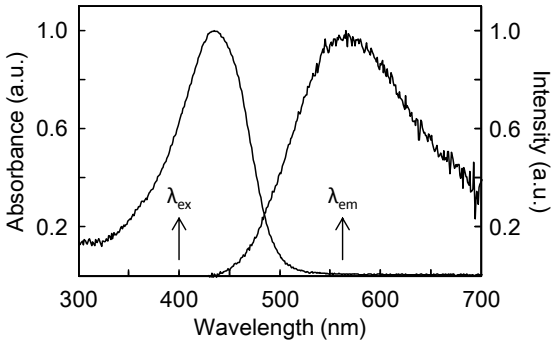

Figure 6.1. Normalised steady-state absorption and fluorescence spectra of curcumin in PAAC18 hydrogel (50 mM phosphate buffer at pH 7.4).

In this study, PAAC18 hydrogel is used to capture and stabilise curcumin in an aqueous environment. The spectroscopic properties of curcumin complexed with the PAAC18 hydrogel reveal the microenvironment of water and curcumin in the octadecyl hydrophobic aggregates of PAAC18. Figure 6.1 shows steady-state UV-visible absorption and fluorescence spectra of curcumin in the PAAC18 hydrogel. The 430-nm absorption peak is attributed to the keto-enol tautomer of curcumin (Scheme 6.1a), which is in agreement with previous studies [22, 26, 28, 59, 70]. The absence of a spectral shoulder around 350 nm in the absorption spectrum indicates that the diketo form of curcumin is present at a negligible level (Scheme 6.1b) [22, 25, 59, 70]. Previous studies have shown that curcumin exists solely as the keto-enol tautomer in a hydrophobic environment [22, 26, 28, 59, 70], which is consistent with the binding of curcumin to the hydrophobic octadecyl aggregates of PAAC18 [36]. The absence of vibronic structures in the absorption spectrum of curcumin in the PAAC18 hydrogel indicates the presence of rapid interactions between curcumin and water molecules at the hydrophobic octadecyl substituents of PAAC18 [59].

The fluorescence spectrum of curcumin in the PAAC18 hydrogel shows an emission band around 560 nm and a Stokes shift value of $5430 \pm 40\,\mathrm{cm}^{-1}$, which indicates the presence of solvation dynamics due to excited-state curcumin. The fluorescence spectral features and Stokes shift value of curcumin in the PAAC18 hydrogel are similar to those of curcumin in sodium dodecyl sulphate (SDS) micellar solutions [25, 59]. In contrast, previous studies have shown low Stokes shift values when curcumin

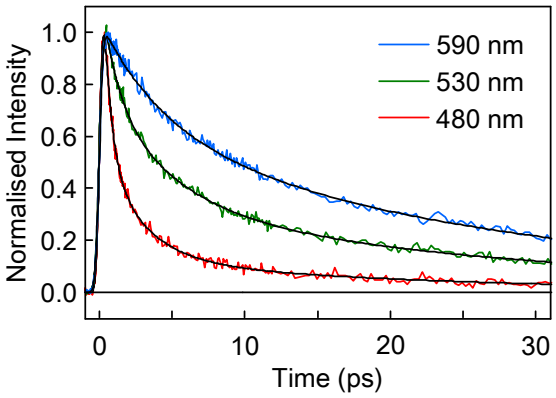

Figure 6.2. Representative normalised time-resolved fluorescence decays of curcumin in the PAAC18 hydrogel at 480, 530 and 590 nm.

binds to Triton X-100 (TX-100), dodecyl trimethyl ammonium bromide (DTAB), bovine serum albumin (BSA) and human serum albumin (HSA) [28–30, 59]. It is well-established that curcumin binds to micelles in the palisade layer, where dynamics of water molecules are similar to bulk water [59]. Therefore, the steady-state spectra of curcumin in the PAAC18 hydrogel suggest that the microenvironment of curcumin complexed with PAAC18 would be similar to that of curcumin bound to micelles, and the solvation dynamics of water in the PAAC18 hydrogel may be similar to that of bulk water. However, steady-state spectroscopy is unable to reveal the dynamics of the excited states. Ultrafast spectroscopic techniques offer insight into solvation dynamics of water and photophysical properties of curcumin in the PAAC18 hydrogel.

6.4.2 Solvation Dynamics of Water in PAAC18 Hydrogel

In a previous study, Jarzeba et al. have shown that the solvation dynamics of bulk water occur with an average time constant of 0.86 ps [60]. Our study offers insight into solvation dynamics of water in the PAAC18 hydrogel, using curcumin as a probe. Curcumin possesses a large dipole moment change of $\Delta\mu = 6.1$ D [71], which is comparable to that of Coumarin 153 ($\Delta\mu \approx 8$ D), a common probe for solvation dynamics [69].

Here we report solvation dynamics of water in the PAAC18 hydrogel using femtosecond fluorescence upconversion spectroscopy. Fluorescence upconversion measurements ranging from 470 nm to 590 nm generate time-resolved fluorescence spectra of curcumin in the PAAC18 hydrogel, as shown in previous studies [58–61, 68, 69]. Figure 6.2 shows the representative normalised time-resolved fluorescence de-

cay traces of curcumin in the PAAC18 hydrogel at 480, 530, and 590 nm. A fast fluorescence decay is observed at 480 nm while the fluorescence decay is slower at 530 nm, which is followed by a further reduction in the rate of decay at 590 nm. These wavelength-dependent changes are indicative of the presence of the solvation dynamics [58–61].

Figure 6.3a shows fluorescence spectra of curcumin in the PAAC18 hydrogel at 0, 0.38 and 3 ps together with the steady-state fluorescence spectrum ($t = \infty$). It is clear that a rapid spectral shift is present within the instrument response function of 0.38 ps. However, the fluorescence spectrum at 3 ps is still evolving to approach the steady-state spectrum, indicating the presence of a slow component in the solvation dynamics of water in the PAAC18 hydrogel. In Figure 6.3b, the solvation correlation function, $C(t)$ (eq 6.1), exhibits the dynamics of water in the PAAC18 hydrogel, and the solvation parameters are summarised in Table 6.1. The fractional solvation value ($f_{380\text{ fs}}$, eq 6.2) shows that approximately 67 % of reorganisation of water molecules in the PAAC18 hydrogel is completed within the instrument response time. This result reflects the rapid appearance of the fluorescence spectrum at 0.38 ps that resembles the steady-state spectrum (Figure 6.3a), which has also been observed in other systems [58, 59]. Moreover, $C(t)$ is well fitted with a triexponential function with time constants of 0.05 ps (58 %), 0.91 ± 0.23 ps (24 %) and 5.70 ± 0.73 ps (18 %), respectively. The presence of ultrafast librational motions is represented as a fixed time constant of 0.05 ps [58, 59, 61]. The average time constant, $\langle\tau\rangle$, for the dynamics of water molecules in the PAAC18 hydrogel is 1.29 ± 0.14 ps. To our knowledge, this is the first study on solvation dynamics of water in a hydrogel using femtosecond fluorescence upconversion spectroscopy. Comparisons to other experimental results provide understandings of the solvation dynamics of water in the PAAC18 hydrogel (Table 6.1).

Jarzeba et al. have shown ultrafast response of bulk water using 7-(dimethylamino)-coumarin-4-acetic acid as a probe [60]. Their instrument response function of 280 fs is unable to resolve the ultrafast librational motions (< 50 fs) of bulk water. However, the diffusion components of bulk water have been shown to have time constants of 0.16 ps (33 %) and 1.2 ps (67 %) [60]. Jimenez et al. have also reported comparable time constants of 0.13 ps (20 %) and 0.88 ps (35 %) using Coumarin 343 as a probe [61], which are in agreement with another study [62]. Similarly, solvation dynamics of bulk water have been examined using L-tryptophan as a probe [64]. In this previous study, the solvation correlation function was fitted with a biexponential function with time constants of 0.18 ps (20 %) and 1.1 ps (80 %). Therefore, there are genuine agreements with solvation dynamics of bulk water molecules, where inertial

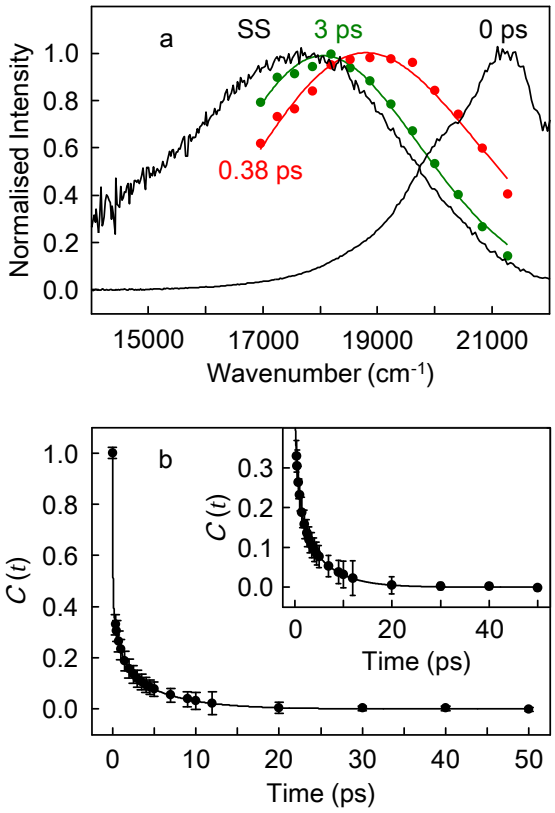

Figure 6.3. (a) Normalised time-resolved fluorescence spectra of curcumin in the PAAC18 hydrogel with spectra at $t = 0$, 0.38, 3 and ∞ ps. The fluorescence spectra at $t = 0$ and ∞ ps are estimated using the steady-state spectra of curcumin in hexane and the PAAC18 hydrogel, respectively [68, 69]. The fluorescence spectra at $t = 0.38$ and 3 ps are re-constructed according to the procedure described by Maroncelli and Fleming [69]. (b) Solvation correlation function, $C(t)$ (eq 6.1), of water in the PAAC18 hydrogel. Note that 67 ± 2 % of the solvation is completed within the instrument response function (380 fs). The inset shows the function from 0.38 ps.

diffusion occurs at ~ 0.2 ps as the minor process and translational diffusion occurs at ~ 1 ps as the major process [62]. For the PAAC18 hydrogel, both time constants of 0.91 ± 0.23 ps and 5.70 ± 0.73 ps are substantially longer than those of bulk water.

Dynamics of water in a confined environment have also been studied using reverse micelles. Riter et al. have investigated solvation dynamics of water/Aerosol OT (AOT)/isooctane reverse micelles with a range of water contents [62]. Reverse micelles contain with $[H_2O]/[AOT] = 7.5$ exhibit solvation dynamic time constants of 0.11 ps (69 %) and 3.0 ps (31 %) [62]. The fast inertial diffusion time constant is similar to that of bulk water, but it becomes a dominant process. In contrast, the translational diffusion at 3.0 ps appears substantially slower than that observed in the dynamics of bulk water (~ 1 ps). These observations were also reported in another study [63]. Additionally, electrostatic charges of electrolytes and hydrophilic moiety of surfactants also contribute to the immobilisation of water [62, 72, 73]. Because the solvation time constants of water in the PAAC18 hydrogel are similar to those for the reverse micellar systems (Table 6.1), it is likely that the slow dynamics of water in the PAAC18 hydrogel are attributed to the motion of confined water molecules in a three-dimensional cross-linking network of the octadecyl substituents of PAAC18. This assignment is supported by the high viscosity of 1 Pa s of the PAAC18 hydrogel (at 1.5 wt%) [48, 49].

Water molecules at the surface of macromolecules and proteins play an important role in biological activities and assemblies [64, 74], which have attracted investigations on dynamics of water molecules in micellar and protein systems [59, 64–66]. Adhikary et al. have demonstrated dynamics of water at the surface of different micelles using curcumin as a probe. Their results show a slow mobility of water molecules. Pal et al. have revealed solvation time constants of 0.8 ps and 38 ps in a protein solution. These slow time constants are comparable to those in other protein solutions [65, 66]. Thus, significantly slower solvation dynamics are reported in these studies than those of bulk and reverse micellar systems. There are possible interactions including hydrogen bonding of water molecules at the surface of macromolecules and proteins, which are expected to result in substantially slow dynamics [64]. As mentioned earlier, curcumin binds to the hydrophobic octadecyl substituent aggregates of PAAC18 [36]. Hence, weak interactions between the hydrophobic octadecyl substituents of PAAC18 and water molecules in vicinity of excited-state curcumin are expected. The lack of strong interactions leads to faster dynamics of water molecules in the PAAC18 hydrogel than those in micellar and protein systems.

Overall, we show that the solvation time components arise from inertial and translational diffusions of water molecules in the PAAC18 hydrogel (Table 6.1) [61, 62,

Table 6.1. Solvation Correlation Function Decay Parameters of Water in Different Systems.

Solvent	a_1	τ_1 (ps)	a_2	τ_2 (ps)	a_3	τ_3 (ps)	$\langle\tau\rangle$ (ps)	References
PAAC18 Hydrogel[a]	0.58 ± 0.01	0.05	0.24 ± 0.01	0.91 ± 0.23	0.18 ± 0.02	5.70 ± 0.73	1.29 ± 0.14	This study
Bulk Water	-	-	0.33	0.16	0.67	1.2	0.86	Ref. [60]
Reverse Micelle[b]	-	-	0.69	0.11	0.31	3.0	1.01	Ref. [62]
Micelle[c]	0.37 ± 0.02	0.31 ± 0.04	0.22 ± 0.03	8	0.41 ± 0.02	∞	1.87	Ref. [59]
Protein[d]	-	-	0.61	0.8	0.39	38	15.3	Ref. [64]

[a] The fractional solvation ($f_{380\ \mathrm{fs}}$, eq 6.2) is $67 \pm 2\,\%$, and τ_1 was fixed to 0.05 ps to represent the ultrafast librational motions [61].

[b] Water/Aerosol OT (AOT)/isooctane reverse micelle when[H_2O]/[AOT] = 7.5.

[c] 0.1 M Triton X-100 micellar solution. The kinetics were fitted with a triexponential function including a fixed $\tau_2 = 8$ ps and a constant $a_3 = 0.41 \pm 0.02$.

[d] Subtilisin *Carlsberg*.

67, 69, 75, 76]. The fast time constant (0.91 ps) is in agreement with those of bulk and reverse micellar systems [60–62]. This fast inertial diffusion in response to dipole change of curcumin is a result of the absence of interactions between water molecules and the hydrophobic octadecyl substituent aggregates of PAAC18, where curcumin is present [36]. In contrast, the relatively slow time constant (5.70 ps) of water in the PAAC18 hydrogel is similar to those of the reverse micellar systems [62, 63], but are faster than those of protein and micellar systems [59, 64–66]. The water molecules in the PAAC18 hydrogel are restricted to undergo translational diffusion in a confined environment owing to the three-dimensional cross-linking network of the octadecyl substituents of PAAC18.

6.4.3 Femtosecond Transient Absorption and Excited-State Kinetics of Curcumin in PAAC18 Hydrogel

Femtosecond transient absorption spectroscopy has been used to study the excited-state dynamics of curcumin in various systems [53, 77]. Figure 6.4a shows transient absorption spectra of curcumin in the PAAC18 hydrogel, with several pump-probe delay times. Curcumin complexed with PAAC18 exhibits rapid excited-state absorption (ESA) peaks around 490 nm and 560 nm at 0.5 ps, followed by evolution of another ESA peak around 500 nm. The 560-nm ESA peak observed at 1 ps evolves into stimulated emission (SE) signals around 640–720 nm, which is still present at 50 ps. The 500-nm ESA peak shows a spectral shoulder around 550 nm, which reaches a maximum ΔOD around 3 ps and decreases thereafter. These spectral features are similar to those of curcumin in methanol and micellar solution [53]. The 500-nm ESA peak is still observable after 500 ps although the SE signals have disappeared, which is discussed below. In Figure 6.4a, the overlap between the ESA and SE signals results in the overall ESA peak observed at 500 nm.

Changes in the transient absorption signals reveal the excited-state relaxation of curcumin in the PAAC18 hydrogel. Figure 6.4b shows the time-dependent 500-nm ESA signal of curcumin in the PAAC18 hydrogel, which is fitted with an exponential function with a growth term (τ_1) and three decay terms (τ_2, τ_3 and τ_4). The τ_4 component represents a slow decay that occurs over several nanoseconds. First, the ESA signals of curcumin in PAAC18 show a growth component with a time constant τ_1 of 0.75 ± 0.03 ps (46 % of the maximum signal amplitude). This growth component at 500 nm represents the solvation dynamics of water in the PAAC18 hydrogel, considering a transition from the lowest vibronic energy level in the first excited state. Therefore, the time constant $\tau_1 = 0.75$ ps is an average solvation time constant, which

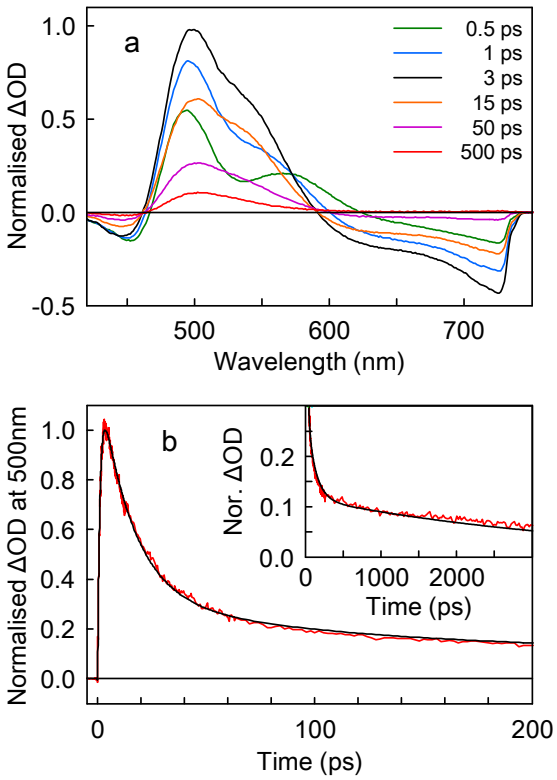

Figure 6.4. (a) Transient absorption spectra of curcumin in PAAC18 hydrogel (50 mM phosphate buffer at pH 7.4) at several pump-probe delay times. The data are normalised to the maximum ΔOD signal. (b) Decay kinetics of the excited-state absorption signals of curcumin in the PAAC18 hydrogel at 500 nm. The inset shows the signals at longer delay times.

Table 6.2. Transient Absorption Kinetic Parameters of Curcumin in the PAAC18 Hydrogel Solutions of Different Solvents.

Solvent	a_1	τ_1 (ps)	a_2	τ_2 (ps)	a_3[a]	a_4[a]
Buffer[b]	-0.46 ± 0.01	0.75 ± 0.03	0.40 ± 0.01	16.6 ± 0.8	0.09 ± 0.01	0.05 ± 0.01
H_2O	-0.47 ± 0.01	0.67 ± 0.07	0.41 ± 0.01	14.0 ± 0.1	0.07 ± 0.01	0.04 ± 0.01
D_2O	-0.46 ± 0.01	0.97 ± 0.01	0.34 ± 0.01	25.8 ± 0.3	0.14 ± 0.01	0.06 ± 0.01

[a] The τ_3 and τ_4 values are fixed to 109 and 5000 ps, respectively [78].

[b] 50 mM phosphate buffer at pH 7.4 as described above.

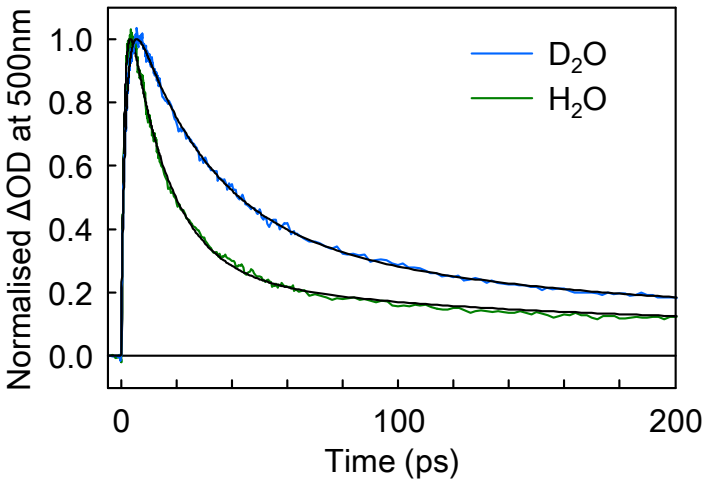

Figure 6.5. Decay kinetics of the 500-nm excited-state absorption signals of curcumin in the PAAC18 hydrogel in H_2O (green) and D_2O (blue) solvent systems. The data are normalised to the maximum ΔOD signal.

is comparable with the average solvation time constant of $\langle\tau\rangle = 1.29 \pm 0.14$ ps (Table 6.1). Second, the time constant τ_2 is 16.6 ± 0.8 ps (40 %), which shows a deuterium isotope effect of 1.8 (Figure 6.5 and Table 6.2). This dominant relaxation process is ESIHT of curcumin as established previously [53–59], which is an important photophysical process of excited-state curcumin. Interactions between the enolic hydrogen of curcumin and polar solvent molecules influence the rate of ESIHT [54–56, 58, 59, 77]. The time constant τ_2 shows relatively fast ESIHT process of curcumin in the PAAC18 hydrogel compared with that in protic solvents [53, 54, 58, 59, 77]. Finally, the time constants τ_3 and τ_4 are fixed to 109 ps (9 %) and 5000 ps (5 %) [78], respectively, which shows insignificant deuterium isotope effects (Table 6.2). In a previous study, the 2D NOESY ^{1}H NMR spectrum of curcumin in PAAC18 has shown cross-peaks arising from interactions between curcumin and octadecyl substituents of PAAC18, and substantial broadening of proton signals of curcumin [36]. The results of the 2D NOESY ^{1}H NMR spectrum indicate that the hydrophobic octadecyl aggregates of PAAC18 where curcumin binds are likely to exhibit dynamic characteristics. Furthermore, similar slow and small-amplitude relaxation components have also been observed from excited-state dynamics of guest molecules encapsulated by γ-cyclodextrins [54, 78]. These studies suggest that the slow decay dynamics may be originated from the fluctuation of the γ-cyclodextrins, diffusive motions of the guest molecules, and/or alkyl host-guest interactions. In this current work, the interactions between curcumin and the octadecyl substituents of PAAC18 are expected to be similar to those between the guest molecule and the hydrophobic annulus of

γ-cyclodextrin. Thus, the time constants of 109 ps and 5000 ps are attributable to relaxation processes of excited-state curcumin in the PAAC18 hydrogel owing to fluctuation of the octadecyl aggregate moieties, diffusive motions of curcumin, and/or alkyl hydrogen-hydrogen vibrational motions between curcumin and the octadecyl aggregates of PAAC18.

6.5 Conclusions

This study highlights the ultrafast dynamics of water and curcumin in a PAAC18 hydrogel. The steady-state spectra show a large Stokes shift value of $5430 \pm 40\,\mathrm{cm}^{-1}$, indicating the presence of solvation response and water-curcumin interactions due to dipole change of curcumin induced by photo-excitation. To our knowledge, we have demonstrated the first results of solvation dynamics of water in a hydrogel using femtosecond fluorescence upconversion spectroscopy. The dominant component at 0.91 ps is bulk-like fast inertial diffusion response, due to a lack of significant interactions between water molecules and the hydrophobic octadecyl substituents of PAAC18. The slow translational diffusion response at 5.70 ps is a result of the confinement of water molecules in the three-dimensional cross-linking network of the octadecyl substituents of PAAC18. Femtosecond transient absorption spectroscopic results provide insight into the time-resolved ESA and SE spectra. The ESA decay profile reveals that the non-radiative relaxation processes of curcumin are solvation (0.75 ps), ESIHT ($\sim$ 17 ps) and other slow motions due to dynamic interactions between curcumin and octadecyl aggregates of PAAC18. In conclusion, we have shown the excited-state dynamics of water and curcumin in the PAAC18 hydrogel using ultrafast spectroscopic techniques.

6.6 References

(1) Leung, M. H. M.; Harada, T.; Kee, T. W. Delivery of Curcumin and Medicinal Effects of the Copper(II)-Curcumin Complexes. *Curr. Pharm. Des.* **2013**, *19*, 2070–2083.

(2) Sa, G.; Das, T. Anti-Cancer Effects of Curcumin: Cycle of Life and Death. *Cell Division* **2008**, *3*, 1–14.

(3) Anand, P.; Sundaram, C.; Jhurani, S.; Kunnumakkara, A. B.; Aggarwal, B. B. Curcumin and Cancer: An "Old-Age" Disease with an "Age-Old" Solution. *Cancer Lett.* **2008**, *267*, 133–164.

(4) Lantz, R. C.; Chen, G. J.; Solyom, A. M.; Jolad, S. D.; Timmermann, B. N. The Effect of Turmeric Extracts on Inflammatory Mediator Production. *Phytomedicine* **2005**, *12*, 445–452.

(5) Aggarwal, B. B.; Kumar, A.; Bharti, A. C. Anticancer Potential of Curcumin: Preclinical and Clinical Studies. *Anticancer Res.* **2003**, *23*, 363–398.

(6) Harada, T.; Giorgio, L.; Harris, T. J.; Pham, D.-T.; Ngo, H. T.; Need, E. F.; Coventry, B. J.; Lincoln, S. F.; Easton, C. J.; Buchanan, G.; Kee, T. W. Diamide Linked γ-Cyclodextrin Dimers as Molecular-Scale Delivery Systems for the Medicinal Pigment Curcumin to Prostate Cancer Cells. *Mol. Pharmaceutics* **2013**, *10*, 4481–4490.

(7) Hatcher, H.; Planalp, R.; Cho, J.; Tortia, F. M.; Torti, S. V. Curcumin: From Ancient Medicine to Current Clinical Trials. *Cell. Mol. Life Sci.* **2008**, *65*, 1631–1652.

(8) Huang, M. T.; Lou, Y. R.; Ma, W.; Newmark, H. L.; Reuhl, K. R.; Conney, A. H. Inhibitory Effects of Dietary Curcumin on Forestomach, Duodenal, and Colon Carcinogenesis in Mice. *Cancer Res.* **1994**, *54*, 5841–5847.

(9) Rao, C. V.; Rivenson, A.; Simi, B.; Reddy, B. S. Chemoprevention of Colon Carcinogenesis by Dietary Curcumin, A Naturally-Occurring Plant Phenolic Compound. *Cancer Res.* **1995**, *55*, 259–266.

(10) Sharma, O. P. Antioxidant Activity of Curcumin and Related Compounds. *Biochem. Pharmacol.* **1976**, *25*, 1811–1812.

(11) Lim, G. P.; Chu, T.; Yang, F. S.; Beech, W.; Frautschy, S. A.; Cole, G. M. The Curry Spice Curcumin Reduces Oxidative Damage and Amyloid Pathology in an Alzheimer Transgenic Mouse. *J. Neurosci.* **2001**, *21*, 8370–8377.

(12) Ono, K.; Hasegawa, K.; Naiki, H.; Yamada, M. Curcumin Has Potent Anti-Amyloidogenic Effects for Alzheimer's β-Amyloid Fibrils In Vitro. *J. Neurosci. Res.* **2004**, *75*, 742–750.

(13) Yang, F. S.; Lim, G. P.; Begum, A. N.; Ubeda, O. J.; Simmons, M. R.; Ambegaokar, S. S.; Chen, P. P.; Kayed, R.; Glabe, C. G.; Frautschy, S. A.; Cole, G. M. Curcumin Inhibits Formation of Amyloid β Oligomers and Fibrils, Binds Plaques, and Reduces Amyloid In Vivo. *J. Biol. Chem.* **2005**, *280*, 5892–5901.

(14) Cartiera, M. S.; Ferreira, E. C.; Caputo, C.; Egan, M. E.; Caplan, M. J.; Saltzman, W. M. Partial Correction of Cystic Fibrosis Defects with PLGA Nanoparticles Encapsulating Curcumin. *Mol. Pharmaceutics* **2010**, *7*, 86–93.

(15) Egan, M. E.; Pearson, M.; Weiner, S. A.; Rajendran, V.; Rubin, D.; Glockner-Pagel, J.; Canny, S.; Du, K.; Lukacs, G. L.; Caplan, M. J. Curcumin, a Major Constituent of Turmeric, Corrects Cystic Fibrosis Defects. *Science* **2004**, *304*, 600–602.

(16) Cheng, A. L.; Hsu, C. H.; Lin, J. K.; Hsu, M. M.; Ho, Y. F.; Shen, T. S.; Ko, J. Y.; Lin, J. T.; Lin, B. R.; Wu, M. S.; Yu, H. S.; Jee, S. H.; Chen, G. S.; Chen, T. M.; Chen, C. A.; Lai, M. K.; Pu, Y. S.; Pan, M. H.; Wang, Y. J.; Tsai, C. C.; Hsieh, C. Y. Phase I Clinical Trial of Curcumin, a Chemopreventive Agent, in Patients with High-Risk or Pre-Malignant Lesions. *Anticancer Res.* **2001**, *21*, 2895–2900.

(17) Sharma, R. A.; Euden, S. A.; Platton, S. L.; Cooke, D. N.; Shafayat, A.; Hewitt, H. R.; Marczylo, T. H.; Morgan, B.; Hemingway, D.; Plummer, S. M.; Pirmohamed, M.; Gescher, A. J.; Steward, W. P. Phase I Clinical Trial of oral Curcumin: Biomarkers of Systemic Activity and Compliance. *Clin. Cancer Res.* **2004**, *10*, 6847–6854.

(18) ClinicalTrials.gov, Trial of Curcumin in Advanced Pancreatic Cancer., M.D. Anderson Cancer Center, `http://clinicaltrials.gov/ct2/show/NCT00094445`.

(19) ClinicalTrials.gov, Curcumin in Patients With Mild to Moderate Alzheimer's Disease., `http://clinicaltrials.gov/ct2/show/NCT00099710`.

(20) Kaminaga, Y.; Nagatsu, A.; Akiyama, T.; Sugimoto, N.; Yamazaki, T.; Maitani, T.; Mizukami, H. Production of Unnatural Glucosides of Curcumin with Drastically Enhanced Water Solubility by Cell Suspension Cultures of Catharanthus Roseus. *FEBS Lett.* **2003**, *555*, 311–316.

(21) Letchford, K.; Liggins, R.; Burt, H. Solubilization of Hydrophobic Drugs by Methoxy Poly(ethylene glycol)-block-polycaprolactone Diblock Copolymer Micelles: Theoretical and Experimental Data and Correlations. *J. Pharm. Sci.* **2008**, *97*, 1179–1190.

(22) Harada, T.; Pham, D.-T.; Leung, M. H. M.; Ngo, H. T.; Lincoln, S. F.; Easton, C. J.; Kee, T. W. Cooperative Binding and Stabilization of the Medicinal Pigment Curcumin by Diamide Linked γ-Cyclodextrin Dimers: A Spectroscopic Characterization. *J. Phys. Chem. B* **2011**, *115*, 1268–1274.

(23) Wang, Y. J.; Pan, M. H.; Cheng, A. L.; Lin, L. I.; Ho, Y. S.; Hsieh, C. Y.; Lin, J. K. Stability of Curcumin in Buffer Solutions and Characterization of Its Degradation Products. *J. Pharm. Biomed. Anal.* **1997**, *15*, 1867–1876.

(24) Iwunze, M. O. Binding and Distribution Characteristics of Curcumin Solubilized in CTAB Micelle. *J. Mol. Liq.* **2004**, *111*, 161–165.

(25) Leung, M. H. M.; Colangelo, H.; Kee, T. W. Encapsulation of Curcumin in Cationic Micelles Suppresses Alkaline Hydrolysis. *Langmuir* **2008**, *24*, 5672–5675.

(26) Tønnesen, H. H.; Másson, M.; Loftsson, T. Studies of Curcumin and Curcuminoids. XXVII. Cyclodextrin Complexation: Solubility, Chemical and Photochemical Stability. *Int. J. Pharm.* **2002**, *244*, 127–135.

(27) Sahu, A.; Kasoju, N.; Bora, U. Fluorescence Study of the Curcumin-Casein Micelle Complexation and Its Application as a Drug Nanocarrier to Cancer Cells. *Biomacromolecules* **2008**, *9*, 2905–2912.

(28) Leung, M. H. M.; Kee, T. W. Effective Stabilization of Curcumin by Association to Plasma Proteins: Human Serum Albumin and Fibrinogen. *Langmuir* **2009**, *25*, 5773–5777.

(29) Barik, A.; Mishra, B.; Kunwar, A.; Kadam, R. M.; Shen, L.; Dutta, S.; Padhye, S.; Satpati, A. K.; Zhang, H.-Y.; Priyadarsini, K. I. Comparative Study of Copper(II)-Curcumin Complexes as Superoxide Dismutase Mimics and Free Radical Scavengers. *Eur. J. Med. Chem.* **2007**, *42*, 431–439.

(30) Barik, A.; Priyadarsini, K. I.; Mohan, H. Photophysical Studies on Binding of Curcumin to Bovine Serum Albumin. *Photochem. Photobiol.* **2003**, *77*, 597–603.

(31) Baglole, K. N.; Boland, P. G.; Wagner, B. D. Fluorescence Enhancement of Curcumin upon Inclusion into Parent and Modified Cyclodextrins. *J. Photochem. Photobiol. A* **2005**, *173*, 230–237.

(32) Singh, R.; Tønnesen, H. H.; Vogensen, S. B.; Loftsson, T.; Másson, M. Studies of Curcumin and Curcuminoids. XXXVI. The Stoichiometry and Complexation Constants of Cyclodextrin Complexes as Determined by the Phase-Solubility Method and UV-Vis Titration. *J. Incl. Phenom. Macro.* **2010**, *66*, 335–348.

(33) Mohanty, C.; Sahoo, S. K. The In Vitro Stability and In Vivo Pharmacokinetics of Curcumin Prepared as an Aqueous Nanoparticulate Formulation. *Biomaterials* **2010**, *31*, 6597–6611.

(34) Shaikh, J.; Ankola, D. D.; Beniwal, V.; Singh, D.; Kumar, M. N. V. R. Nanoparticle Encapsulation Improves Oral Bioavailability of Curcumin by at Least 9-fold when Compared to Curcumin Administered with Piperine as Absorption Enhancer. *Eur. J. Pharm. Sci.* **2009**, *37*, 223–230.

(35) Bisht, S.; Feldmann, G.; Soni, S.; Ravi, R.; Karikar, C.; Maitra, A.; Maitra, A. Polymeric Nanoparticle-Encapsulated Curcumin ("Nanocurcumin"): A Novel Strategy for Human Cancer Therapy. *J. Nanobiotechnology* **2007**, *5*, 18.

(36) Harada, T.; Pham, D.-T.; Lincoln, S. F.; Kee, T. W. The Capture and Stabilization of Curcumin Using Hydrophobically Modified Polyacrylate Aggregates and Hydrogels. *J. Phys. Chem. B* **2014**, *118*, 9515–9523.

(37) Agnihotri, S. A.; Mallikarjuna, N. N.; Aminabhavi, T. M. Recent Advances on Chitosan-Based Micro- and Nanoparticles in Drug Delivery. *J. Controlled Release* **2004**, *100*, 5–28.

(38) Dong, L. C.; Yan, Q.; Hoffman, A. S. Controlled Release of Amylase from a Thermal and pH-Sensitive, Macroporous Hydrogel. *J. Controlled Release* **1992**, *19*, 171–177.

(39) Ende, M. T. A.; Peppas, N. A. Transport of Ionizable Drugs and Proteins in Crosslinked Poly(acrylic acid) and Poly(acrylic acid-co-2-hydroxyethyl methacrylate) Hydrogels. 2. Diffusion and Release Studies. *J. Controlled Release* **1997**, *48*, 47–56.

(40) Peppas, N. A.; Hilt, J. Z.; Khademhosseini, A.; Langer, R. Hydrogels in Biology and Medicine: From Molecular Principles to Bionanotechnology. *Adv. Mater.* **2006**, *18*, 1345–1360.

(41) Suh, J. K. F.; Matthew, H. W. T. Application of Chitosan-Based Polysaccharide Biomaterials in Cartilage Tissue Engineering: A Review. *Biomaterials* **2000**, *21*, 2589–2598.

(42) Yan, Q.; Hoffman, A. S. Synthesis of Macroporous Hydrogels with Rapid Swelling and Deswelling Properties for Delivery of Macromolecules. *Polymer* **1995**, *36*, 887–889.

(43) Tuntikulwattana, S.; Sinchaipanid, N.; Ketjinda, W.; Williams, D. B.; Mitrevej, A. Fabrication of Chitosan-Polyacrylic Acid Complexes as Polymeric Osmogents for Swellable Micro/Nanoporous Osmotic Pumps. *Drug Dev. Ind. Pharm.* **2011**, *37*, 926–933.

(44) Torrado, S.; Prada, P.; de la Torre, P. M.; Torrado, S. Chitosan-Poly(acrylic) Acid Polyionic Complex: In Vivo Study to Demonstrate Prolonged Gastric Retention. *Biomaterials* **2004**, *25*, 917–923.

(45) Grimm, S.; Giesa, R.; Sklarek, K.; Langner, A.; Gosele, U.; Schmidt, H. W.; Steinhart, M. Nondestructive Replication of Self-Ordered Nanoporous Alumina Membranes via Cross-Linked Polyacrylate Nanofiber Arrays. *Nano Lett.* **2008**, *8*, 1954–1959.

(46) Xie, B. J.; Parkhill, R. L.; Warren, W. L.; Smay, J. E. Direct Writing of Three-Dimensional Polymer Scaffolds using Colloidal Gels. *Adv. Funct. Mater.* **2006**, *16*, 1685–1693.

(47) Wang, K. T.; Iliopoulos, I.; Audebert, R. Viscometric Behaviour of Hydrophobically Modified Poly(sodium acrylate). *Polym. Bull.* **1988**, *20*, 577–582.

(48) Guo, X.; Abdala, A. A.; May, B. L.; Lincoln, S. F.; Khan, S. A.; Prud'homme, R. K. Rheology Control by Modulating Hydrophobic and Inclusion Associations in Modified Poly(acrylic acid) Solutions. *Polymer* **2006**, *47*, 2976–2983.

(49) Wang, J.; Li, L.; Ke, H.; Liu, P.; Zheng, L.; Guo, X.; Lincoln, S. F. Rheology Control by Modulating Hydrophobic and Inclusive Associations of Side-Groups in Poly(acrylic acid). *Asia-Pac. J. Chem. Eng.* **2009**, *4*, 537–543.

(50) Chan, W.-H.; Wu, H.-J. Anti-Apoptotic Effects of Curcumin on Photosensitized Human Epidermal Carcinoma A431 Cells. *J. Cell. Biochem.* **2004**, *92*, 200–212.

(51) Koon, H. K.; Leung, A. W. N.; Yue, K. K. M.; Mak, N. K. Photodynamic Effect of Curcumin on NPC/CNE2 Cells. *J. Environ. Pathol. Toxicol. Oncol.* **2006**, *25*, 205–216.

(52) Park, K.; Lee, J.-H. Photosensitizer Effect of Curcumin on UVB-Irradiated HaCaT Cells through Activation of Caspase Pathways. *Oncol. Rep.* **2007**, *17*, 537–540.

(53) Leung, M. H. M.; Pham, D.-T.; Lincoln, S. F.; Kee, T. W. Femtosecond Transient Absorption Spectroscopy of Copper(II)-Curcumin Complexes. *Phys. Chem. Chem. Phys.* **2012**, *14*, 13580–13587.

(54) Harada, T.; McTernan, H. L.; Pham, D.-T.; Lincoln, S. F.; Kee, T. W. Femtosecond Transient Absorption Spectroscopy of the Medicinal Agent Curcumin in Diamide Linked γ-Cyclodextrin Dimers. *J. Phys. Chem. B* **2015**, *119*, 2425–2433.

(55) Nardo, L.; Paderno, R.; Andreoni, A.; Másson, M.; Haukvik, T.; Tønnesen, H. H. Role of H-bond Formation in the Photoreactivity of Curcumin. *Spectroscopy* **2008**, *22*, 187–198.

(56) Nardo, L.; Andreoni, A.; Bondani, M.; Másson, M.; Tønnesen, H. H. Studies on Curcumin and Curcuminoids. XXXIV. Photophysical Properties of a Symmetrical, Non-Substituted Curcumin Analogue. *J. Photochem. Photobiol. B: Biol.* **2009**, *97*, 77–86.

(57) Mandal, S.; Ghosh, S.; Banik, D.; Banerjee, C.; Kuchlyan, J.; Sarkar, N. An Investigation into the Effect of the Structure of Bile Salt Aggregates on the Binding Interactions and ESIHT Dynamics of Curcumin: A Photophysical Approach to Probe Bile Salt Aggregates as a Potential Drug Carrier. *J. Phys. Chem. B* **2013**, *117*, 13795–13807.

(58) Adhikary, R.; Mukherjee, P.; Kee, T. W.; Petrich, J. W. Excited-State Intramolecular Hydrogen Atom Transfer and Solvation Dynamics of the Medicinal Pigment Curcumin. *J. Phys. Chem. B* **2009**, *113*, 5255–5261.

(59) Adhikary, R.; Carlson, P. J.; Kee, T. W.; Petrich, J. W. Excited-State Intramolecular Hydrogen Atom Transfer of Curcumin in Surfactant Micelles. *J. Phys. Chem. B* **2010**, *114*, 2997–3004.

(60) Jarzeba, W.; Walker, G. C.; Johnson, A. E.; Kahlow, M. A.; Barbara, P. F. Femtosecond Microscopic Solvation Dynamics of Aqueous Solutions. *J. Phys. Chem.* **1988**, *92*, 7039–7041.

(61) Jimenez, R.; Fleming, G. R.; Kumar, P. V.; Maroncelli, M. Femtosecond Solvation Dynamics of Water. *Nature* **1994**, *369*, 471–473.

(62) Riter, R.; Willard, D.; Levinger, N. Water Immobilization at Surfactant Interfaces in Reverse Micelles. *J. Phys. Chem. B* **1998**, *102*, 2705–2714.

(63) Corbeil, E.; Riter, R.; Levinger, N. Cosurfactant Impact on Probe Molecule in Reverse Micelles. *J. Phys. Chem. B* **2004**, *108*, 10777–10784.

(64) Pal, S.; Peon, J.; Zewail, A. Biological Water at the Protein Surface: Dynamical Solvation Probed Directly with Femtosecond Resolution. *Proc. Natl. Acad. Sci. U. S. A.* **2002**, *99*, 1763–1768.

(65) Qiu, W.; Zhang, L.; Okobiah, O.; Yang, Y.; Wang, L.; Zhong, D.; Zewail, A. Ultrafast Solvation Dynamics of Human Serum Albumin: Correlations with Conformational Transitions and Site-Selected Recognition. *J. Phys. Chem. B* **2006**, *110*, 10540–10549.

(66) Halder, M.; Mukherjee, P.; Bose, S.; Hargrove, M. S.; Song, X.; Petrich, J. W. Solvation Dynamics in Protein Environments: Comparison of Fluorescence Upconversion Measurements of Coumarin 153 in Monomeric Hemeproteins with Molecular Dynamics Simulations. *J. Chem. Phys.* **2007**, *127* 055101.

(67) Horng, M.; Gardecki, J.; Papazyan, A.; Maroncelli, M. Subpicosecond Measurements of Polar Solvation Dynamics - Coumarin-153 Revisited. *J. Phys. Chem.* **1995**, *99*, 17311–17337.

(68) Fee, R.; Maroncelli, M. Estimating the Time-Zero Spectrum in Time-Resolved Emission Measurements of Solvation Dynamics. *Chem. Phys.* **1994**, *183*, 235–247.

(69) Maroncelli, M.; Fleming, G. R. Picosecond Solvation Dynamics of Coumarin-153 - The Importance of Molecular Aspects of Solvation. *J. Chem. Phys.* **1987**, *86*, 6221–6239.

(70) Wang, Z. F.; Leung, M. H. M.; Kee, T. W.; English, D. S. The Role of Charge in the Surfactant-Assisted Stabilization of the Natural Product Curcumin. *Langmuir* **2010**, *26*, 5520–5526.

(71) Khopde, S. M.; Indira Priyadarsini, K.; Palit, D. K.; Mukherjee, T. Effect of Solvent on the Excited-State Photophysical Properties of Curcumin. *Photochem. Photobiol.* **2000**, *72*, 625–631.

(72) Riter, R. E.; Undiks, E. P.; Levinger, N. E. Impact of Counterion on Water Motion in Aerosol OT Reverse Micelles. *J. Am. Chem. Soc.* **1998**, *120*, 6062–6067.

(73) Pant, D.; Riter, R.; Levinger, N. Influence of Restricted Environment and Ionic Interactions on Water Solvation Dynamics. *J. Chem. Phys.* **1998**, *109*, 9995–10003.

(74) Bagchi, B. Water Dynamics in the Hydration Layer around Proteins and Micelles. *Chem. Rev.* **2005**, *105*, 3197–3219.

(75) Fleming, G.; Cho, M. Chromophore-Solvent Dynamics. *Annu. Rev. Phys. Chem.* **1996**, *47*, 109–134.

(76) Stratt, R. M.; Maroncelli, M. Nonreactive Dynamics in Solution: The Emerging Molecular View of Solvation Dynamics and Vibrational Relaxation. *J. Phys. Chem.* **1996**, *100*, 12981–12996.

(77) Ghosh, R.; Mondal, J. A.; Palit, D. K. Ultrafast Dynamics of the Excited States of Curcumin in Solution. *J. Phys. Chem. B* **2010**, *114*, 12129–12143.

(78) Vajda, S.; Jimenez, R.; Rosenthal, S.; Fidler, V.; Fleming, G.; Castner, E. Femtosecond to Nanosecond Solvation Dynamics in Pure Water and Inside the γ-Cyclodextrin Cavity. *J. Chem. Soc. Faraday Trans.* **1995**, *91*, 867–873.

Appendix A

Supporting Information for Chapter 2: Diamide Linked γ–Cyclodextrin Dimers as Molecular-Scale Delivery Systems for the Medicinal Pigment Curcumin to Prostate Cancer Cells

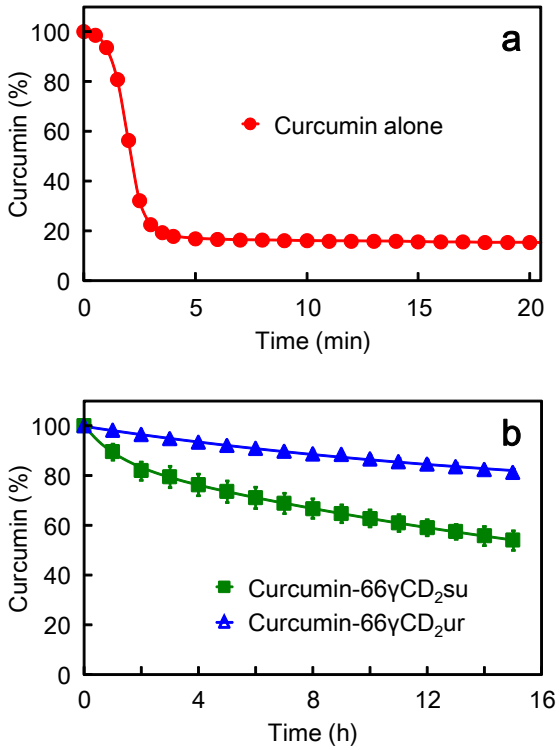

Figure A.1. Degradation kinetics of 15.0 µM curcumin in (a) pH 7.4 phosphate buffer, (b) 66γCD_2su and (c) 66γCD_2ur at 37 °C. The mole ratio of curcumin to either 66γCD_2su or 66γCD_2ur is 1 : 1. Signals were recorded for (a) 20 min, and (b) 15 h.

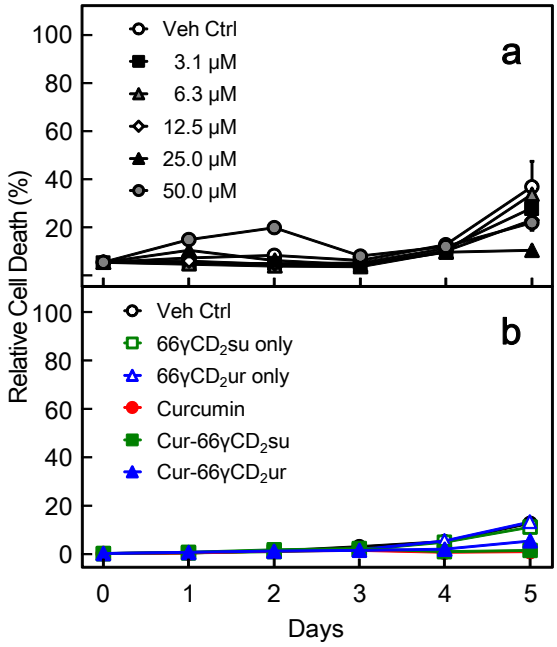

Figure A.2. Cell viability assays performed using human epithelial prostate cancer PC-3 cells. (a) Dead PC-3 cells with increasing concentrations of curcumin over 5 days, with respect to the corresponding vehicle control. (b) Dead PC-3 cells treated with 12.5 µM curcumin, curcumin-66γCD$_2$su or curcumin-66γCD$_2$ur over 5 days, with respect to the corresponding vehicle control.

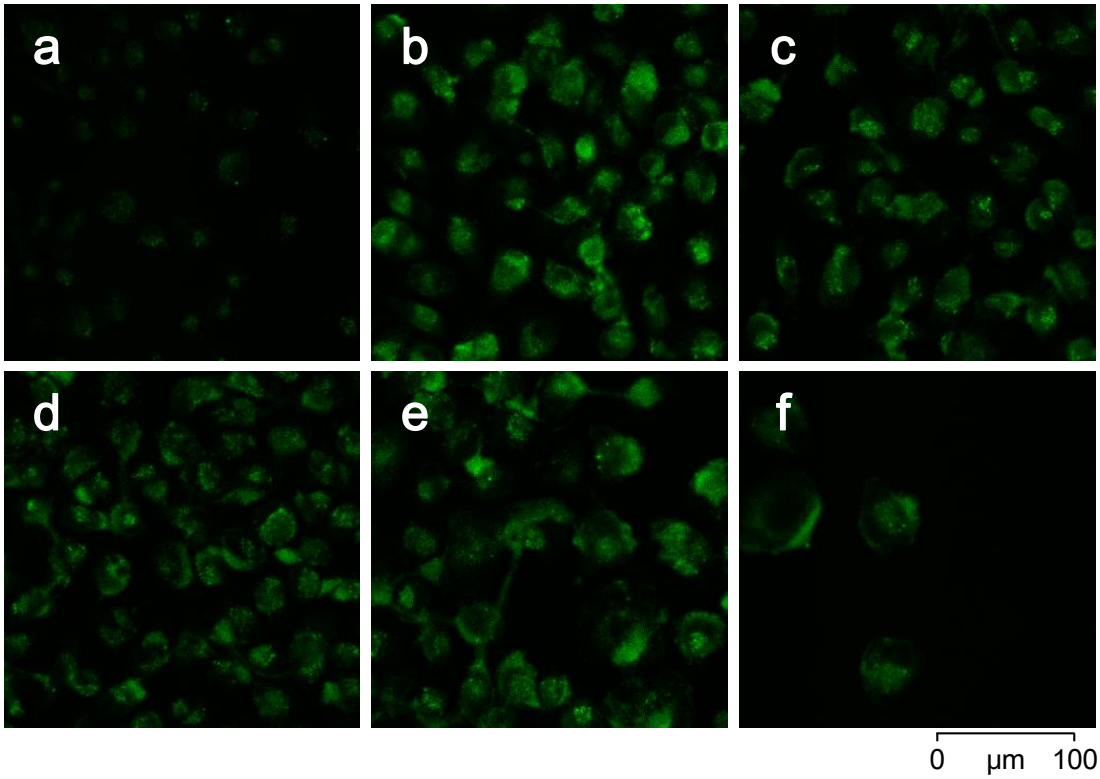

Figure A.3. Confocal fluorescence images of PC-3 cells treated with (a) 0.08 %v/v DMSO (vehicle control) and 12.5 µM of curcumin for (b) 1, (c) 2, (d) 3, (e) 4 and (f) 5 days.

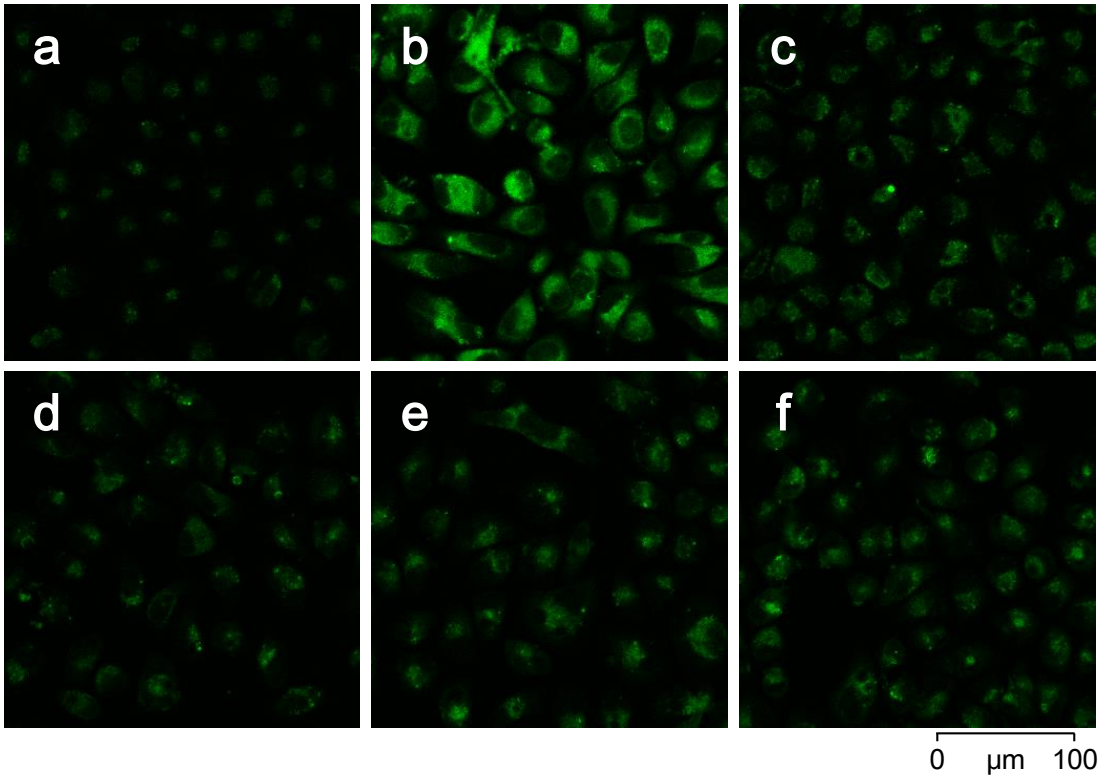

Figure A.4. Confocal fluorescence images of PC-3 cells treated with (a) 12.5 µM of 66γCD$_2$su (0.08 %v/v DMSO) and 12.5 µM of curcumin-66γCD$_2$su for (b) 1, (c) 2, (d) 3, (e) 4 and (f) 5 days.

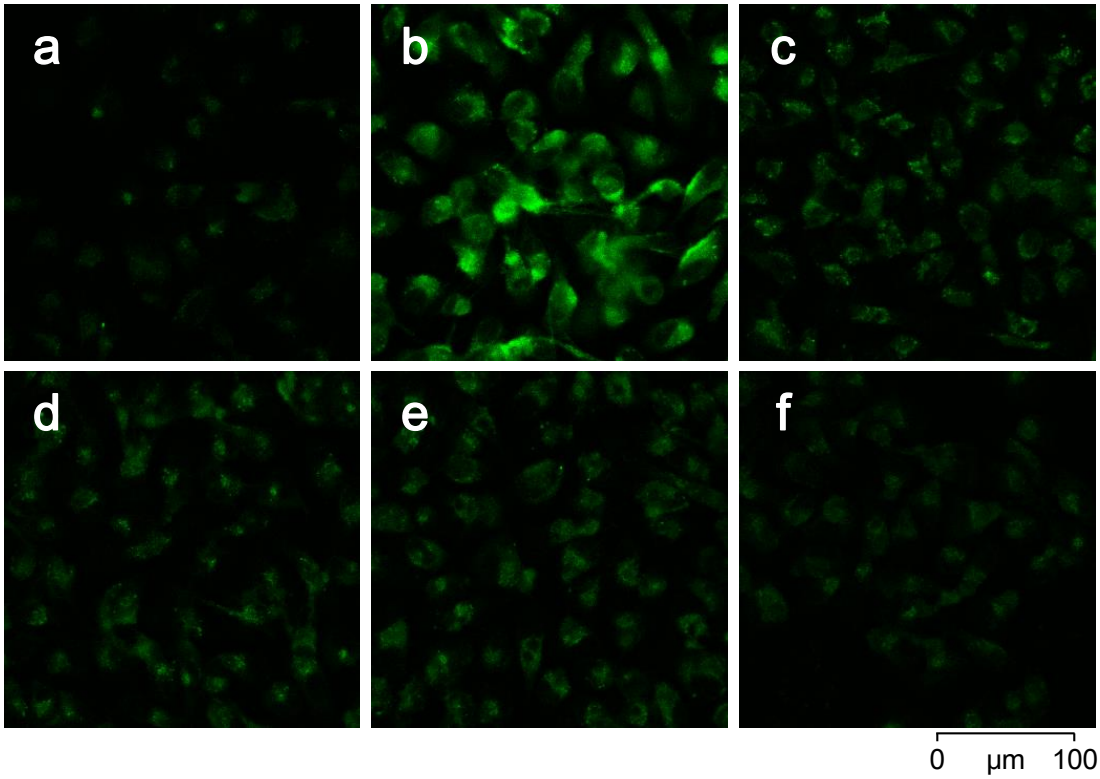

Figure A.5. Confocal fluorescence images of PC-3 cells treated with (a) 12.5 µM of 66γCD$_2$ur (0.08 %v/v DMSO) and 12.5 µM of curcumin-66γCD$_2$ur for (b) 1, (c) 2, (d) 3, (e) 4 and (f) 5 days.

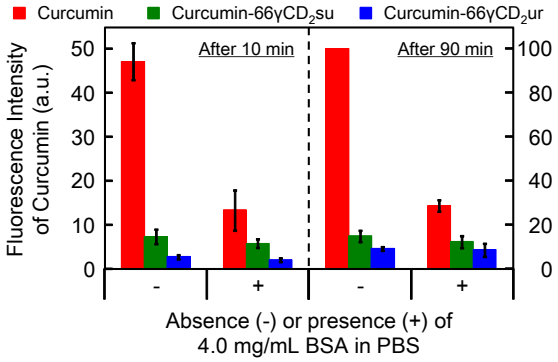

Figure A.6. Effects of BSA on cellular uptake of curcumin in the absence and presence of either 66γCD$_2$su or 66γCD$_2$ur. The PBS solutions contain 0.0 or 4.0 mg/mL of BSA. PC-3 cells were incubated with 12.5 µM of each solution for 10 (left) and 90 min (right). Fluorescence intensities were normalised to the saturation intensity of the curcumin-only sample without BSA after 90-min incubation, showing it is comparable to Figure 2.5. Note the different scales for the left and right panels. Asterisk symbols in the figure represent very significant decrease in fluorescence intensity of curcumin due to the presence of BSA ($p < 0.001$).

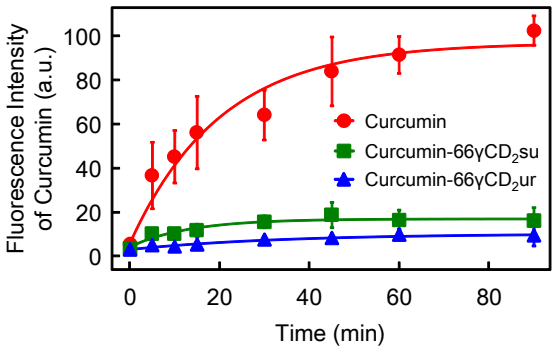

Figure A.7. Kinetics of cellular uptake of curcumin in the absence and presence of either 66γCD$_2$su or 66γCD$_2$ur in PBS. PC-3 cells were incubated with 12.5 µM of each treatment up to 90 min.

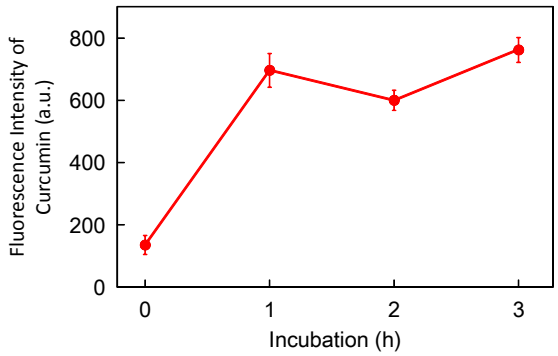

Figure A.8. Kinetic of cellular uptake of curcumin in the absence of either 66γCD_2-su or 66γCD_2ur in PBS. PC-3 cells (4×10^4 cells/well) were incubated with 80 µM curcumin up to 3 h. The resultant amount of DMSO is 0.06 %v/v. This kinetic shows cellular uptake may cease within 1–2 h.

Table A.1. An example of normalisation process in the cellular uptake study.[a]

Incubation Time (min)	Fluorescence Intensity of Curcumin (a.u.)	ΣSD	Normalised Fluorescence Intensity of Curcumin	Normalised ΣSD
0.083	434	35	3.692	0.296
5	3744	146	31.870	1.244
10	4889	163	41.609	1.389
15	6732	198	57.295	1.685
30	7575	250	64.477	2.125
45	10479	322	89.194	2.743
60	11375	328	96.813	2.796
90	11514	336	98.003	2.861
Plateau	11749			
Intrinsic fluorescence	155	59	1.321	0.504

[a] Fluorescence intensity of curcumin is the difference in intensity between cells treated with curcumin and vehicle control to obtain the fluorescence intensity of curcumin only. This intensity is fitted with a first order kinetics to estimate the plateau value. All the fluorescence intensities of curcumin are then normalised with respect to this plateau value. The intrinsic fluorescence is the difference in intensity between vehicle control and methanol, that is, the fluorescence intensity due to cells, which is very small compared to that of curcumin.

Appendix B

Supporting Information for Chapter 5: The Capture and Stabilisation of Curcumin Using Hydrophobically Modified Polyacrylate Aggregates and Hydrogels

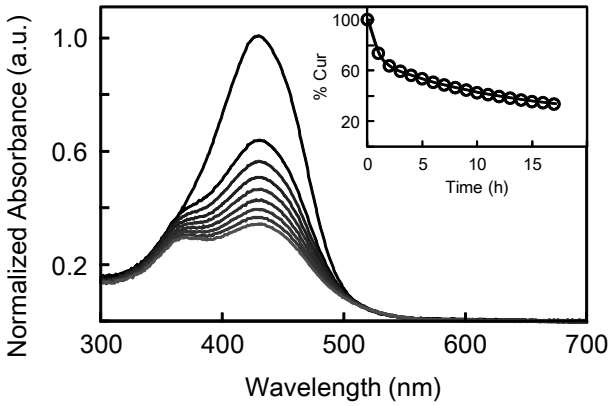

Figure B.1. UV-Vis absorption spectra of 30 µM curcumin in 2.9 wt%, at 37 °C. Signals were recorded for 18 h. The inset shows the decay of the absorption maxima due to decomposition of curcumin. The 2.9 wt% PAAC12 possesses an equivalent number of carbon atoms on the substituent as 2.0 wt% PAAC18. The 2.9 wt% PAAC12 shows a similar viscosity as 1.0 wt% PAAC18 in a previous study. However, PAAC12 exhibits insignificant suppression of curcumin decomposition at 37 °C.

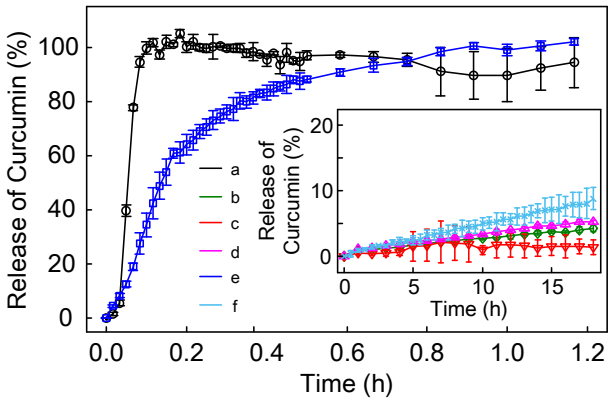

Figure B.2. Release kinetics of curcumin in (a) pH 7.4 phosphate buffer solution, those in PAAC18 at (b) 0.3 wt%, (c) 1.0 wt% and (d) 2.0 wt%, and those in (e) PAAC12 at 1.0 wt% and (f) 10%-PAAC12 at 0.5 wt%, at 37 °C. The kinetics were determined by the evolution of the absorbance around 350 nm with respect to the maximum absorbance of curcumin around 430 nm. Absorbance around 350 nm corresponds to degradation products of curcumin as a result of its release from the polyacrylate micelle-like aggregates or hydrogels. Curcumin in buffer (a) shows rapid formation of degradation products. Curcumin in PAAC18 (b–d) shows sustained release profiles over 18 h. PAAC12 releases curcumin rapidly (e) within 1 h, while 10%-PAAC12 exhibits a sustained release of curcumin (f).

Table B.1. Binding constants, K_n, of PAAC18-curcumin complexes for n = 1–10

n	K_n ($\times 10^4 M^{-1}$)
1	–
2	0.36 ± 0.01
3	0.70 ± 0.01
3.5	1.04 ± 0.01
4	1.48 ± 0.06
4.25	1.65 ± 0.06
4.5	1.85 ± 0.10
4.75	2.06 ± 0.13
5	2.08 ± 0.13
5.25	1.86 ± 0.18
5.5	1.67 ± 0.26
5.75	1.39 ± 0.18
6	1.36 ± 0.12
6.5	1.14 ± 0.15
7	0.92 ± 0.09
7.5	0.85 ± 0.08
8	0.75 ± 0.06
9	0.67 ± 0.05
10	0.61 ± 0.05

Table B.2. Chemical shifts of curcumin (1,7-bis(4-hydroxy-3-methoxyphenyl)hepta-1,6-diene-3,5-dione) in different solvent systems and 1.0 wt% PAAC18

		Chemical shifts (ppm)		
Curcumin Hydrogens		d_6-DMSO	$CDCl_3$	PAAC18 in D_2O
trans	H1, H7	7.55	7.57	7.39
Ph	H5	7.32	7.32	6.80–6.97
Ph	H1	7.15	7.16	
Ph	H2	6.82	6.85	
trans	H2, H6	6.76	6.76	6.40
Alpha	H4	6.06	6.06	*D-Exchange*
Methoxy	–	3.90	3.85	3.82

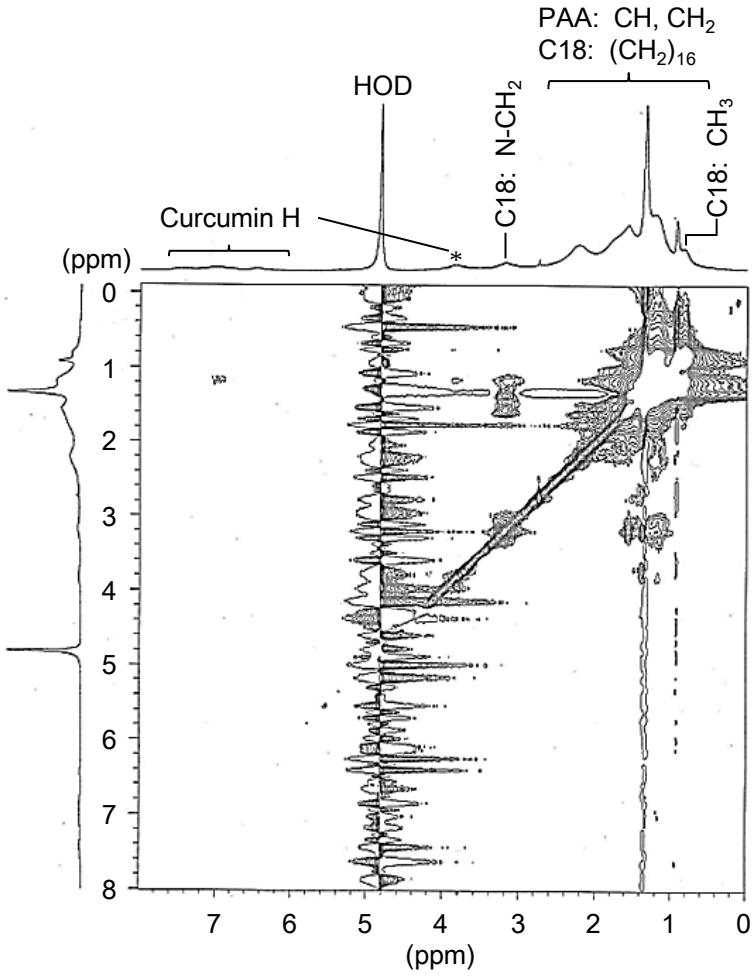

Figure B.3. 2D NOESY ^{1}H NMR spectrum of curcumin in 2.0 wt% 10%-PAAC12 in D_2O at pD 7. No cross-peaks arising from the interactions between the dodecyl substituent protons and the curcumin CH and CH_3O (as indicated as asterisk) are observed.